Magnetically Actuated Hybrid Brake for Autonomous, Electrified Vehicles

Vom Fachbereich Maschinenbau an der
Technischen Universität Darmstadt
zur Erlangung des Grades eines
Doktor-Ingenieurs (Dr.-Ing.)
genehmigte

Dissertation

vorgelegt von

Lennart Alexander Guckes M. Sc.
aus Wiesbaden

Berichterstatter:	Prof. Dr. rer. nat. Hermann Winner
Mitberichterstatter:	Prof. Dr.-Ing. Ralph Mayer
Tag der Einreichung:	29.11.2022
Tag der mündlichen Prüfung:	25.01.2023

Darmstadt 2023
D 17

Preface

This dissertation was written during my time at the Institute of Automotive Engineering (FZD) of Technical University of Darmstadt from February 2019 to September 2022 as part of the research project "Systems for Wheel Brake Actuation" in collaboration with the Innovation Department of Continental Teves AG & Co.oHG.

My thanks go to all people who made writing this dissertation possible. First and foremost, my doctoral supervisor Prof. Dr. rer. nat. Hermann Winner, who supervised me during my time at FZD, including many scientific discussions and constructive feedback. Also, for his willingness to continue to supervise the outgoing Ph.D. candidates until the doctoral examination, even after the start of his retirement.

Furthermore, thanks to Prof. Dr.-Ing. Ralph Mayer for the co-examination of this academic work.

I would especially like to thank my colleagues at FZD for the many events and experiences we had together during this time, which had a great impact on me. Not only the Ph.D. candidates, but also all the technical and administrative staff at FZD, who supported me in all organisational or manufacturing-related aspects.

I would like to thank my colleagues in the research project at Conti, especially Prof. Dr.-Ing. Jens Hoffmann and Dr.-Ing. Christian Vey, who played a significant role in my professional orientation during my studies and in the research project. Special thanks go to Michael Richter and Stefan Imhof, who supported me in the setup of the prototypes, the test benches and sensors.

I would especially like to thank my family for their constant support, both moral and financial, during my academic education.

And of course, my thanks go to my wife Iris, who stands by my side for over 13 years, endured all my moods and always managed to take my mind off things.

Table of Contents

Abbreviations

Abbreviation	Description
ABS	Antilock Braking System
AMS	Auto Motor Sport
BFD	Brake force distribution
CD	City Descent
EMB	Electromechanical wheel brake
ES	Emergency Stop
ESC	Electronic Stability Program
EV	Electric vehicle
FM	Fleet manager
FZD	Fahrzeugtechnik Darmstadt
GG	Großglockner
HFT	High Speed Fading Test
HMI	Human machine interface
L	Legislator
NAO	Non-asbestos organics
NVH	Noise Vibration Harshness
ODD	Operational Design Domain
OEM	Original Equipment Manufacturer
P	Passenger
rot	rotational
RU	Road users
SAE	Society of Automotive Engineers
SoC	State of charge
STO	Standard Transport Operation
trans	translational
UN	United Nations

Symbols

Symbol	Unit	Description
a	m/s^2	Acceleration
A	m^2	Area
B	T	Magnetic flux density
c^*	-	Brake factor
f	Hz	Frequency
F	N	Force
h	m	Height
H	A/m	Magnetic Field Strength
I	A	Current
j	m/s^3	Jerk
K	-	Geometric coefficient for brake factor calculation
l	m	Length
m	kg	Mass
M	Nm	Torque
N	-	Count (e.g. winding count)
p	bar	Pressure
P	W	Power
q	-	road gradient
r	m	Radius
R	Ohm	Resistance
s	m	Distance
SoC	-	State of charge
t	s	Time
T	°C	Temperature
U	V	Voltage
v	m/s	velocity
W	J	Energy
x	m	Displacement
z	-	Normalized deceleration

Symbol	Unit	Description
α	°	Angle
δ	m	Air Gap
Δ	-	Difference
μ	-	Coefficient of Friction
μ_0	Vs/Am	Permeability of free space
μ_r	-	Relative Permeability
φ	-	Displacement angle
Ψ	-	Rear axle ratio
χ	-	Height of center of gravity in relation to wheelbase
τ	s	Duration

List of Figures

List of Tables

Kurzzusammenfassung

Autonomes Fahren, die Elektrifizierung des Antriebsstrangs und die Senkung der Emissionen sind drei große Entwicklungstrends in der Automobilindustrie. Neue Mobilitätslösungen wie beispielsweise elektrifizierte, autonome Shuttles zum Personen- und Gütertransport in Städten werden erdacht und fordern ein entwicklungstechnisches Umdenken nicht nur softwareseitig, sondern auch auf der Fahrwerksseite.

Für Bremssysteme ergeben sich für diese Fahrzeuge Änderungen in den Anforderungen. Bestehende Testspezifikationen zur Überprüfung der Leistungsfähigkeit einer Pkw Radbremse sind vor allem auf Extremfälle ausgelegt, welche von einem menschlichen Fahrer ausgelöst werden können. Anhand einer Stakeholder Analyse sowie einer Use-Case Betrachtung werden im Rahmen der Arbeit Anforderungen spezifiziert und in neuen Testvorschriften umgesetzt, die auf autonome Shuttles zugeschnitten sind. Besonders die Einschränkung des Einsatzgebietes im Rahmen der Operational Design Domain des autonomen Shuttles bedingt wesentlich geringere thermische Anforderungen an die Radbremse im Vergleich zum konventionellen Pkw. Dennoch werden aufgrund der hohen Fahrzeugmassen und dem Szenario der Nichtverfügbarkeit der regenerativen Bremse hohe Bremsmomente gefordert.

Anhand der identifizierten Anforderungen und Entwicklungsziele aus der Analyse wird der Lösungsraum der Bremssysteme im Stand der Technik durchsucht und die Eignung verschiedener Wirkprinzipien diskutiert. Bisherige hydraulische Konzepte für Pkw erfüllen zwar die dynamischen und thermischen Anforderungen, bergen aber wenig Potential zur Emissionsminderung und neigen zu Korrosionen durch die steigende Dauer zwischen den Betätigungen bei Verwendung der regenerativen Bremse. Als Alternative stehen vor allem elektromechanische Konzepte im Fokus der Entwicklung für einzelne Radbremsmodule mit elektromotorischer Betätigung, welche in einem Fehlerfall nur zum Ausfall einer der vier Radbremsen führen. Bisherige Konzepte elektromotorisch betätigter Bremsen zeigen einen Entwicklungskonflikt darin, dass wegen der nötigen, hoch übersetzenden Getriebe viele Getriebestufen nötig sind, die aufgrund der verwendeten Schmierstoffe eine hohe Wirkungsgradvarianz über der Temperatur besitzen. Im Lösungsraum der elektromechanischen Aktoren sind neben den Elektromotoren auch Elektromagneten zu finden. Im Stand der Technik und der Forschung sind jedoch nur wenige Konzeptuntersuchungen veröffentlicht, obwohl eine elektromagnetische Betätigung im Gegensatz zu einer elektromotorischen einige Vorteile verspricht. Unter anderem sind dies eine weniger komplexe Ansteuerung, geringerer Bauraum, sowie eine geringere mechanische Komplexität. Aufgrund der offenbarten Lücke im Stand der Forschung wird ein elektromagnetisches Konzept ausgewählt, um es auf seine Eignung als Radbremse für ein autonomes Shuttle zu untersuchen. Dafür lassen sich als Aktoren entweder Haftmagneten oder Hubmagneten einsetzen, wobei Haftmagneten wesentlich höhere Magnetkräfte versprechen.

Zur Untersuchung wird eine erste Auslegung einer mit einem Haftmagneten betätigten Trommelbremse prototypisch realisiert. Das Konzept umfasst eine Kombination einer haftmagnetisch betätigten Vollbelagsscheibenbremse mit einer nachgeschalteten Trommelbremse in Duplex Bauform. Die Verschaltung der beiden Bremsen verspricht eine Ausnutzung des Raddrehwinkels zur Betätigung der Trommelbremse und eine redundante Aktorausführung durch die Verwendung von zwei Erregerspulen in der magnetischen Scheibenbremse.

Für den Nachweis der Eignung des Konzepts werden Aktorkräfte, Dynamik, Gesamtbremsmomente und Scheibenbremsmomente des Konzepts im Betrieb untersucht. Die größten Abweichungen zur Modellvorstellung treten im Momentenverlauf der Bremse über der Drehzahl auf, welche mittels eines hypothesen- und testbasierten Vorgehens näher untersucht werden. Neben Untersuchungen bezüglich des Einflusses von magnetfeldschwächenden Effekten, wie beispielsweise Wirbelströmen, wird auch der Reibwert der Reibpartner am Haftmagnetaktor bestimmt und als Hauptursache für die Momentenabnahme identifiziert. Es zeigt sich eine Abhängigkeit sowohl von der Drehzahl als auch von der erreichten Axialkraft. Die beteiligten Reibpartner übernehmen sowohl die Funktion der Feldführung als auch der Reibkrafterzeugung. Der zur Feldführung notwendige Reibkontakt zwischen metallischer Scheibe und metallischem Magnetjoch zeigt einen großen Einfluss auf den Reibwert des Scheibenbremssystems. Die Untersuchung der Hysterese des Gesamtbremssystems zeigt die Schwierigkeit beim Stellen kleiner Momente, da der Magnet zum Durchfahren des Initialluftspalts einen hohen Strombedarf hat, der beim Auftreffen auf die Scheibe bereits mittlere Momente erzeugt. Ein Vorschlag zur Aktuierung mittels einer Stromvorsteuerung wird ebenfalls getestet und bewertet.

Durch die getätigten Untersuchungen ist der Entwicklungskonflikt bei der Verwendung eines haftmagnetischen Aktorkonzepts zur Betätigung einer Radbremse messtechnisch erfasst und durch das hypothesenbasierte Vorgehen wird der ursächliche Effekt der Momentenabnahme identifiziert. Das realisierte Haftmagnetkonzept erfüllt die Anforderungen an die Dynamik und den Wunsch nach emissionsarmen, kompakten Bremskonzepten, erreicht jedoch nicht die geforderten Bremsmomente über den gesamten Betriebsbereich eines autonomen Shuttles. Im Ausblick wird ein konzeptueller Lösungsvorschlag einer Betätigung mittels Hubmagnetaktorik diskutiert, der den erfassten Entwicklungskonflikt zu lösen verspricht, aber wegen des geringeren Kraftpotentials wiederum einen höheren Übersetzungsbedarf aufweist.

Summary

Autonomous driving, the electrification of the powertrain and the reduction of emissions are three major development trends in today's automotive industry. New mobility solutions such as electrified, autonomous shuttles for transporting people and goods in cities are being conceived and require a change of view in development, not only on the software level but also on chassis components.

For braking systems, there are changes in the requirements for these vehicles. Existing test specifications for the performance of wheel brakes for passenger cars are primarily designed for the worst-case scenarios that can be caused by a human driver. Based on a stakeholder analysis as well as a use-case consideration new requirements are generated and new test specifications are developed, which are tailored to autonomous shuttles. Especially the restriction of the Operational Design Domain of the autonomous shuttle results in significantly lower thermal requirements for the wheel brake compared to conventional passenger cars. Nevertheless, high braking torques are still required due to high vehicle masses and the scenario of non-availability of the regenerative brake.

Based on the identified requirements and development goals from the analysis, the solution space of braking systems in the state of the art is considered and the suitability of different brake concepts is discussed. Although current hydraulic concepts for passenger cars meet the dynamic and thermal requirements, they have little potential for reducing emissions and tend to corrode due to the increasing duration between actuations when regenerative brakes are in use. As an alternative, the focus of development lies on electromechanical concepts for individual wheel brake modules with electromotive actuation, which in the event of a fault only leads to the failure of one of four wheel brakes. Previous concepts of electromotively actuated brakes show a development conflict in the fact that many gear stages are necessary due to the high transmission ratios, which show a high efficiency variance over temperature due to their lubricants. In the concept space of electromechanical actuators, electromagnets can be found in addition to electric motors. However, only a few concept studies have been published regarding the state of the art and research, although electromagnetic actuation promises some advantages over electromotive actuation. These include less complex actuation, smaller installation space, and less mechanical complexity. Due to the revealed gap in the state of the art, an electromagnetic concept is selected to be investigated for its suitability as a wheel brake for an autonomous shuttle. For this purpose, either holding magnets or solenoids can be used as actuators, with holding magnets promising significantly higher magnetic forces at small air gaps.

For the investigations, a first design of a drum brake actuated by a holding magnet is prototypically realized. The concept comprises a combination of a magnetically actuated solid disc brake with a downstream duplex drum brake. The interconnection of the two brakes

promises the utilization of the wheel rotation angle for actuation of the drum brake and a redundant actuator design through the use of two excitation coils in the magnetic disc brake.

To evaluate the suitability of the concept, actuator forces, dynamics, total torques and disc brake torques are measured in operation. The largest deviations from the design considerations occur in the torque curve of the brake over speed, which are investigated in more detail using a hypothesis- and test-based approach. In addition to investigations into the influence of magnetic field weakening effects, such as eddy currents, the coefficient of friction of the friction partners on the holding magnet actuator is also determined and identified as the main cause of the torque drop. A dependence on both the velocity and the axial force is examined.

The investigation of the torque hysteresis of the overall braking system shows the difficulty in setting small torques, since the magnet has a high current demand to pass the initial air gap, which then generates medium torques when it hits the disc. A proposal for control by means of a current pre-control is also being tested and evaluated.

Through the investigations carried out, the development conflict in the use of a holding-magnetic actuator concept for the actuation of a wheel brake is recorded, and through the hypothesis-based approach the causal effect of the torque drop is identified. The realized magnetic actuator concept fulfills the requirements for dynamics and the wish for low-emission, compact braking concepts, but does not achieve the required braking torques over the entire operating range of an autonomous shuttle. In the outlook a proposed conceptual solution of actuation by means of solenoid actuators is discussed, which promises to solve the described development conflict, but in turn requires a higher transmission ratio due to the lower force potential.

„Wenn wir wüssten, was wir tun, würde man es nicht Forschung nennen.“

Albert Einstein

„If we knew what we are doing, it wouldn't be called research.“

Albert Einstein

1 Introduction

1.1 Motivation

Modern vehicle technology is currently undergoing a technical transformation. Three major trends are shaping the development directions of car manufacturers: automated driving, electrification of the powertrain and the strive for the lowest possible emissions. Car manufacturers, start-ups and suppliers are developing vehicle concepts that illustrate these development trends and serve as a show case for their own development potential. The concept of an autonomous shuttle is often set into focus by automotive developers. According to the manufacturers, it promises to become an automated, electrified and ecologic fleet vehicle for on-demand transport of passengers in metropolitan areas or even cross country.

The technical goal of developing a vehicle with SAE Level 4 or 5 also means rethinking the requirements for all chassis systems. The complete separation of the human driver and the actuator system changes the assumed loads on the vehicle systems, including powertrain, brakes, steering and chassis. Classically, these systems are designed to endure the worst-case loads by a human driver, but in an automated vehicle this load is reducible. Electrification of the powertrain in particular entails the ability of regenerative braking, which reduces the frequency of using friction brakes for comfort brakings and produces no particulate emissions.

The first central research question for this work is therefore:

1. *What are the requirements for wheel brakes of highly automated, electrified shuttles?*

Answering the first question leads directly to the next stage in the development process:

2. *Which wheel brake concepts are particularly suitable for highly automated, electrified shuttles?*

It is not the aim of this work to generate a complete list of all requirements for autonomous shuttles, but rather to show the greatest differences to the requirements for today's passenger car braking systems. Out of the answer to the second research question and the research to actuation principles for wheel brakes a third research question arose:

3. *Is a magnetically actuated hybrid brake able to fulfill the requirements for an autonomous shuttle and are the presumed advantages valid?*

1.2 Methodology and Structure

The central research questions are answered using a developed methodology, which is explained in the following and determines the structure of the thesis.

Chapter 1 motivates the research topic and presents the methodology and structure of the thesis. Chapter 2 describes the state of the art of autonomous shuttles, the requirements for car braking systems and wheel brake concepts used in modern cars. In addition, wheel brake concepts that are still in the research stage are presented. Chapter 3 describes the procedure for the definition of requirements for wheel brakes of autonomous shuttles by means of a stakeholder analysis and the comparison with requirements for wheel brakes of today's passenger cars. Chapter 4 discusses the suitability of today's known wheel brake concepts and highlights the research gap in the field of electromechanically actuated brakes. Chapter 5 presents the magnetic hybrid brake mentioned in the title, its design and construction. Chapter 6 shows the results of performance tests to check on the fulfilment of the set requirements by means of test bench trials and simulation. In chapter 7, an effect analysis is carried out to identify the cause of a torque drop of the brake using hypothesis-based tests. In chapter 8, a conclusion is drawn and an outlook is given on possible fields of research in the area of magnetic brake actuation. Figure 1-1 shows the chapters and the underlying questions.

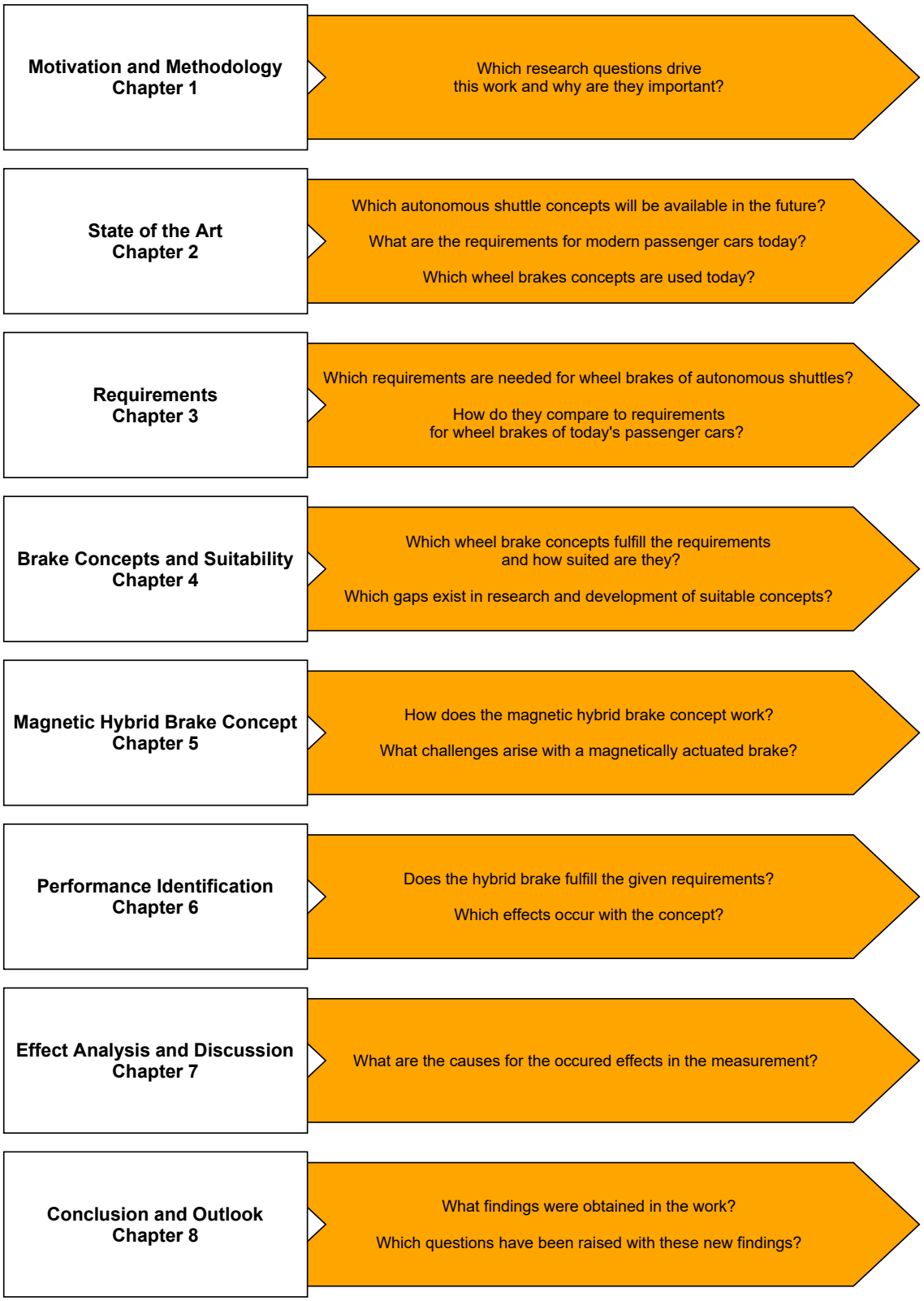

Figure 1-1: Structure of the work and corresponding research questions

2 State of the Art

2.1 Autonomous Shuttles

Global trends in vehicle development today show three main development directions. Electrification of the powertrain is fundamentally changing the propulsion concepts of modern vehicles and its equipment rate is steadily increasing[1]. Automated driving is gradually becoming established in the modern vehicle market [2] and, in addition to powertrain emissions, emissions from tires and wheel brakes in particular are being researched more closely and will be standardized in the future by a United Nations (UN) working group [3]. Some manufacturers as well as suppliers publish various concepts of automated shuttles to demonstrate their own innovative capacity in those fields (Figure 2-1).

Figure 2-1: Example of an autonomous shuttle built by Easy Mile and Continental[4]

The ideas behind these concepts are very similar: the autonomous driving shuttle is a vehicle concept that should reach at least level 4 of the Society of Automotive Engineers (SAE) [5] standard, is electrically driven and is part of a vehicle fleet operation as a transport-on-demand vehicle. In the future, they are expected to replace parts of the public transport system, especially in cities, and will not operate as regular bus services with fixed schedules, but on-demand and thus covering the so-called last mile.

[1] Carlier, M.: Number of electric vehicles in use by type 2016-2020 (2021).

[2] Katharina Buchholz: Cars Increasingly Ready for Autonomous Driving (2021).

[3] UNECE: UNECE to develop global methodology to measure particle emissions from vehicles' braking systems (2021).

[4] Miriam Baum: Entwicklungsfahrzeug CUbE.

[5] SAE International: Taxonomy and Definitions for Terms Related to Driving Automation Systems for On-Road Motor Vehicles (2021), p. 30.

Early vehicles of this type were developed by the company Navya and 2getthere. The shuttles on the market now each differ in their specifications. Table 2-1 shows a selection of these vehicles and their technical data, as far as they were published.

Table 2-1: Vehicle data on different autonomous shuttles

Manufacturer and Model	Speed in trials in km/h	Maximum speed in km/h	Drivetrain power in kW	Admissible mass in kg	Maximum gradient in %	Capacity seated	Overall capacity
2getthere GRT[6]	20	60		6418	10	8	22
2getthere PRT[7]	20	40		2050	10	6	6
E.Go Mover[8]		60	78	3500		5	15
Easy Mile EZ10	25	45	12	3130	15		15
Local Motors Olli[9]	20	40		3266			12
Navya Arma[10]	12	25	15	3450	12	11	15
Schaeffler Mover[11]			13			4	6

Except for the 2getthere GRT, all vehicles are in the M1 class of the UNECE[12] with a maximum permissible total mass lower than 3500 kg. On the chassis side, the vehicles are equipped either with a front steering axle or with all-wheel steering including individual steering angle control like the Schaeffler Mover. Schaeffler demonstrates a developed rolling chassis with maximum maneuverability and the possibility for individual setups for passenger transport or delivery tasks. Further differences in vehicle design result from the specification of a preferred driving direction or completely free choice of driving direction. From an economic point of view, the concepts with preferred direction and front-axle steering offer

[6] 2getthere: GRT vehicle: automated minibus (2018).

[7] 2getthere: PRT vehicle: automated taxi (2018).

[8] e.GO MOOVE GmbH: Our Concept (2020).

[9] Local Motors: Meet Olli (2020).

[10] Navya: Arma Autonomous Shuttle (2020).

[11] Schaeffler: Urbanes Fahrzeugkonzept für die Zukunft (2019).

[12] UNECE: Concerning The Common Definitions of Vehicle Categories, Masses and Dimensions (2005).

the advantage of lower component complexity and more effective temperature management (because of the radiator). The stated maximum speeds of the vehicles vary between 25 – 60 km/h, but in current test studies a maximum of 25 km/h is stated, with the vehicles being monitored by a safety driver[13]. The maximum gradient of the road is stated as 10 – 15 %.

2.2 Requirements on Wheel Brakes for Passenger Cars

Today's requirements for wheel brakes are primarily set in the three categories of performance, comfort and lifetime. Based on regulatory activities of the UN in the Particle Measurement Programme Informal Working Group (PMP), particle emissions will also become a focus of requirements in the near future[14]. These categories can be broken down even further, like shown in Figure 2-2.

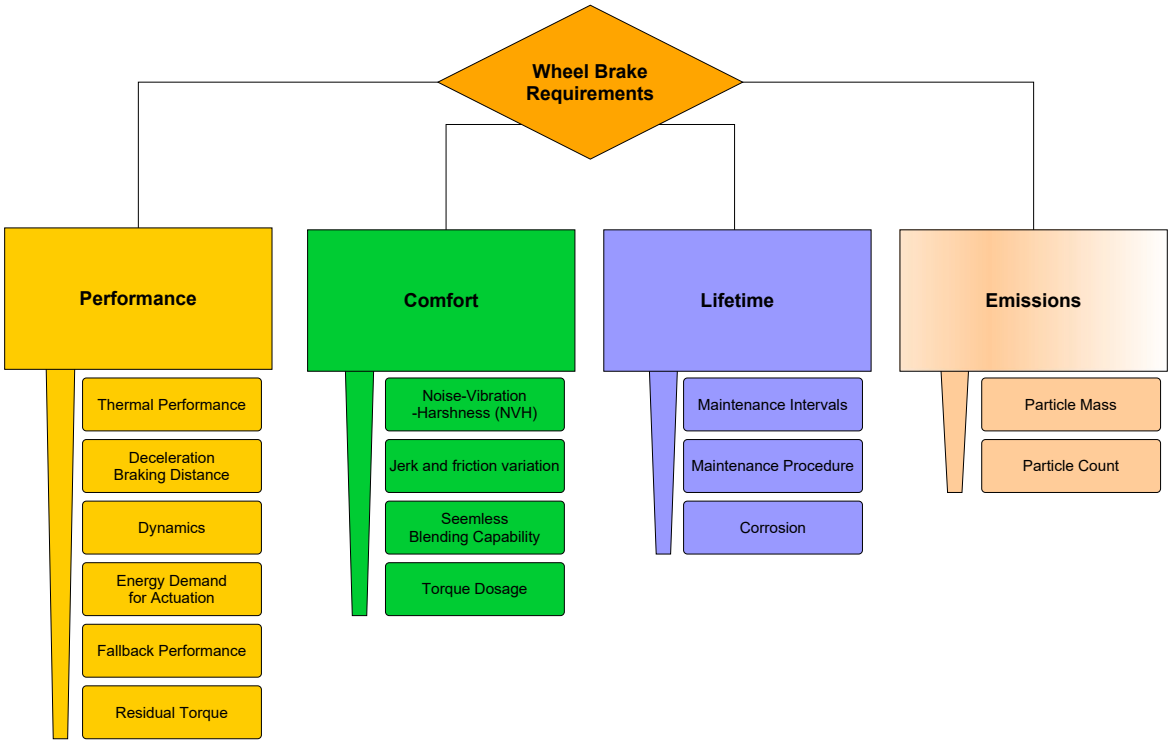

Figure 2-2: Categories of wheel brake requirements for today’s passenger cars

[13] RMV: Probefahrt in die Zukunft.

[14] UNECE: UNECE to develop global methodology to measure particle emissions from vehicles’ braking systems (2021).

The regulatory rules for the approval of braking systems for new vehicle models are based on the UN ECE-R13-H [15]. It contains requirements for thermal performance, stopping distance, dynamics and deceleration. These represent the minimum development targets of every passenger car braking system. The average deceleration to be achieved with a maximum force on the pedal of 500 N for a cold brake at a starting speed of 100 km/h must be at least $6.43\ \frac{\mathrm{m}}{\mathrm{s}^2} = 0.66g$ (Type 0 test). In order to characterize the hot behavior of the brake, it is conditioned in the Type 1 test, in which 15 brake applications from 80 % of the maximum speed to 40 % of the maximum speed with a deceleration of $3\ \frac{\mathrm{m}}{\mathrm{s}^2}$ are performed. This is followed by another Type 0 test. The average deceleration should correspond to at least 60 % of the average deceleration with the cold brake. For the braking system, a response time of 600 ms applies for the dynamics from the start of pedal actuation until the desired braking force is reached at each wheel.

However, the requirements from the automotive industry usually are set more strictly compared to these values. The thermal performance of the wheel brake is determined on the basis of the OEM's specifications. The OEM, in turn, also bases its specifications on benchmark tests, for example the "Auto Motor Sport" (AMS) test, which is used by the German magazine of the same name to evaluate the performance of the braking system of a new vehicle model[16]. For this purpose, the vehicle is accelerated ten times to 100 km/h and then brought to a stop with an emergency braking maneuver. As the brakes heat up, the stopping distance extends accordingly. This test is therefore a generic comparative test that is not based on a real-life scenario. Another of the so-called "fading tests" is the High Speed Fading Test (HFT), which corresponds to a conceivable worst-case motorway scenario. The vehicle drives at 90 % of its maximum speed and is decelerated to 90 km/h with a $0.6g$ deceleration. This corresponds to a fast motorway drive on the left lane with a lorry pulling out of its right lane in front of the driver's vehicle, starting to overtake another vehicle at 90 km/h. This scenario is repeated 15 times and the cooling time corresponds only to the acceleration time of the driver's vehicle to the target speed[17]. The criteria for passing the test depend on the OEM's specifications and relate to the friction value loss due to the increased temperature, functional integrity of the components as well as hydraulic pressure and volume requirements for the brake fluid to apply the hot brake.

Another test to check on the thermal performance is a hill descent, usually the Grossglockner descent (GG) is chosen as the reference test cycle. The underlying scenario represents a quite probable scenario of a hill descent on the Grossglockner Hochalpenstraße, where low speeds are dominant and a very long braking time is required and a high amount of potential energy needs to be dissipated. As with the HFT, the change in friction coefficient and the necessary

[15] UN: ECE R13-H (2018).

[16] Pickenhahn, J.; Straub, T.: Auslegung und Simulation von Pkw-Bremsanlagen (2017), p. 103.

[17] Marschner, H. et al.: Bremsentechnisches Versuchswesen (2017), p. 695.

braking pressure and fluid volume are considered and evaluated after the test[18]. Table 2-2 gives an overview of the various tests described.

Table 2-2: Test cycles for evaluating thermal performance of wheel brakes

	ECE	**AMS**	**HFT**	**GG**
Load	laden	partially laden	partially laden	laden
Number of brakings	15	10	15	1
Deceleration	$3\,\frac{\mathrm{m}}{\mathrm{s}^2}$	$10\,\frac{\mathrm{m}}{\mathrm{s}^2}$	$6\,\frac{\mathrm{m}}{\mathrm{s}^2}$	based on $v = \text{const.} \cap \mathrm{q} = -0.095$
Velocity targets	$0.4\ v_{\max}$ $\rightarrow 0.8\ v_{\max}$ $\rightarrow 0.4\ v_{\max}$	0 $\rightarrow 100\,\frac{\mathrm{km}}{\mathrm{h}}$ $\rightarrow 0$	$90\,\frac{\mathrm{km}}{\mathrm{h}}$ $\rightarrow 0.9\ v_{\max}$ $\rightarrow 90\,\frac{\mathrm{km}}{\mathrm{h}}$	$40\,\frac{\mathrm{km}}{\mathrm{h}}$
Cool down time	depending on acceleration capability	depending on acceleration capability	depending on acceleration capability	none
Passing criteria (simplified)	$\Delta\mu < 0.4$	$\Delta\mu < 0.3$	$\Delta\mu < 0.3$	$\Delta\mu < 0.3$

2.2.1 Changes in Requirements for Electrified Vehicles

Due to the increasing number of electrified vehicles, the proportion of vehicles that use regenerative braking to recover the vehicle's kinetic energy is also rising. However, the legislators and also OEMs do not seem to step down on performance requirements or performance tests, but the topic is heavily discussed on braking conferences and tier one suppliers. The use in real life driving shows that the temperatures of the brake discs differ greatly between electric vehicles and combustion vehicles. Hoffmann et al.[19] show this in a drive through the Taunus region with two vehicles of the same class but different drive types (electric and internal combustion engine). Due to the low frequency of application, the brake disc temperature of a vehicle with regenerative brakes is at an average temperature of 20 °C, while

[18] Marschner, H. et al.: Bremsentechnisches Versuchswesen (2017), p. 694.

[19] Hoffmann, J.; Wörsdörfer, K.-F.: End of oversizing: smart designing of brake systems for BEVs (2020), pp. 10–12.

the average temperature of an internal combustion vehicle on the same route is in the 70 – 80 °C range. The energy input of the combustion vehicle to the friction brakes is 10 times higher than that of the electric vehicle.

Nevertheless, it should be noted that a regenerative brake is mainly dependent on the battery condition (state of charge (SoC) and temperature [20]) as well as the temperatures of the motor windings and inverters, and is therefore not continuously available. For this reason, the braking torque from the regenerative brake is not considered in the performance tests of OEMs or magazines.

Possible starting points for an argumentation to mitigate the power tests, lie in the acceleration time of the vehicles. Depending on the design, a derating of the allowed propulsion power for the drive takes place during several successive acceleration maneuvers under high power. This means that after, for example, 3 or 4 acceleration maneuvers in a performance test, the following ones are carried out with lower acceleration rates in order to protect the electric motor. Thereby an increased cooling time for the wheel brake is generated during the acceleration phases and the final temperature of the components during such a test are affected.

2.3 Wheel Brake Concepts and Actuation Principles

The state of the art in service brakes, especially for passenger cars and commercial vehicles, is dominated by disc and drum brakes. These are friction brakes that have proven themselves for over 100 years in passenger cars. In addition to friction brakes, which are based on Coulomb friction, there are also other operating principles which generate a force against a vehicle's direction of movement:

- Aerodynamic brakes (parachute brake, adjustable spoiler)
- Lorentz forces (eddy current brakes, electrical machines)
- Rheological forces (electro- or magnetorheological brakes)
- Fluidic forces (fluid retarders)
- Hysteresis brakes

The mentioned braking principles are capable of a wear-free operation or nearly wear-free operation. Aerodynamic brakes are used in today's sports cars, for example in the Bugatti Veyron[21]. Due to the physical principle of air resistance the aerodynamic brake only works at high velocities.

[20] Robert Syrnik: Diss., Fahrdynamische Potenziale eines elektromotorischen Traktionsantriebs (2015), p. 22.

[21] Bugatti Automobiles S.A.S.: Bugatti Veyron Technik (2022).

The same also applies to eddy-current brakes, that are in use for trucks to relieve the friction brakes during longer descents[22]. Gay[23] tests a small prototype brake that has a diameter of 64 mm and generates a maximum torque of 2 Nm.

Wang et al.[24] present a magnetorheological brake, that resembles a multidisc brake filled with a rheological fluid, which generates a torque depending on the viscosity of the fluid. The viscosity is controllable via magnetic flux, that is generated using electromagnets. The specification of the brake shows a diameter of 492 mm and a width of 325 mm. The brake is able to achieve up to 1000 Nm but needs additional cooling because of otherwise unstable torque generation.

The fluid retarders, that are also used in trucks to dissipate potential energy during descents, can deliver high torques which are speed dependent. For braking to stop, the friction brakes have to be used.

For the purpose of this thesis the focus is set on friction brakes, as these have a particularly high gravimetric and volumetric power density and offer the functionality of braking into standstill. Figure 2-3 shows an overview of the actuation principles and design concepts of disc and drum brakes from the state of the art and state of research as well as their degree of maturity.

---

[22] Hans Wegmüller AG: Wirbelstrombremsen (2022).

[23] Gay, S.: Diss., Contactless Magnetic Brake (2005), p. 145.

[24] Wang, D. M. et al.: A novel high-torque magnetorheological brake with a water cooling method for heat dissipation (2013).

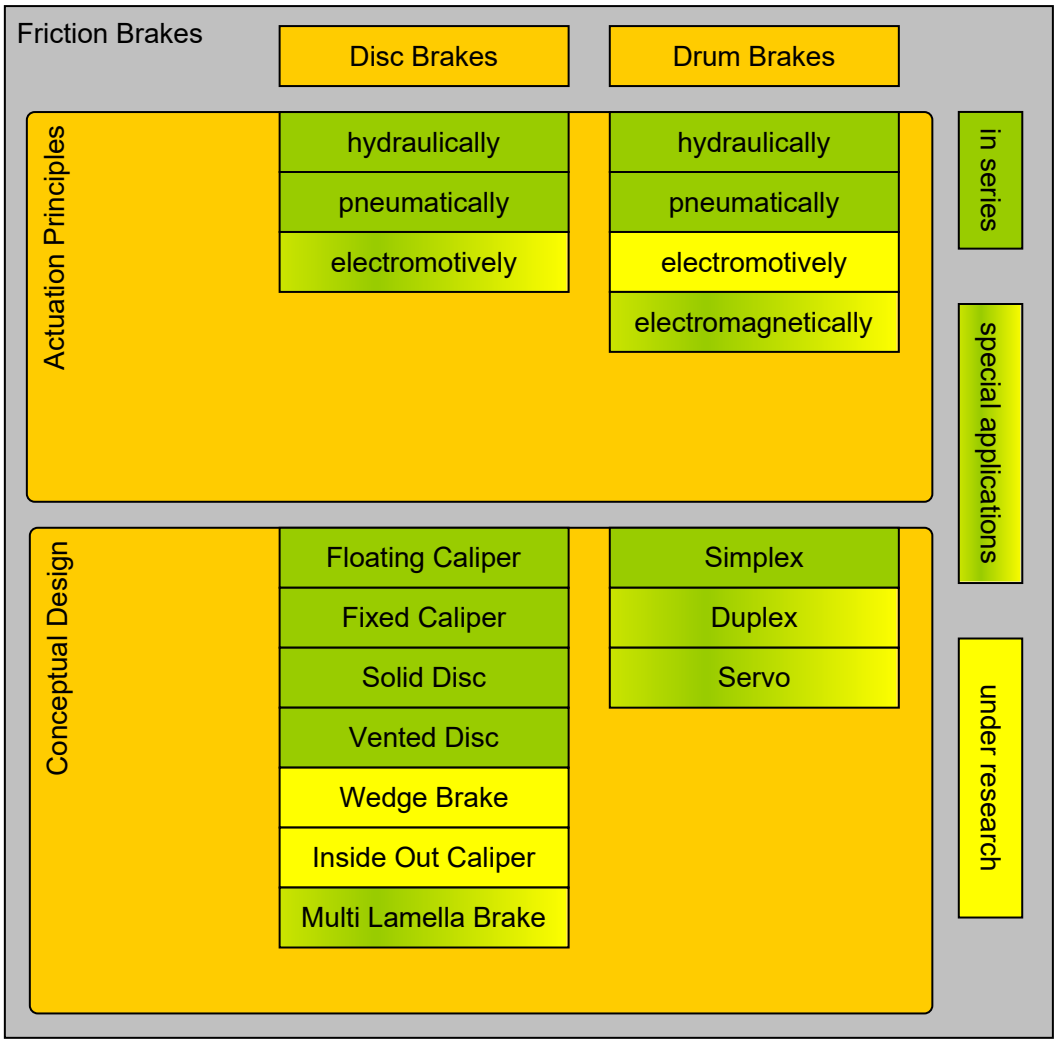

Figure 2-3: Known actuation principles and designs of friction brakes (sources: see descriptions below)

The disc and drum brakes of today's passenger cars are predominantly hydraulically actuated. The conventional hydraulic brake system consists of three functionally separable groups [25]:

1. Actuation
2. Modulation
3. Foundation Brake

Actuation includes the generation of pressure from the driver's pedal force and an auxiliary force (pedal, brake booster, tandem master cylinder). Modulation includes the functions for wheel-specific control of the brake pressure, primarily for stabilizing the vehicle (Anti-lock braking system (ABS) and electronic stability control (ESC)). The Foundation Brake

[25] Remfrey, J. et al.: Aufbau und Komponenten von Pkw-Bremsanlagen (2017), p. 126.

represents the conversion from brake pressure to brake torque at the wheel (disc brake or drum brake).

Figure 2-3 shows the level of maturity of various combinations of actuation concepts and designs for disc and drum brakes. While disc brakes can be found hydraulically and pneumatically actuated in passenger cars and commercial vehicles today, there are only small series for electric motor-actuated disc brakes, such as the Audi R8 e-tron[26] with electric motor-actuated brake calipers on the rear axle.

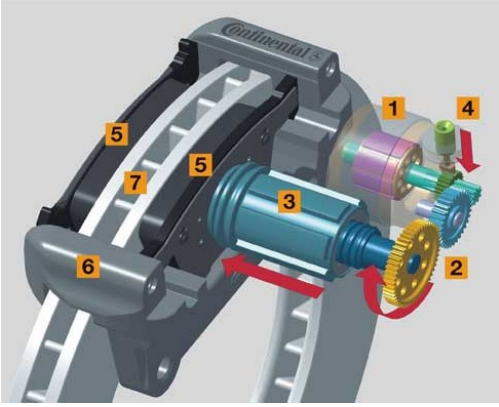

Figure 2-4: Concept and components of an electromechanical disc brake[27]; 1: electric motor, 2: gearing, 3: spindle, 4: parking brake lock, 5: brake pads, 6: caliper, 7: brake disc

However, market penetration has not been achieved for large series until today, since its presentation in 2015. In addition to the fixed and floating calipers with solid or ventilated discs available in series production, other concepts are currently being researched, including the wedge brake[28] with increased self-reinforcement shown in Figure 2-5.

[26] Diehl, P.: Schraubzwinge (2015).

[27] Autoteile Ralf Schmitz Handel GmbH: Was wurde eigentlich aus der Keilbremse? (2022).

[28] Semsch, M.: Entwurf einer elektromechanisch betätigten Radbremse mit Selbstverstärkung (2010).

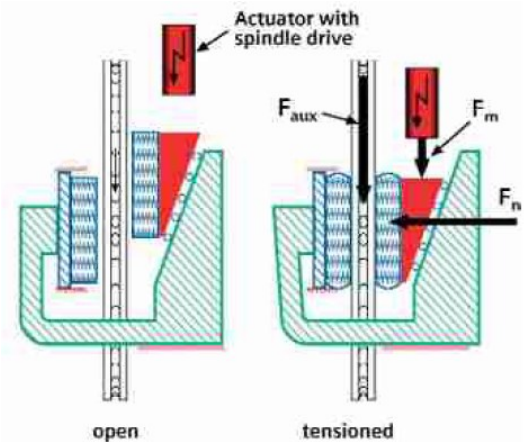

Figure 2-5: Operating principle of wedge brake in released and applied state[29]

The additional usage of the auxiliary force originating from the friction force itself amplifies the actuator force, thus reducing the force demand (Figure 2-6). The diagram also shows that there is a limit for the coefficient of friction at which the brake is locking without an actuation force, which should be prevented for safety reasons with a sufficient safety margin.

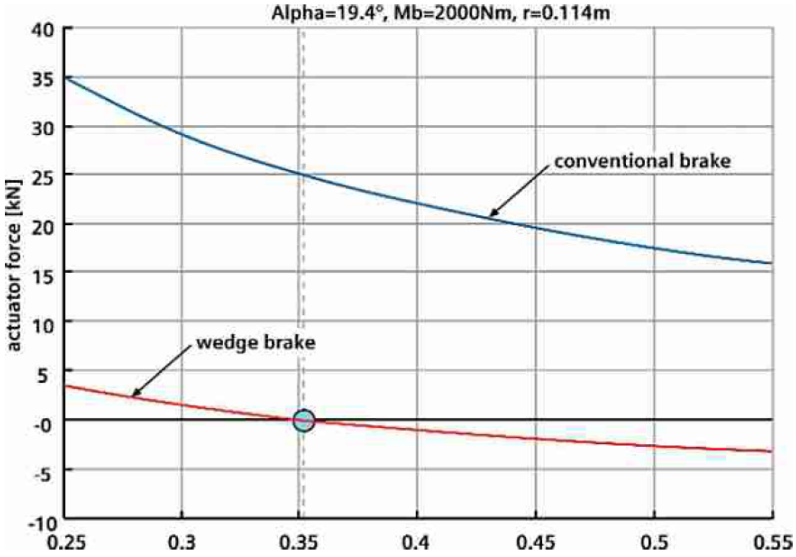

Figure 2-6: Actuator force demand of conventional disc brake and wedge brake for different friction coefficients between disc and pad[30]

For EVs Continental developed a brake concept with the goal to minimize corrosion. It is called the "New Wheel Concept", a floating caliper wrapped around an aluminum ring on the inside (Figure 2-7). Due to the bigger radius at which the friction force is working, lower actuation forces are needed than in conventional disc brakes.

[29] Gombert, B.; Gutenberg, P.: Die elektronische Keilbremse (2006).

[30] Gombert, B.; Gutenberg, P.: Die elektronische Keilbremse (2006), p. 906.

Figure 2-7: New wheel concept with aluminum brake disc and an inside out floating caliper[31]

Another development impulse for brake concepts for passenger cars originates from the agricultural and construction sector, which is the multi lamella brake[32]. It resembles a fully encapsulated brake with multiple, stacked discs that are running in a fluid. The encapsulation ensures a protection from corrosion and the fluid enhances the lifetime of the discs and padded discs between them.

Historically, there have also been hydraulic and pneumatic applications for the drum brake in series development. Whereas in earlier times less auxiliary power was available and variants with a high degree of self-reinforcement were installed (e.g. Duo Servo), today simplex drum brakes are used in modern passenger cars for reasons of comfort, e.g. in the electrically driven VW ID.3[33]. However, in 2021 the supplier Continental demonstrated the possibility of installing a Duo-Servo drum brake on the front axle of a vehicle [34] and demonstrated it at a press event. The series drum brakes of passenger cars are mainly hydraulically operated. Electromotively actuated drum brakes [35], which follow a brake-by-wire approach, are currently being researched (Figure 2-8).

[31] Continental AG: New Wheel Concept (2017).

[32] Knott Group: Bremsenübersicht (2022).

[33] Harloff, T.: Warum die Trommelbremse des ID.3 sinnvoll ist (2020).

[34] Huber, A.: Continental Trommelbremse für die Vorderachse (2021).

[35] Vey, C. et al.: Design of an Electromechanical Drum Brake (2019).

Figure 2-8: Electromotively actuated simplex drum brake with torque sensor

Electromagnetically actuated drum brakes are marketed for trailer applications by Warner Electric [36] and work according to the duo-servo principle and use a holding magnet that pulls on to the rotating drum and transmits the resulting frictional force via a lever as the actuation force to the drum brake shoes (Figure 2-9).

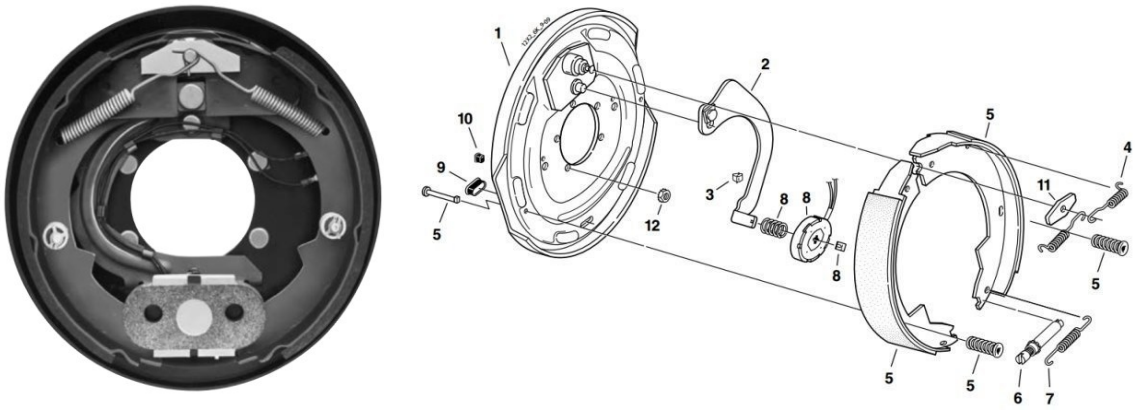

Figure 2-9: Electromagnetical Warner Brake concept (1: backplate, 2: actuation lever, 4: return springs, 5: brake shoes, 8: magnet assembly)[37]

2.3.1 Electromechanical Wheel Brake Concepts

The following chapter deals with the operation principles of wheel-specific, electromechanical wheel brakes (EMBs). Compared to hydraulically actuated wheel brakes, these offer the potential for the following advantages[38]:

[36] Warner Electric: Electric Wheel Brake (2014).

[37] Ray: Faulty Dexter Trailer Brake (2013).

[38] Reichenbach, M.: Wir sind auf dem besten Weg zur trockenen Bremse (2022), p. 24.

- Easier implementation of driver-independent operation and individual control (brake blending, assistance systems)
- Elimination of individual, distributed hydraulic modules and fluid (ESC, vacuum pump, brake booster)
- No necessity for filling and bleeding in final assembly by the manufacturer
- Modular, decentralized design, thus lower risk of total brake system failure (in case of redundant energy supply)

The basic structure of an EMB consists of the components shown in Figure 2-10.

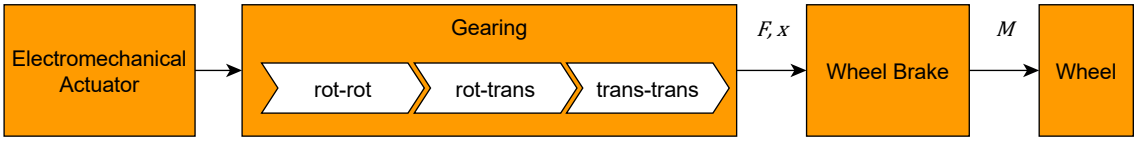

Figure 2-10: Block Diagram of electromechanical brakes based on Bill[39]

An EMB uses electrical energy that is converted into mechanical energy in an electromechanical actuator (e.g. an electric motor). The wheel brake itself has a force-displacement characteristic (like in Figure 2-11) that must be overcome with the help of the actuator.

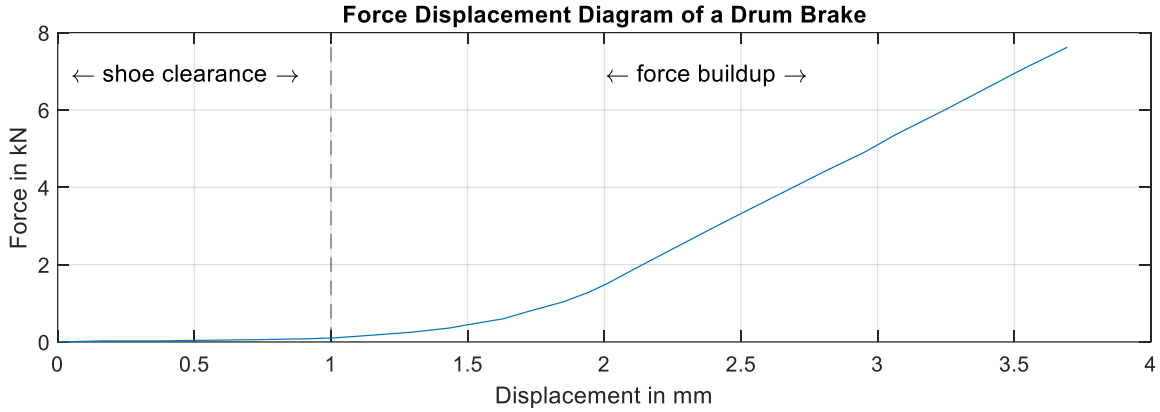

Figure 2-11: Example of a force displacement diagram of a wheel brake

The characteristic is divided into two basic sections:

1. Shoe clearance
2. Force buildup

Small forces are needed to move through the clearance, but a high force is needed to generate the axial force or clamping force for the required friction force. This clearly shows the conflict between dynamics and maximum force for the design of the actuator. Since the electric motors used have a low maximum torque for cost and weight reasons, a transmission in the form of gears is necessary to build up the maximum force at the brake. These consist of rot-rot converters (rotation to rotation, e.g. spur gears), rot-trans converters (rotation to

[39] Bill, K. H.: Grundlagen elektrisch betätigter Pkw-Bremssysteme (2017), p. 445.

translation, e.g. ball screws) and rarely also trans-trans converters (e.g. wedge gears). All electromechanical concepts mentioned in chapter 2.3 fit into this principle except for the Warner Brake.

The electromagnet in the Warner Brake concept also belongs to the group of electromechanical actuators, but its required displacement is not the actuating displacement of the drum brake itself, but the air gap to the inner, axial surface to the drum. The actual actuating displacement of the drum brake shoes is taken from the wheel rotation angle, which means that this plays a subordinated role in the design of the actuator itself (Figure 2-12).

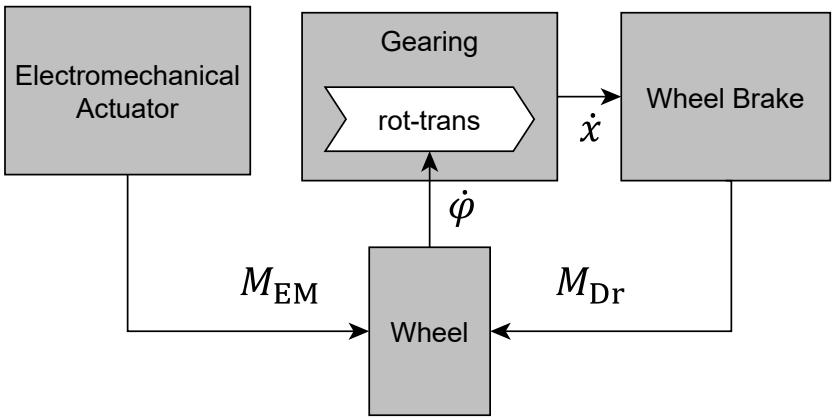

Figure 2-12: Block diagram of the electromagnetic Warner Brake

2.3.2 Electromagnetic Actuators

Electromagnets are part of the electromechanical actuators and are suitable for translatory and rotatory movements with limited paths or angles. They convert electrical energy into magnetic energy and ultimately into mechanical energy. The basic forms and components of an electromagnet are shown in Figure 2-13.

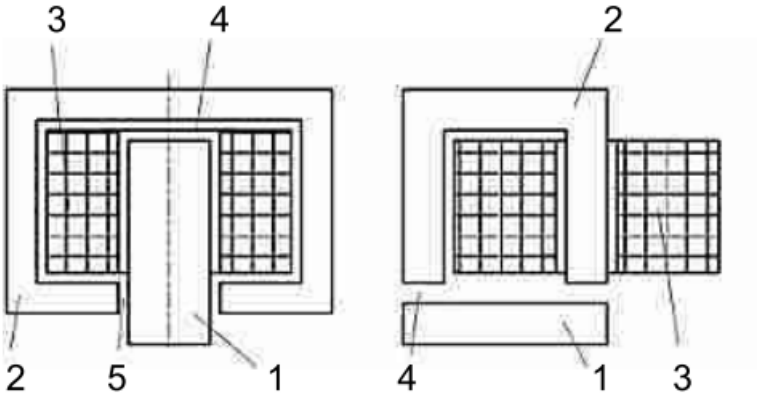

Figure 2-13: Basic forms of electromagnets (1: armature, 2: yoke, 3: winding, 4: air gap, 5: parasitic air gap)[40]

An electric voltage is applied to the coil of the magnet, causing a current to flow through the windings. This creates a magnetic field around the coil, which can be described by the magnetic field strength H and depends on the number of windings and the current:

$$\oint_l H\mathrm{d}l = N \cdot I = \Theta \tag{2-1}$$

The quantity l describes the path of the field lines that run through the armature, the yoke and the air gaps of the magnet. The magnetic flux density B is formed as a function of the so-called permeability, which depends on the material through which the flux is flowing:

$$B = \mu_\mathrm{m} H \tag{2-2}$$

For the most commonly used ferrous materials in the magnetic circuit, the permeability of the material depends on the magnetic field strength and is non-linear. It represents the gradient in the diagram in Figure 2-14 for different materials.

[40] Kallenbach, E. et al.: Elektromagnete (2018), p. 11.

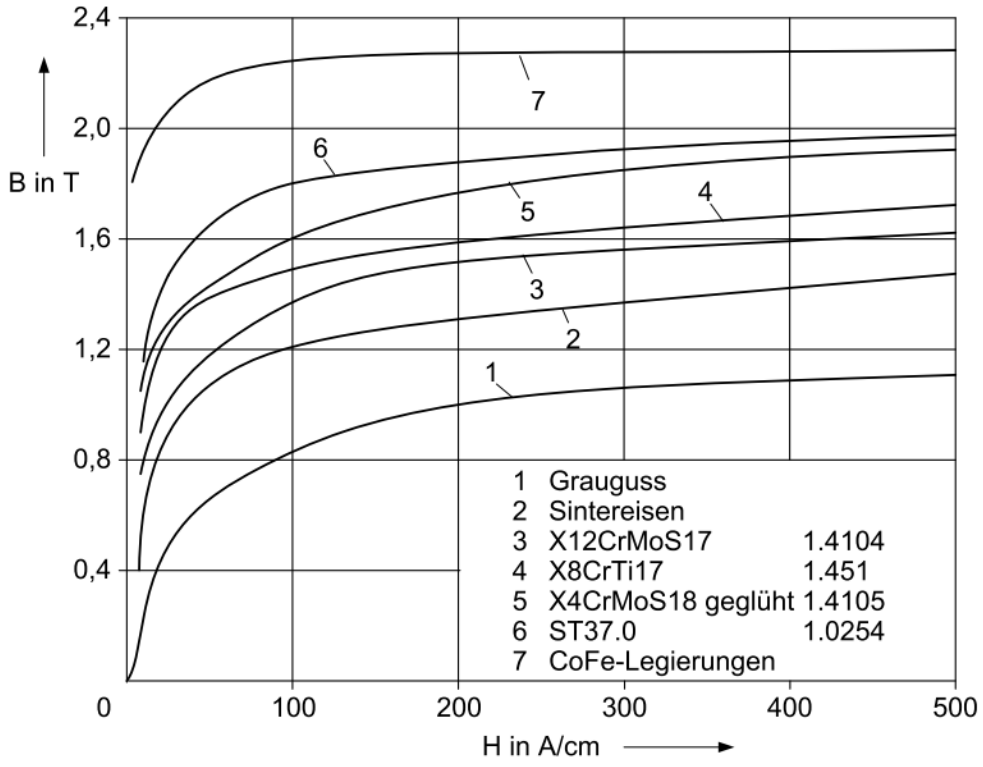

Figure 2-14: B-H-curves for different materials[41] (1: grey cast iron, 2: sintered iron, 6: construction steel, 7: cobalt iron alloys)

In areas of higher magnetic field strength, the flux density reaches saturation. The remaining gradient of the flux density then equals the permeability of the vacuum:

$$\mu_0 = 4\pi \cdot 10^{-7} \frac{\mathrm{Vs}}{\mathrm{Am}} \tag{2-3}$$

The materials not only differ in their permeability but also show different hystereses in the relation between the field strength H and the flux density B, like shown in Figure 2-15. For actuators this effect means, that after an actuation with high field strength and a subsequent release, the material stays magnetized with a certain flux density and so-called remanence forces are still acting on the actuator's armature and yoke. The cause for those forces is the so-called remanent flux density, which can be found in the diagram for $H = 0$.

[41] Kallenbach, E. et al.: Elektromagnete (2018), p. 46.

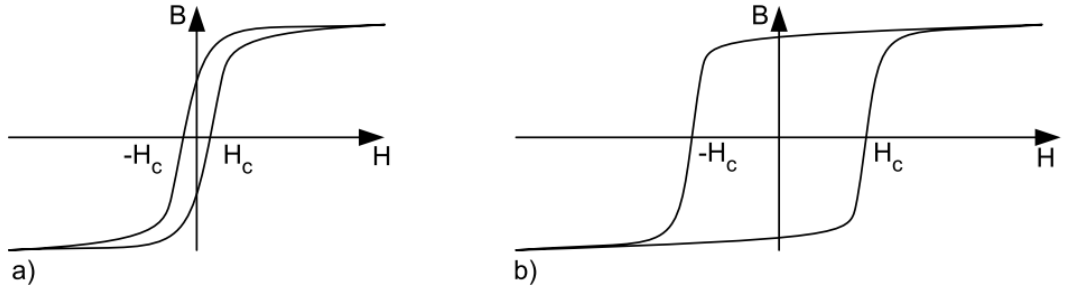

Figure 2-15: Hystereses curves for a soft magnetic material (a) and a hard magnetic material (b)[42]

The magnetic actuator forces that are created in the air gap at the interface between the yoke and the armature can be simplified to Maxwell's traction force formula[43] with the assumption of a perpendicular flux at a density of B through the surface A:

$$F_{\mathrm{mag}} = \frac{B^2 A}{2\mu_0} \tag{2-4}$$

Depending on the design of the magnet, different force-air gap characteristics can be achieved. Examples are shown in Figure 2-16.

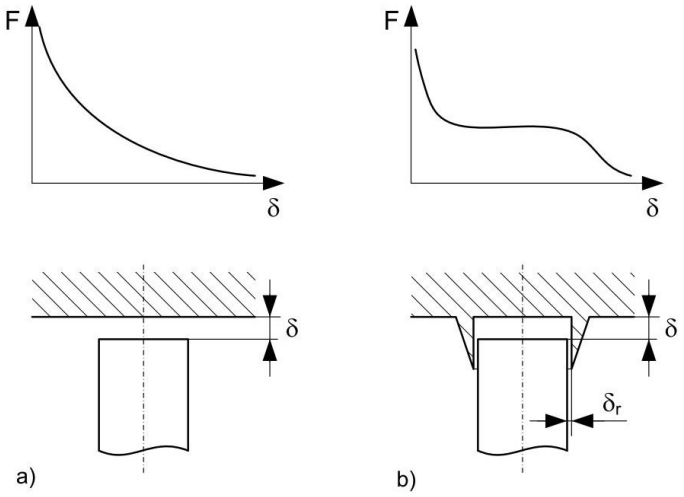

Figure 2-16: Force - air gap diagrams for different yoke designs[44]

Form a) is particularly suitable for large forces with small air gaps, such as those used for holding magnets on cranes. The force is strongly dependent on the current air gap. The range in which the magnet is actually used is in the smallest air gap possible. With form b), a section of the characteristic curve is independent of the air gap and thus forms a favorable working range in which the magnetic force only depends on the current and not on its

[42] Kallenbach, E. et al.: Elektromagnete (2018), p. 37.

[43] Kallenbach, E. et al.: Elektromagnete (2018), p. 74.

[44] Kallenbach, E. et al.: Elektromagnete (2018), p. 85.

position/air gap. The range of small air gaps is avoided, only the range with a constant force is used.

In this thesis, a magnet with the design shown in a) is referred to as a holding magnet and in b) as a solenoid.

2.3.3 Electromagnetically Actuated Safety Brakes for Industrial Applications

Magnetically actuated brakes are commonly used for industrial applications in the form of so-called safety brakes, which are normally closed brakes. They are used in areas where a moving shaft needs to be stopped in case of an energy outage, for example in elevators, escalators and wind turbines. Figure 2-17 shows the basic principle behind the magnetically released safety brakes. When the magnet is energized, it pulls the anchor disc off the rotating disc, which is mounted on the shaft. The magnet works against an application spring. When the magnet is demagnetized, the application spring pushes the anchor disc against the rotating disc. Usually the anchor disc is coated with friction material to achieve a high friction coefficient.

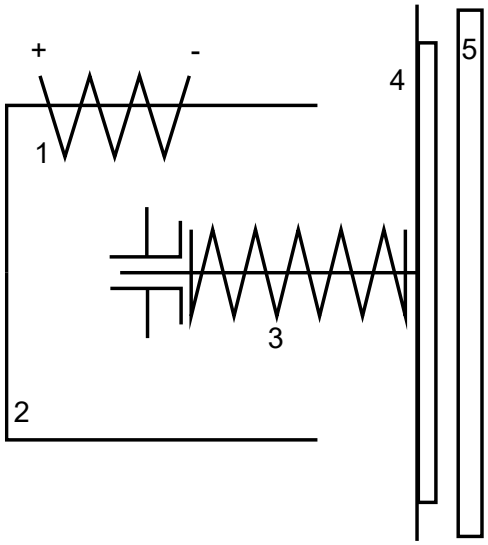

Figure 2-17: Operating principle of normally closed industrial brakes (1: coil, 2: yoke, 3: application spring, 4: friction disc, 5: rotating disc)

Magnetic safety brakes are not suitable for class M1 vehicles of UNECE, as they work according to the normally close principle. For those vehicles the UNECE[45] requires the service brakes to be released in the case of a power outage or the absence of application forces. An application against the driver's intention can lead to vehicle instability and is therefore forbidden.

[45] UN: ECE R13-H (2018), p. 14.

3 Requirements on Wheel Brakes of Autonomous Shuttles

This chapter addresses the first research question:

What are the requirements for wheel brakes of highly automated, electrified shuttles?

The method and findings were already published by the author in a research paper in 2021[46].

3.1 Methodical approach

While the requirements for wheel brakes of passenger cars today are defined by numerous specifications and tests, for new vehicle concepts that drive electrically and automated a holistic view of the installed hardware, the vehicle functions and the application purpose is necessary to derive the requirements. Due to the similarity of the autonomous shuttle to the passenger car in terms of performance class and permissible total mass, the requirements set for passenger cars are checked for their relevance to the new vehicle concept. For this purpose, the self-developed method in Figure 3-1 is applied. The methodical approach is based on the definition of use-cases for the vehicle, from which the so-called edge cases are subsequently derived. The edge cases are the use cases that place the highest demands on the vehicle hardware. In order to define the use cases, the following influencing factors are determined in advance:

1. Vehicle hardware
2. Operational Design Domain (ODD)
3. Vehicle functions
4. Economic goals
5. Ecologic goals
6. Stakeholders

In order to enhance the coverage of the requirements definition process, specifications for current passenger cars are collected and their underlying edge cases are extracted. These are then examined for their relevance based on the use cases of the autonomous shuttle. The collected, relevant edge cases are formulated as requirements for the vehicle's braking system and transformed down to the corresponding requirements for the wheel brake.

[46] Guckes, L. et al.: Requirements and Test Cycles for Brake Systems of Autonomous Vehicle Concepts on the Example of an Autonomous Shuttle (2021).

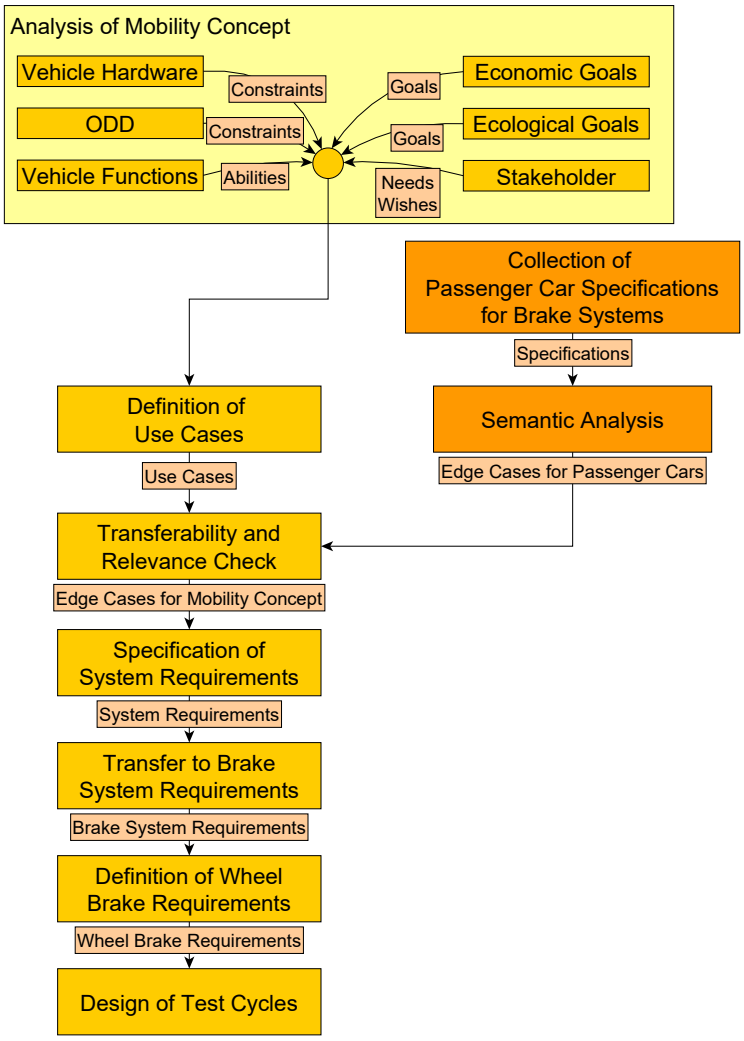

Figure 3-1: Methodology for requirements derivation

The feasibility of this method is demonstrated in the following using an example vehicle, an autonomous shuttle from the company Easy Mile.

3.2 Analysis of Mobility Concept

3.2.1 Vehicle Hardware

The EZ10 from the Easy Mile company is used as an example vehicle for an autonomous shuttle. The vehicle data for all driving dynamics calculations are shown in Table 3-1. The vehicle is driven by an electric motor on the rear axle and has a preferred direction of travel with front axle steering.

Table 3-1: EZ10 vehicle data

Parameter	Value	Parameter	Value
Unladen mass m_{ul}	1700 kg	Brake force distribution FA/RA	2/1
Admissible vehicle weight m_{l}	2700 kg	Position Motor	RA
wheelbase l	2.8 m	Continuous traction power P_{con}	60 kW
Height center of gravity h_{CoG} (unladen)	0.58 m	Maximum regenerative power $P_{\mathrm{reg,max}}$	30 kW
Longitudinal position center of gravity l_{f} (unladen)	1.4 m		

3.2.2 Operational Design Domain (ODD)

The Operational Design Domain (ODD) defines the limitations of an automated system and the circumstances under which it is specified as functional. In SAE J3016[47] the ODD is defined as follows:

"Operating conditions under which a given driving automation system or feature thereof is specifically designed to function, including, but not limited to, environmental, geographical, and time-of-day restrictions, and/or the requisite presence or absence of certain traffic or roadway characteristics."

Compared to a conventional car, this means that the automated vehicle is limited in terms of where it can be used, for example, that certain routes cannot be driven on the basis of their parameters such as road gradient. For the example vehicle, this means that it can be limited to an urban environment, which in turn restricts the maximum speed and expected differences in altitude on the route.

3.2.3 Vehicle Functions

For the definition of the requirements, as visualized in the methodical approach, the vehicle functions are described, that are assumed to be implemented when the set development goal is achieved. These include:

1. The autonomous shuttle drives automated at level 4.

[47] SAE International: Taxonomy and Definitions for Terms Related to Driving Automation Systems for On-Road Motor Vehicles (2021).

2. The electric driveline is capable of regenerative braking, provided the conditions of the motor and the battery allow it. The electric motor is also used for braking to stop, even if electric energy is required for this.
3. The route planning is automated and uses available map data and traffic information.
4. The vehicle automatically moves to a charging point if the battery charge level falls below a threshold value and automatically charges up to a set SoC value.

3.2.4 Economic Goals

The economic goals associated with the operation of autonomous shuttles originate primarily from the business model of fleet operators who offer a mobility on demand service. For them, a profitable operation of the fleet is desired, which means that in addition to the acquisition costs for the vehicles, the costs for operation and maintenance must also be as low as possible. Due to the automation of the driving functions, no operating staff is required in the vehicle for the transport task.

3.2.5 Ecologic Goals

The ecologic goals behind the vehicle concepts of the autonomous shuttles are based on the wish to fulfil a transport task that is as sustainable as possible, but more flexible than a regular service with buses. This consequently includes emission issues such as CO_2 emissions (reduction of climate-damaging gases) but also fine dust particles (to reduce health damage to human organs). The argument of a sustainable mode of transport can also be used to gain an economic advantage in the marketing strategy of the fleet operator.

3.2.6 Stakeholders and Use Cases

The stakeholders for an autonomous shuttle are all persons or institutions that in some way interact with the vehicle or have an influence on its usage. By identifying the stakeholders, the different needs and desires of these become apparent and different perspectives are gained for requirements identification. The stakeholders include:

1. Passengers (P)
2. Road Users (RU)
3. Legislators (L)
4. Fleet Manager (FM)
5. Original Equipment Manufacturer (OEM)

By looking at the vehicle concept from the perspective of the respective stakeholders, their needs and wishes can be identified. The result is documented in Table 3-2. For structuring purposes, the resulting use cases were divided into the groups of transport, safety and business.

Table 3-2: Use cases for the stakeholders of the autonomous shuttle

Group	#	Description	Stakeholder
Transport	A1	call vehicle to point a	P
	A2	set desired target point b	P
	A3	be transported with a low ecologic footprint accelerate with low emissions decelerate with low emissions	P, L
	A4	be transported comfortably be accelerated comfortably be decelerated comfortably be jerked comfortably be protected from noise and vibrations	P
	A5	be transported quickly	P, RU
	A6	board vehicle ergonomically board vehicle with walking aids or wheel chairs board vehicle with low physical effort board vehicle with additional luggage	P
	A7	be entertained	P
Safety	B1	be transported injury free be seated safely be supported if standing	P, L
	B2	drive collision free control vehicle remotely control vehicle locally decelerate vehicle quickly	P, FM, RU
Business	C1	transport passengers in defined region without need of driver	FM
	C2	profit from service	FM, OEM
	C3	economic maintenance of fleet	FM
	C4	charging of vehicles charge vehicles in short time charge vehicles effectively	FM

A passenger's transport demand begins with the ordering of a vehicle via app to a starting point and the setting of the desired destination point. The passenger wishes for a safe, sustainable, comfortable and fast transport to the destination with the possibility to attend to other diversions in the meantime (use case A7).

3.3 Transferability and Relevance of Passenger Car Requirements

In this chapter, the requirements for modern wheel brakes of passenger cars are examined and discussed in terms of their transferability to the autonomous shuttle.

3.3.1 Performance Requirements

The range of requirements for the performance of the wheel brake primarily includes the topics of thermal performance, stopping distance, dynamics and, especially since the use of electric drive trains, also the residual braking torques.

The brake performance tests described in the state of the art (Table 2-2) and their underlying scenarios will be examined in the following with regard to their transferability on the basis of the use cases of the autonomous shuttle (Figure 3-2).

The Grossglockner test is not relevant for the autonomous shuttle in its regional definition, as the shuttle has an ODD limited to a certain area of operation and thus no such hill descent will occur. Still relevant, however, is the abstract edge case behind the GG test that the vehicle must be able to dissipate a certain potential energy determined by the ODD.

The AMS test is used to compare vehicles and to quantify the thermal braking behavior for the buyers of passenger cars. For autonomous shuttles, however, it is not relevant for several reasons, since

- the ODD limits the vehicle to a maximum velocity allowed in a city
- the acceleration of the shuttle will be limited for comfort reasons
- no 10 repetitions of the AMS test's highly dynamic driving maneuvers shall be performed in real road traffic with a shuttle, on the one hand for reasons of comfort and on the other hand to protect the electric drive train from thermal overload

However, a number of full decelerations with intermediate acceleration times that the vehicle has to undergo remain relevant from the AMS test. These acceleration times must not be based on the maximum power of the drive, but on the maximum comfort acceleration defined by the driving function.

The same applies to the HFT, which requires a velocity above the ODD of the shuttle and additionally is based on a motorway scenario, which is also excluded in the ODD of the shuttle. The edge case, which resembles a selected worst-case scenario for the vehicle's everyday task, remains relevant.

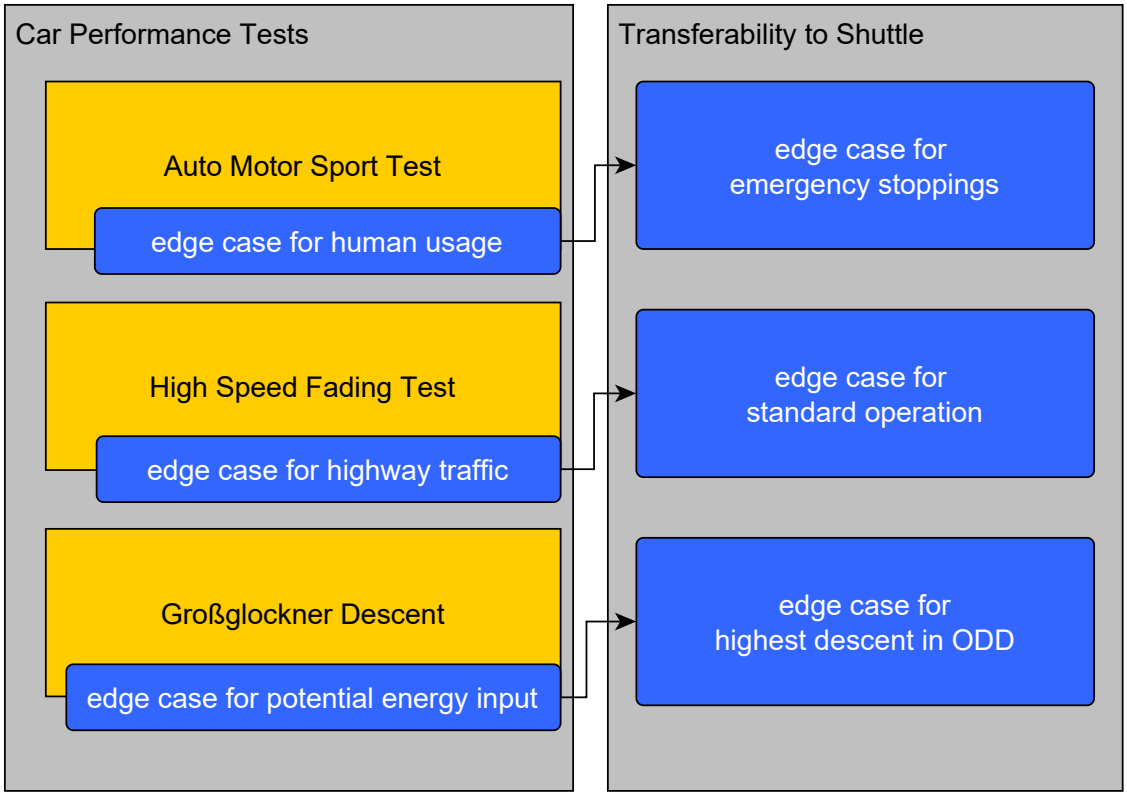

Figure 3-2: Transferability of car performance tests to the autonomous shuttle

To avoid collisions, full deceleration with full usage of the friction coefficient between road and tire is still required. The necessity of vehicle stabilization also applies in order to be able to maintain the controllability of the vehicle. Consequently, the wheel brake must achieve the dynamics necessary for ABS control for the change of different torque levels.

3.3.2 Comfort Requirements

In terms of comfort, there are two fundamental changes compared to the passenger car based on use case C1:

1. Pedal feel
2. Noise Vibration Harshness (NVH)

The development goals in the area of comfort for the actuation of the brake become completely irrelevant due to the automated driving function. Whereas in a passenger car, the pedal actuation forces and the force-displacement characteristic of the actuation determine the comfort for pedal feel, in an autonomous shuttle the actuation is completely automated. The usual development effort for the human-machine interface to the brake is therefore eliminated or reduced to an emergency stop interface.

For comfortable passenger transport, a certain range of comfortable deceleration and jerk must be maintained by the vehicle (see use case A4 in Table 3-2). Bae et al. put this range at

a deceleration of up to 1.5 m/s^2 and a jerk of up to 0.9 m/s^3 and regard these as limit values for comfortable longitudinal control of an automated vehicle[48]. This range can be covered by the regenerative brake, provided there is sufficient friction between the road surface and the tires.

If the electric drive is used for comfort braking into standstill, the requirements for the brake in the shuttle regarding NVH behavior do not apply to this speed range. In the area of comfortable passenger transport, the friction brake is thus not in use and the typical noises do not occur, such as squeal, groan or howl[49] (use case A4).

3.3.3 Lifetime Requirements

There are also changes in brake lifetime requirements based on the use cases compared to the passenger car. Above all, the administration and maintenance of the vehicles by a fleet manager reveals the necessity of an economic consideration (use cases C2, C3).

Modern components for passenger cars are usually designed and tested for a lifetime mileage of 300,000 km. An application similar to the shuttle is a city bus and the requirements on the components for its operation offer indications for the shuttle. Research on the mileage requirements of public buses gives a value of 1.2 million km[50]. The autonomous shuttle will presumably be placed between a regular bus and a passenger car in terms of mileage requirements. However, the mentioned mileage does not apply to the usual wear parts, such as brake pads.

3.3.4 Emission Requirements

For an ecologic service (use case A3) the emissions of the vehicle should be as low as possible. This applies to the drivetrain, tires and brake system and other systems which emit hazardous particles or gases. Currently the UNECE[51] is developing a method to measure brake emissions which forms the basis for future vehicle emission regulations.

---

[48] Bae, I. et al.: Toward a Comfortable Driving Experience for a Self-Driving Shuttle Bus (2019), p. 2.

[49] Marschner, H. et al.: Schwingungen und Geräusche (2017), p. 630.

[50] Oberhavel Verkehrsgesellschaft mbH: Lastenheft (2019), p. 1.

[51] UNECE: UNECE to develop global methodology to measure particle emissions from vehicles' braking systems (2021).

3.4 Requirements for the Brake System of an autonomous Shuttle

The following chapter summarizes the findings from the requirements definition procedure for some basic requirements for the autonomous shuttle. In particular, the deceleration capabilities, the dynamics for applying and releasing the brake and the cycles for thermal performance are examined.

3.4.1 Longitudinal Dynamics Requirements

Table 3-3 shows the requirements regarding the longitudinal dynamics of the vehicle. The maximum acceleration in operation is conservatively rounded up to 2 m/s² from the comfortable acceleration mentioned in the chapter 3.3.2. For the maximum permissible deceleration, the question of avoiding injuries arises for the transport of standing passengers. It is debatable whether the maximum deceleration shall be set below the friction coefficient limit in order to protect the passengers from injury. However, nowadays strong decelerations are also applied in buses at high values, even though standing passengers can be injured in the process. The primary objective of such a maneuver is collision avoidance. This goal is therefore also assumed to be valid for the autonomous shuttle. Consequently, the braking system must be able to achieve a deceleration of $1g$ at high friction coefficients. The regenerative braking system cannot be included in the collision avoidance task, as its availability depends on the State of Charge (SoC) and the temperatures of its components [52].

Table 3-3: Longitudinal dynamics requirements for the brake system

Description	Parameter	Value	Based on
Maximum acceleration	$a_{\mathrm{p,max}}$	$2\ \mathrm{m/s^2}$	passenger comfort
Maximum deceleration	$z_{\max} = \frac{-a_{\max}}{g}$	1	collision avoidance
Maximum velocity	$v_{\max}$	$20\ \mathrm{m/s}$	Area of operation
Maximum gradient	$q_{\max}$	0.2	Area of operation
Maximum jerk	$j_{\max}$	$0.9\ \mathrm{m/s^3}$	Passenger comfort

[52] Robert Syrnik: Diss., Fahrdynamische Potenziale eines elektromotorischen Traktionsantriebs (2015), p. 22.

3.4.2 Performance Requirements

The requirements for evaluating the performance of the system are determined in the following with a focus on thermal performance. In Figure 3-2 the extracted edge cases are derived from the car tests. Based on these, three cycles are developed that transfer these edge cases to the autonomous shuttle:

1. Standard Transport Operation Test (STO)
2. City Descent (CD)
3. Emergency Stop (ES)

The STO maps the classic transport task of the shuttle and follows the determined edge case of the HFT in the passenger car. This includes acceleration to maximum velocity after the passengers have boarded and comfortable deceleration until the vehicle comes to a stop to allow the passengers to disembark. In order to develop the test on the basis of the edge case, the maximum permissible acceleration is used for the acceleration phase, and is lower than the maximum acceleration available due to the vehicle's drive power. For deceleration, the same deceleration level is used and an exit duration of 5 s is anticipated. Ten repetitions are scheduled for the test. The energy thus entering the friction brake causes the friction surface to heat up and is accompanied by a drop in the coefficient of friction. The pass criterion for an automated vehicle cannot be set on the basis of the necessary foot force, but on the deceleration that the vehicle can still perform with a hot brake. The pass criterion after the heating cycle is therefore a full deceleration from $v_{\max}$. The actuator has to provide the necessary displacement and force to reach the full deceleration.

The City Descent represents the edge case of the Grossglockner test from the passenger car. It is therefore defined by the highest possible height difference within the ODD of the vehicle. In an urban environment, the city of San Francisco can serve as an edge case with its "Cable Car Route" on California Street as a worst case scenario. The elevation profile of the route can be found in Figure 3-3. Due to the steepness, however, the maximum velocity of $v = 10\ \mathrm{m/s}$ is set for such a steep route. The route has a length of 1.6 km and an altitude difference of approx. 91 m [53].

[53] Copernicus: California Street (2020).

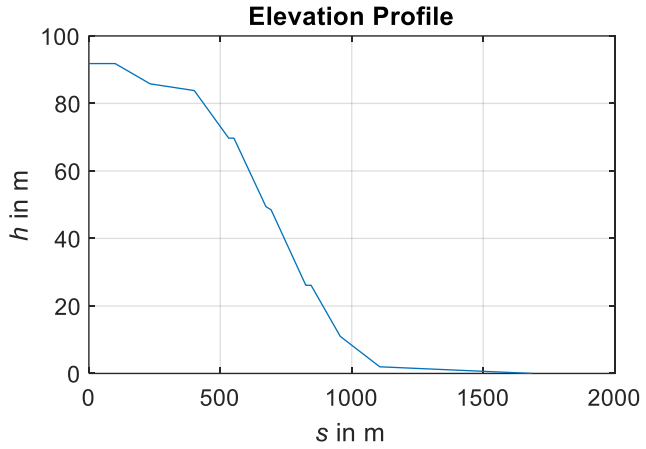

Figure 3-3: Elevation profile of the cable car route in San Francisco

Again, the passing criterion is a subsequent full deceleration that must be realized by the actuation of the brake after heating up.

Based on the edge case derived from the AMS test, the Emergency Stop Test contains the full decelerations still required for collision avoidance. For the passengers of the autonomous shuttle, full deceleration means a dangerous situation with a high risk of injury, which is why it should be avoided in advance by all means by the vehicle's control system. For this reason, a repetition number of ten brakings as in the AMS test is not feasible. Already after one full deceleration, the passengers need a short time period of at least 10 s until they have taken their place again and a continuation of the journey is possible. Therefore, two repetitions of emergency brakings are assumed and one subsequent full deceleration like in the other tests after the heating cycle that the actuation still has to reach.

Table 3-4: Test cycles for the autonomous shuttle

	STO	**CD**	**ES**
Load	laden	laden	laden
Number of brakings	10	1 (for 1.6 km)	2
Deceleration	$a = -2\ \frac{\mathrm{m}}{\mathrm{s}^2}$	Based on $v = \text{const}$ and $q(s)$	$a = -10\ \frac{\mathrm{m}}{\mathrm{s}^2}$
Velocity targets	$0 \rightarrow v_{\max} \rightarrow 0$	$v = 10 \frac{\mathrm{m}}{\mathrm{s}}$	$0 \rightarrow v_{\max} \rightarrow 0$
Cool down time	acceleration time at $a = \min(2\ \frac{\mathrm{m}}{\mathrm{s}^2}, a(P_{\max}))$	0	10 s + acceleration time at $a = \min(2\ \frac{\mathrm{m}}{\mathrm{s}^2}, a(P_{\max}))$
Passing criteria	Actuation capable of one consecutive emergency braking to stop from $v_{\max}$ with $a = -10\ \frac{\mathrm{m}}{\mathrm{s}^2}$ (given a sufficient tire to road friction coefficient and flat road)		

To illustrate the developed cycles, the vehicle is modelled using the vehicle data from chapter 3.2.1 and the simulation tool IPG Car Maker 8 and Matlab Simulink. The cycles are driven virtually.

The brake force distribution (BFD) is calculated as ideal depending on the current deceleration. The required braking forces are calculated according to Pickenhahn et al.[54]:

$$z = \frac{a}{g} \tag{3-1}$$

$$F_{\mathrm{B,f}} = F_{\mathrm{G}} \cdot \mu \cdot (1 - \Psi + \mathrm{z} \cdot \chi) \tag{3-2}$$

$$F_{\mathrm{B,r}} = F_{\mathrm{G}} \cdot \mu \cdot (\Psi - \mathrm{z} \cdot \chi) \tag{3-3}$$

$$\text{with } \Psi = \frac{l_{\mathrm{f}}}{l_{\mathrm{WB}}} \tag{3-4}$$

$$\text{and } \chi = \frac{h_{\mathrm{CoG}}}{l_{\mathrm{WB}}} \tag{3-5}$$

Under the assumption of a sufficient friction coefficient $\mu = z$ for a dry asphalt road equal to all wheels, the brake force distribution of the vehicle diagram is generated (Figure 3-4). The lines of constant deceleration for an emergency braking with $z = 1$ and a comfortable braking for $z = 0.2$ are shown.

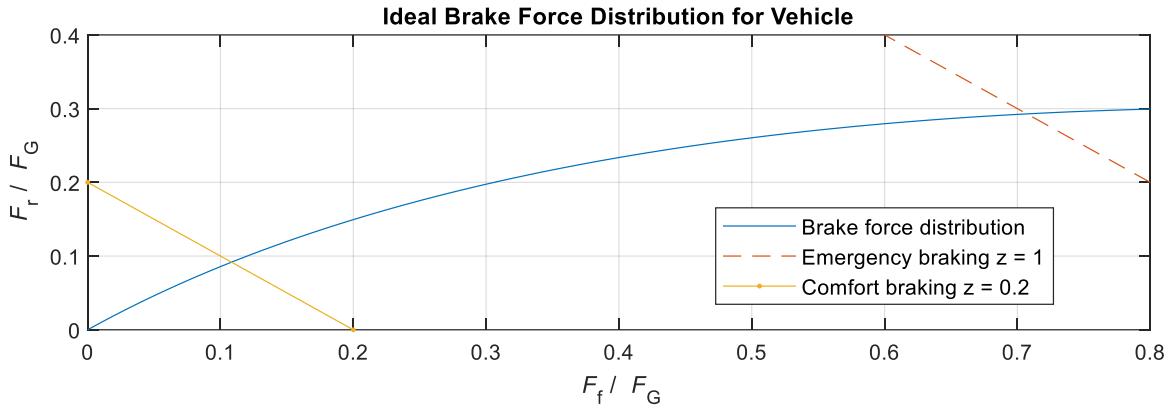

Figure 3-4: Ideal brake force distribution of example shuttle

With the vehicle model the proposed test cycles are virtually tested with the IPG driver. For the regenerative brake the usual control algorithm is used, which is based on the daisy chain control[55] which prioritizes the regenerative brake until the maximum available regenerative brake torque is reached. After that, the friction brakes are applied to add up to the total torque demand.

[54] Pickenhahn, J.; Straub, T.: Auslegung und Simulation von Pkw-Bremsanlagen (2017), pp. 95–96.

[55] Buffington, J.; Enns, D.: Daisy chain control allocation, p. 1537.

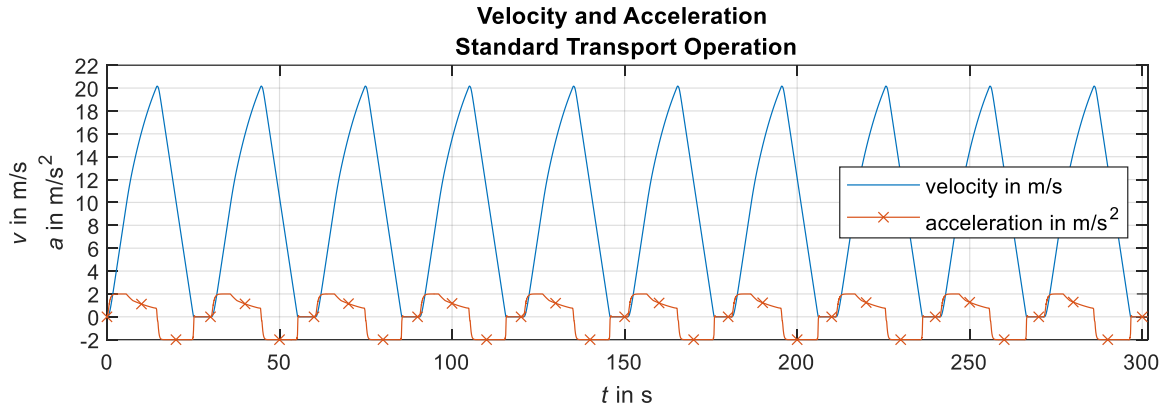

Figure 3-5: Velocity and acceleration during the Standard Transport Operation Test

In the diagram of Figure 3-5 the ten decelerations of the STO with 2 $\mathrm{m/s^2}$ and the accelerations including the power limit of the drive are shown.

The ES test shows the highest deceleration and thus the highest torques for the brake. For the wheel brake of the front axle these are $M_{\mathrm{B,f}} = 2320\ \mathrm{Nm}$ and for the rear axle brake $M_{\mathrm{B,r}} = 1180\ \mathrm{Nm}$. The course of speed and acceleration can be found in Figure 3-6.

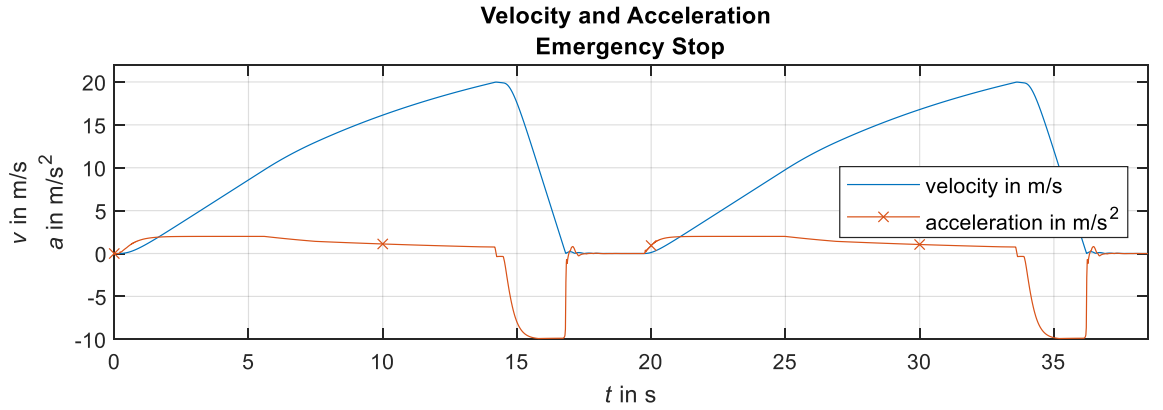

Figure 3-6: Velocity and acceleration profile for Emergency Stop Test

No velocity profile is plotted for the City Descent, as the velocity is kept constant during the test. The torques that occur are $M_{\mathrm{B,f}} = 290\ \mathrm{Nm}$ and $M_{\mathrm{B,r}} = 260\ \mathrm{Nm}$ at a maximum road gradient of $q_{\max} = 0.17$.

With the torques and velocities, the required friction energy for the different cycles can be calculated. For comparison, the required energy of an AMS test at 100 km/h top speed is shown in Figure 3-7. In order to additionally demonstrate the influence of the regenerative brake when it is available, the developed cycles are shown with 100 % SoC (without regenerative brake) and 50 % SoC (full availability of the regenerative brake) each.

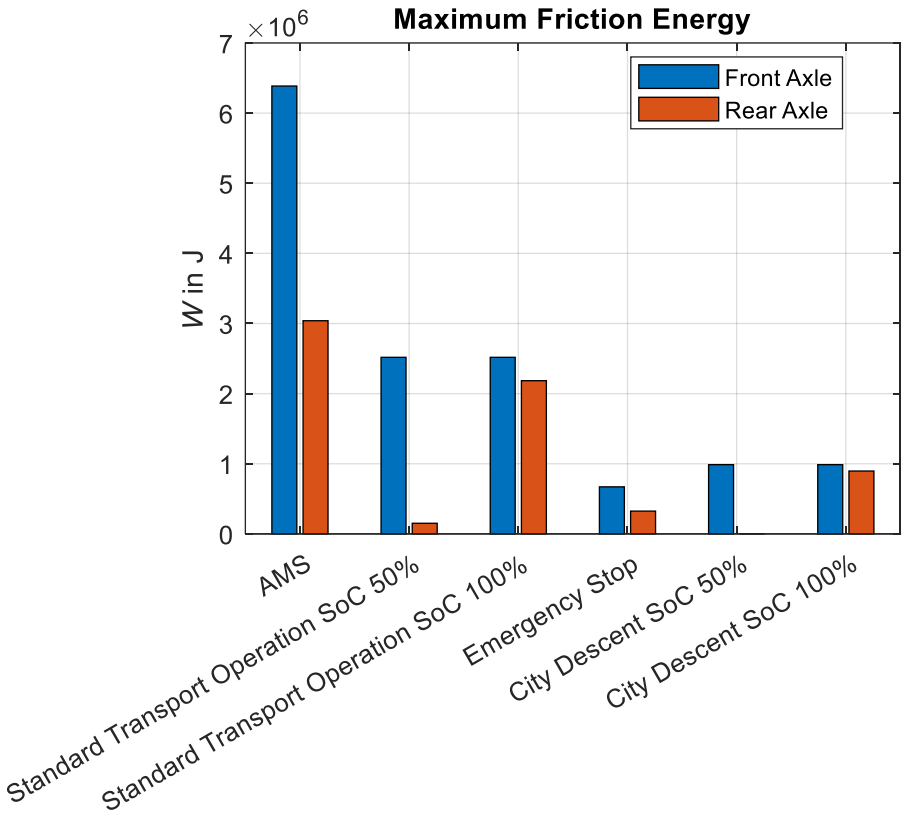

Figure 3-7: Friction energy demand of developed cycles

Considering maximum torques there is no change in the specifications between an autonomous shuttle and a car, as the highest required decelerations have not changed (see use case B1 and B2).

The most demanding cycle (excluding the AMS shown for comparison) regarding friction energy dissipation is the STO test, with $W_{\mathrm{B,f}} = 2.5$ MJ on the front axle and $W_{\mathrm{B,r}} = 2.2$ MJ at the rear axle at 100 % SoC. Table 3-5 gives an overview over the relative differences in energy dissipation demand for the test cycles with different availabilities of the regenerative brake.

Table 3-5: Comparison of energy dissipation demand for different cycles and SoCs

AMS $W_{\mathrm{B,f}} = 6.4$ MJ $W_{\mathrm{B,r}} = 3$ MJ	**STO** (no reg) $W_{\mathrm{B,f}} = 2.5$ MJ $W_{\mathrm{B,r}} = 2.2$ MJ	**Relative difference** $\Delta W_{\mathrm{f}} = 61$ % $\Delta W_{\mathrm{r}} = 27$ %
STO (no reg) $W_{\mathrm{B,r}} = 2.18$ MJ	**STO** (with reg) $W_{\mathrm{B,r}} = 0.15$ MJ	**Relative difference** $\Delta W_{\mathrm{r}} = 93$ %
CD (no reg) $W_{\mathrm{B,r}} = 0.9$ MJ	**CD** (with reg) $W_{\mathrm{B,r}} = 0$	**Relative difference** $\Delta W_{\mathrm{r}} = 100$ %

The relative difference between the STO and the AMS test shows that the classic specifications for passenger cars are not suitable for the development of wheel brakes for autonomous

shuttles. A lot of potential to reduce the energy dissipation demand lies in the availability of the regenerative brake. While in manual driven cars with electric drivetrains there is no possibility to enhance the availability of the regenerative brake significantly, autonomous shuttles might be able to plan ahead and e.g., manage their SoC depending on the route or manage the thermal situation of the battery cells a priori. This requires a development approach that connects wheel brake developers with powertrain and software developers.

3.5 Requirements Conclusion

To answer the research question, a requirements definition method was developed that provides a comprehensive view of the application area and circumstances for the use of an autonomous shuttle through a stakeholder analysis and at the same time includes the basic ideas for establishing specifications for passenger car wheel brakes.

By carrying out the method, essential findings for the development goal of a braking system for this vehicle class are obtained:

- Autonomous, electrified vehicles have a great impact on brake system requirements

The ODD of the vehicle and the elimination of the possibility of excessive usage by a human driver are particularly significant for the braking system. For reasons of passenger comfort, the actuation load caused by automated longitudinal control is considerably reduced compared to the worst-case scenario of today's passenger cars, such as the HFT. In addition, the expected maximum speeds and accelerations are lower than in passenger cars. For the rear axle of a shuttle, even in the case of a non-available regenerative brake, this means a reduction of the energy input by about one third, which will result in a much lower maximum temperature of the brake or the possibility to reduce the thermal capacity of the parts. The nonexistence of the usual human machine interface (HMI) eliminates the need to evaluate pedal feel in the development of the braking system. Since the longitudinal control is completely taken over by the automated driving function, a brake-by-wire system is essential. Furthermore, by using the electric engine when braking into standstill, a considerable amount of development effort can be saved for NVH development of the wheel brake even in the low-speed areas. In this case, the wheel brake is only needed for braking at medium to high decelerations, especially for collision avoidance in the case of unpredictable obstacles. As a result, the actuation frequency of the brake will drop considerably and the corrosion resistance of the components will have a higher priority. There is no change in the required maximum deceleration compared to passenger cars, which, due to the non-guaranteed availability of the regenerative brake, still has to fully utilize the coefficient of friction between tire and road surface. The same applies to the need for vehicle stabilization as used in passenger cars today in the form of electronic stability controls.

For the lifetime of the components, stricter requirements with the longest possible maintenance intervals apply due to the economic goals of an existing fleet operator. The basic idea

of an environmentally friendly transport will also set a focus on the emissions of the vehicle, or even be required by law. For this reason, a brake for an autonomous shuttle must be developed with the aim of minimizing particle emissions.

The used method to derive the requirements can also be transferred to other vehicles with autonomous driving functions, as an example, autonomous road sweepers or parcel delivery vehicles, which will generate deviating requirements in the stakeholder analysis and the expected accelerations and decelerations.

4 Brake Concepts and Suitability

This chapter discusses the suitability of the different braking concepts from chapter 2.3 and asseses the research question:

Which wheel brake concepts are particularly suitable for highly automated, electrified shuttles?

Both the friction brake design and the actuation principles are discussed on the basis of the derived changes to the requirements. Since the example vehicle has an electric drive including regenerative braking capability on the rear axle, a concept search for the rear axle is done to take it into account.

4.1 Friction Brake Concept

For an autonomous shuttle, there is the question of the appropriate brake concept for the rear axle; the pending decision is whether to use a drum or a disc brake.

There are many arguments in favor of using a drum brake. On the basis of the consideration of thermal energies in chapter 3.4.2 it becomes clear that a considerably lower maximum input of frictional energy is to be expected for the autonomous shuttle than for today's passenger cars. In addition to the energy input, a longer cooling time is to be expected due to the comfortable acceleration values and lower maximum speeds than in a passenger car. Due to the less frequent actuation of the friction brake on the regeneratively braked axle, the friction surfaces are more prone to corrosion, as the necessary cleaning effect of the application is reduced.

The drum brake is advantageous because the components are better protected from external influences by the surrounding drum and the backplate and are therefore less prone to corrosion. According to Harloff, this is one of the reasons why a drum brake is used on the rear axle of the Volkswagen ID.3[56]. For the same reason, Hagino et al.[57] attribute a comparably smaller share of particulate emissions to drum brakes than to disc brakes. Harloff also sees the manufacturing costs as an advantage for the manufacturer compared to a disc brake, as well as the lower maintenance effort with regard to wear or the necessity of early component replacement due to the aforementioned corrosion of the brake disc and pads. A conceptual

[56] Harloff, T.: Warum die Trommelbremse des ID.3 sinnvoll ist (2020).

[57] Hagino, H. et al.: Laboratory testing of airborne brake wear particle emissions using a dynamometer system under urban city driving cycles (2016), p. 272.

advantage of the drum brake compared to a disc brake is the lower clamping force requirement, which is based on the higher nominal brake value c^*[58].

In addition, the brake shoes of the drum brake are reset by the return springs once the clamping force has been released, which results in lower residual torques than with the disc brake. The piston of the disc brake is only reset by the deformation of the piston's seal ring, which, however, does not reset the pads themselves.

The conceptual, thermal advantage of the disc brake over a drum brake does not cancel out the disadvantages mentioned. With regard to the reduced friction energy requirement, the thermal disadvantage of the drum brake does not carry much weight in the discussion. Even if a particularly thin brake disc alternative adapted to the frictional energy requirement represents a favorable alternative, the further advantages of the drum brake cannot be achieved with it.

Table 4-1 gives an overview of the advantages and disadvantages of a drum brake compared to a disc brake for the intended application in an autonomous shuttle.

Table 4-1: Advantages and disadvantages of drum brakes over disc brakes for the rear axle of an autonomous shuttle (source: see text in chapter 4.1)

Advantages	Disadvantages
▪ Better protection of brake components due to inherent housing o Less Corrosion o Less Degradation of friction coefficient due to seldom usage of brake ▪ Lower particle emissions ▪ Lower manufacturing costs ▪ Lower actuating forces needed ▪ Lower drag torques due to return springs ▪ Lower maintenance effort and cost	▪ Higher torque sensitivity on friction coefficient due to higher brake factor

4.1.1 Thermal Performance of Drum Brakes

To illustrate the influence of the changed thermal performance conditions, a thermal simulation is carried out for a 10" drum brake. The underlying model was developed by Nowald et al. and validated using dynamometer tests[59]. It is based on a finite volume approach and a

[58] Remfrey, J. et al.: Aufbau und Komponenten von Pkw-Bremsanlagen (2017), p. 131.

[59] Nowald, G.; Siegl, B.: Thermal Simulation Tool for Early Sizing of Nonstandard Brake Concepts (2021).

rotationally symmetric geometry input. The geometry of the drum is described via its section contour in cylindrical coordinates, the area for the power input is defined and the evaluation points for the temperature curve are determined (Figure 4-1).

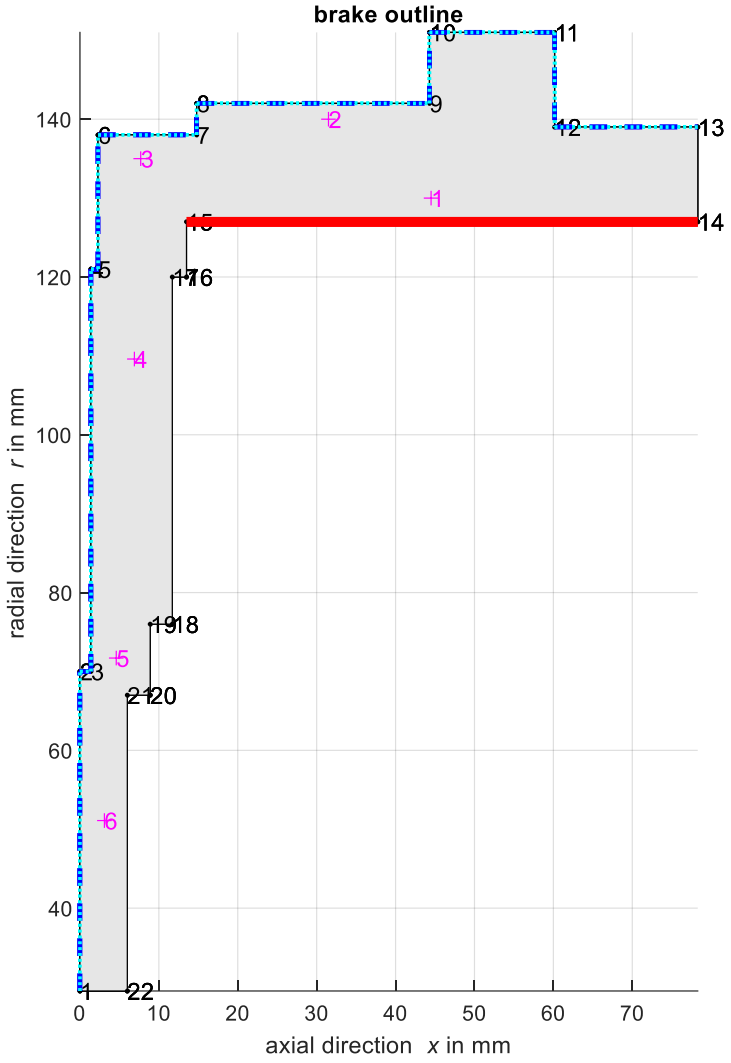

Figure 4-1: 10" brake drum geometry outline (magenta: points for temperature evaluation, red: surface for heat input, blue: surface for convection)

The material selected is grey cast iron, which corresponds to the state of the art of today's drum brakes. The AMS test and the STO test developed for the shuttle are compared as

maneuvers, as the STO shows the highest energy input of the developed tests. The results of the thermal simulation are shown in Figure 4-2 and Figure 4-3.

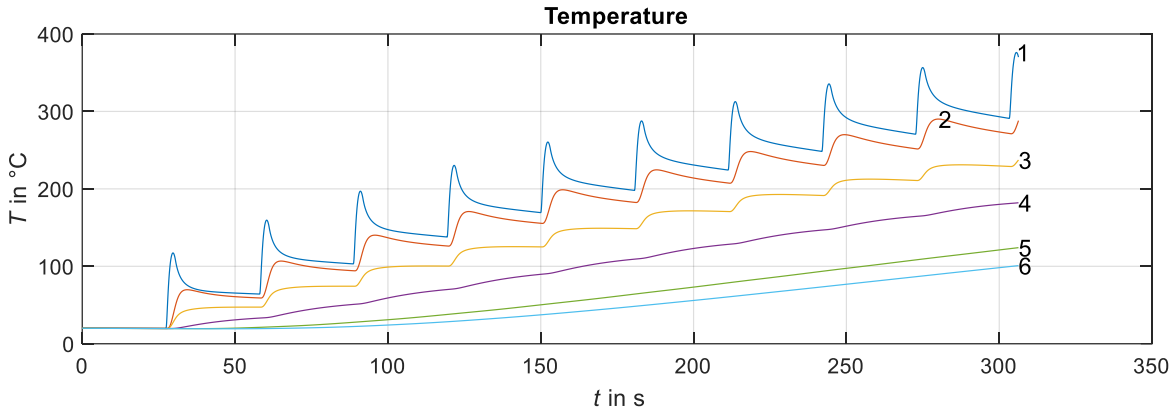

Figure 4-2: Temperature curve of drum for AMS Test

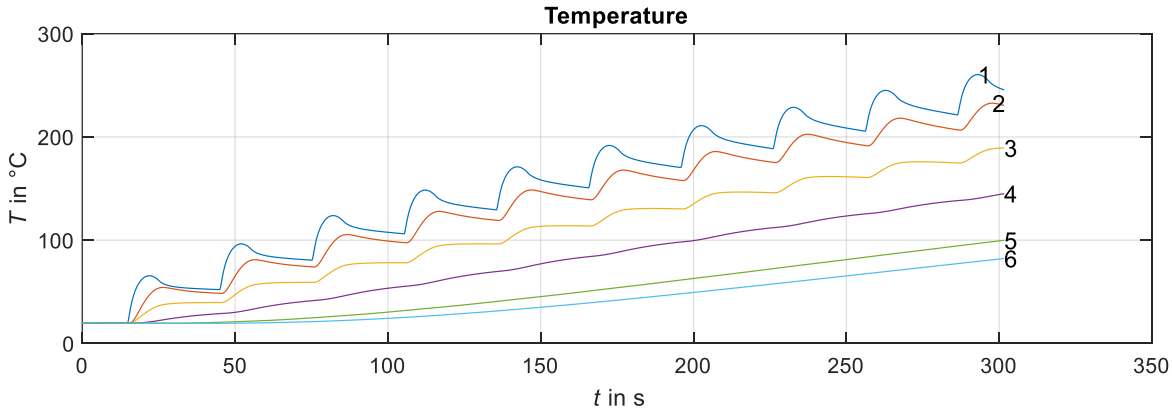

Figure 4-3: Temperature Curve for STO Test

The 10" drum reaches temperatures of up to 380 °C in the immediate vicinity of the friction surface (point 1) in the AMS test. In the STO test this temperature amounts to 250 °C, 130 K less than in the AMS test. Due to the lower temperatures on the drum friction surfaces, a smaller fluctuation in the coefficient of friction is to be expected than with the AMS test. The thermal advantage of a disc brake compared to a drum brake, will not play out in those lower temperatures beneath 250 °C.

4.2 Actuation Principles

Due to the driverless driving function, a brake-by-wire system is required to actuate the brake, which fulfils the deceleration and braking torque demands of the longitudinal control without having to rely on external foot forces. The hydraulic so-called integrated brake systems, that currently are in series production, fulfil this requirement. They consist of a combined electromechanical pressure control system including the usual valve block for stability

control (ABS and ESC). The state of research shows further brake-by-wire solutions besides hydraulic systems. These include the electromechanical wheel brakes in various designs.

As shown in the state of the art, the development and research focus lies on brakes actuated by electric motors. The conflict when using electric motor actuators for actuation lies in the high transmission demand and the conversion of the rotational energy of the actuator into the translational actuation displacement. This requires complex, multi-stage mechanical gears. In the case of the electromechanical drum brake, a spur gear intermediate stage is also required to transmit the torque for actuation, just to overcome the radial distance between the electric motor's axle and the spread unit.

When the actuator current falls to 0 in case of failure, the release of the brake is opposed by the geared-up moment of inertia of the electric motor, as well as the geared-up frictional torques. This leads to the wheel brake to only release very slowly, which can lead to instability of the vehicle when driving on a low-friction road. In addition, there is the necessary lubrication of the components, which has a significant influence on the efficiency of the gearing, but is itself dependent on temperature, age condition and lubricant displacement. The necessary mechanical complexity consequently leads to lower robustness against faults.

The magnetic concept shown in the state of the art, on the other hand, is far less complex, which is mainly due to the type of actuation. In the holding magnet design, the electromagnet as actuator delivers high forces at low possible displacement. However, the state of research shows few publications on the subject of electromagnetically actuated brakes, which is why the potential for the expansion of knowledge in this area is considered particularly great here.

4.3 Suitability of Brake Concepts Conclusion

During the research and selection of possible braking concepts, the following findings emerged:

- Wear-free, contactless brake concepts do not meet the requirements for shuttles
- Enclosed brakes such as drum brakes or wet-running multi-disc lamella brakes promise a higher degree of requirement fulfilment compared to disc brakes

All brake-by-wire systems are suitable for actuating the wheel brake of a shuttle, but the individual dry wheel brake modules have ecologic advantages over the central hydraulic systems and promise shorter installation times for manufacturers.

The following findings result from the consideration of mechatronic actuation in the state of research:

- Electric motor-operated wheel brakes have a high mechanical complexity due to the high transmission demand

- Electromagnetic actuators promise less mechanical complexity, but are not sufficiently researched as an actuation concept for wheel brakes in passenger transport vehicles

To close the revealed research gap, a combined electromagnetically actuated disc brake with a downstream duplex brake was designed for the underlying research project that is based on a holding magnet as actuator, the so-called hybrid brake. The structure and the presumed advantages are explained in the following chapter 5. From the combination and the findings on the two underlying research questions in chapters 3 and 4 a third research question is raised:

Is a magnetically actuated hybrid brake able to fulfill the requirements for an autonomous shuttle and are the presumed advantages valid?

5 Magnetic Hybrid Brake Concept

5.1 Concept Description

The wheel brake concept under investigation is based on a patent from the Knott company[60], which was further developed in cooperation with the Institute of Automotive Engineering of TU Darmstadt[61] and Continental Teves[62]. It comprises a 10" duo-duplex drum brake (1,Figure 5-1), inside which a coaxial holding magnet (3) is situated. The holding magnet is attracted to the armature disc (2) rotating with the wheel when the magnet's coils are energized. The resulting frictional torque on the magnetically actuated disc brake is transmitted as an actuating force to the drum brake shoes (4) via the teeth on the back of the magnet (5). The concept therefore represents a combination of a duo-duplex drum brake in series connection with a magnetically actuated full-pad disc brake. The system can be powered by a current controller working at 9 V. To release the brake, the magnet is pulled against the back plate with return springs.

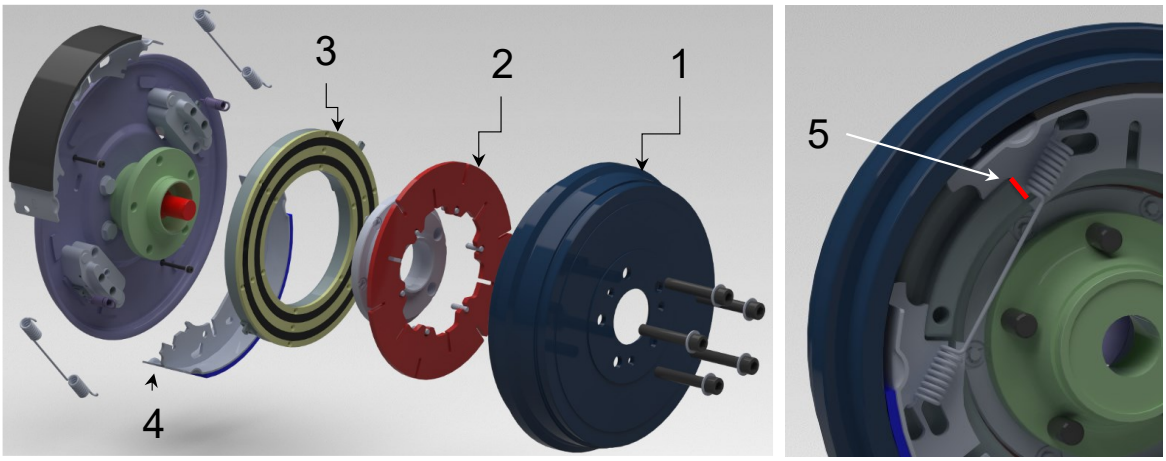

Figure 5-1: Magnetic hybrid drum brake exploded view and view towards the outside of the vehicle

The block diagram in Figure 5-2 shows the technical function with the respective state variables.

[60] Klumpner, A.; Klumpner, B.: Innenbackenbremse mit elektromagnetischer Betätigungseinrichtung (2011).

[61] Lennart Guckes: Master Thesis, Optimierung einer magnetisch aktuierten Trommelbremse (2018).

[62] Bach, U. et al.: Trommelbremse für ein drehbares Element (2019).

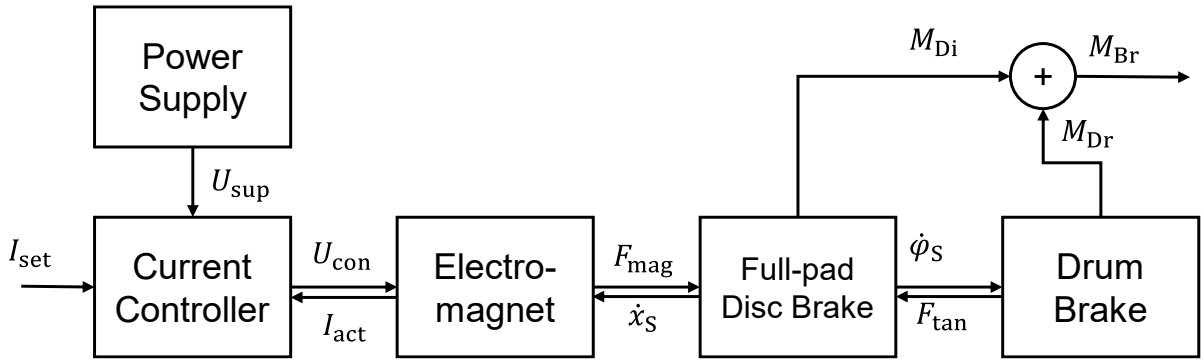

Figure 5-2: Block diagram of hybrid brake concept

In detail, the brake actuation process can be described as follows: In the beginning the brake is in its released state. A current setpoint is set for the coils, which is adjusted by a current controller. The clearance or the initial air gap of the magnetic disc brake is closing as soon as the magnetic force is large enough to overcome the return springs. When the magnet attaches to the disc, a friction torque is generated. The friction torque causes the magnetic ring to rotate in a small angle and the tangential force is transmitted to the actuation surfaces of the drum brake shoes via the ring's teeth. This force is used to actuate the brake shoes which generate a friction torque at the drum. Figure 5-3 shows the prototype in different assembly stages and mint condition.

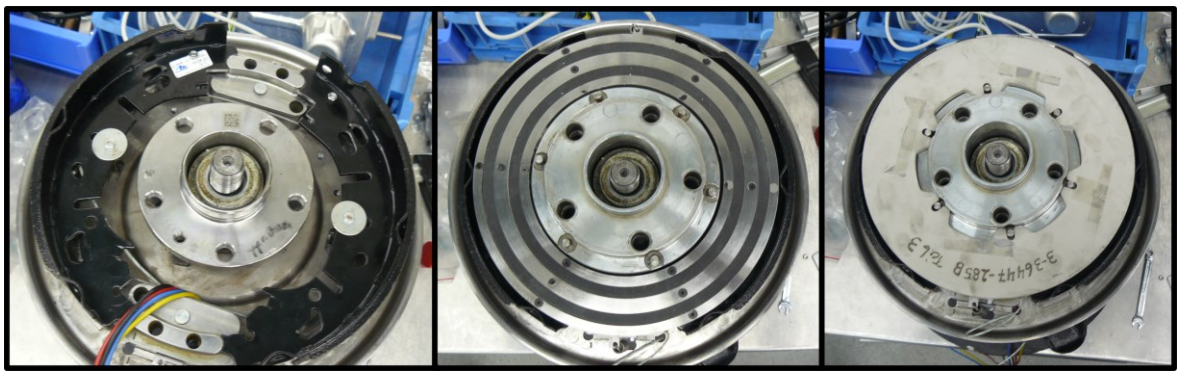

Figure 5-3: Hybrid drum brake in different stages of assembly (left: drum brake shoes, middle: friction surface of magnet, right: fully assembled except drum)

For testing purposes, the prototype can be configured in different setups:

1. Hybrid Setup: Disc and drum brake (as shown in Figure 5-1)
2. Disc Setup: Disc brake only, where the holding magnet is rotationally fixed to the backplate

5.2 Dimensioning of the Components

5.2.1 Dimensioning of the Wheel Brake

The case of an emergency braking procedure with a deceleration of $a = -1g$ on a high friction coefficient requires a braking torque of approximately 1100 Nm at the rear wheel (see Appendix, Figure 8-4). The dimensioning of the concept is based on this value.

The total braking torque is calculated according to Figure 5-2:

$$M_{\mathrm{Br}} = M_{\mathrm{Dr}} + M_{\mathrm{Di}} = \frac{M_{\mathrm{Di}}}{r_{\mathrm{act}}} \cdot r_{\mathrm{Dr}} \cdot c^* + M_{\mathrm{Di}} = M_{\mathrm{Di}} \left(\frac{r_{\mathrm{Dr}}}{r_{\mathrm{act}}} \cdot c^* + 1 \right)$$
$$= F_{\mathrm{mag}} \cdot \mu_{\mathrm{Di}} \cdot r_{\mathrm{eff}} \cdot \left(\frac{r_{\mathrm{Dr}}}{r_{\mathrm{act}}} \cdot c^* + 1 \right) \tag{5-1}$$

The necessary actuator force is then calculated:

$$F_{\mathrm{mag}} = \frac{M_{\mathrm{Br}}}{\mu_{\mathrm{Di}} \cdot r_{\mathrm{eff}} \cdot \left(\frac{r_{\mathrm{Dr}}}{r_{\mathrm{act}}} \cdot c^* + 1 \right)} \tag{5-2}$$

The design variables in Table 5-1 are estimated or determined geometrically:

Table 5-1: Design parameters and assumptions for dimensioning

M_{Br}	Total braking torque	1100 Nm
μ_{Di} (assumed)	Friction coefficient on disc	0.3
r_{eff} (assumed)	Effective friction radius on disc	0.1 m
r_{Dr}	Friction radius on drum surface	0.127 m
r_{act}	Actuation radius of drum brake shoes	0.09 m
c^* (assumed)	Self-amplification of drum brake	2.5 – 4.6 (with $0.3 < \mu < 0.4$)

The calculated necessary magnetic force therefore lies between $F_{\mathrm{mag}}(c^* = 2.5) = 8$ kN and $F_{\mathrm{mag}}(c^* = 4.6) = 5$ kN.

The torque ratio of the disc brake torque to the total torque is calculated as follows:

$$\frac{M_{\mathrm{Di}}}{M_{\mathrm{Br}}} = \frac{1}{\frac{r_{\mathrm{Dr}}}{r_{\mathrm{act}}} \cdot c^* + 1} \tag{5-3}$$

The equation yields the values $\frac{M_{\mathrm{Di}}}{M_{\mathrm{Br}}}(c^* = 2.5) = 0.22$ and $\frac{M_{\mathrm{Di}}}{M_{\mathrm{Br}}}(c^* = 4.6) = 0.14$. Since the drum and armature disc have the same angular velocity, the power contribution of the armature disc to the total frictional braking power lies also at $14 - 22\ \%$.

5.2.2 Dimensioning of the Actuator

A holding magnet, which works at minimal airgaps, is used as the actuator, which consists of multiple individual parts.

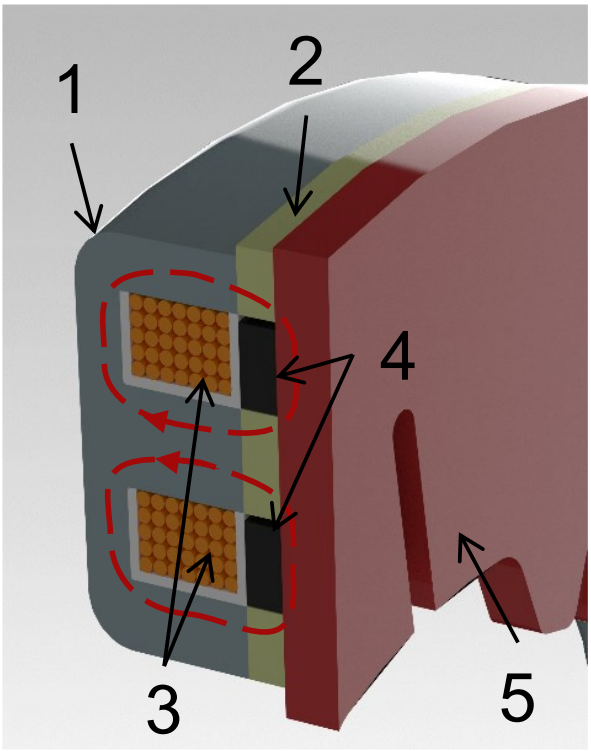

Figure 5-4: Section view of actuator

The cross-section and the choice of materials are the result of the master thesis[63] of the author, with the aim to optimize the magnetic force yield in the available installation space by means of finite element calculations. The parts carrying the magnetic flux are the steel yoke with “E” cross-section (1), the cast friction rings (2) and the armature disc made of steel (5).

[63] Lennart Guckes: Master Thesis, Optimierung einer magnetisch aktuierten Trommelbremse (2018).

In addition, two excitation coils (3) are inserted as well as two friction rings made of a metal-free non-asbestos (NAO) friction material (4). The two excitation coils carry currents in different directions so that the resulting flux is amplified. In the event of failure of one coil, the brake can still be operated, but with lower maximum torque if they are connected in parallel.

Table 5-2 gives an overview over the functions of each component. The cast friction rings were chosen as a compromise between high saturation flux density (about 1.5 T) and graphite content (about 3.5 %) of the material. For reasons of manufacturing, they were designed with a thickness of 4 mm.

Table 5-2: Functional overview of the components of the magnetic ring

Part	Name	Functions
1	Steel yoke	1. Guidance of magnetic flux with high permeability 2. Enclosure and containment of all components of the magnetic ring 3. Transmission of the tangential forces generated by friction to actuate the drum brake shoes
2	Cast friction rings	1. Guidance of magnetic flux with high permeability 2. Lubrication of the friction surface by means of embedded graphite spheres 3. Generation of the friction torque in combination with disc
3	Copper coils	Generation of the necessary excitation for the magnetic flux
4	NAO - friction rings	Improvement of the friction properties of the ring and armature plate pairing
5	Armature disc	1. Guidance of magnetic flux with high permeability 2. Friction partner for magnetic ring 3. Transmission of the braking torque to the wheel

The design of the magnetic ring was made with the requirement of operation of the brake with a lower on-board voltage of 9 V. Each coil of the electromagnet carries 28 turns with a

wire diameter of 1.5 mm. The FEM simulation used in the student thesis results in a static force map as a function of current and air gap, which can be found in Figure 5-5.

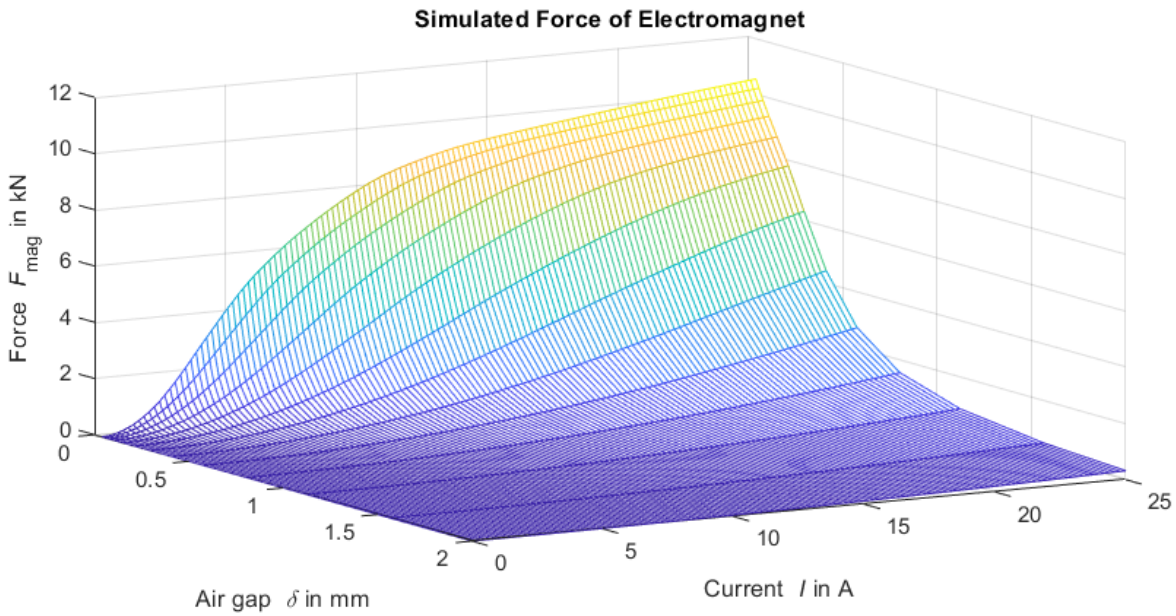

Figure 5-5: Simulated force of electromagnet over current and air gap[64]

The curve shows the strong dependence of the magnetic force on the air gap. The necessary 8 kN clamping force is achieved at the minimum air gap and about 10 A. It also shows the saturation that occurs for higher currents. At higher air gaps, saturation occurs in higher areas of current, because the bigger air gap reduces the magnetic flux density of the magnetic circuit.

[64] Lennart Guckes: Master Thesis, Optimierung einer magnetisch aktuierten Trommelbremse (2018), p. 61.

6 Performance Identification

To investigate the suitability and performance of the brake, different tests are carried out.

1. The actuator itself is examined for the actuator force it can generate.
2. The dynamics of the application of the electromagnet to the disc is measured.
3. The dynamics for the actuation of the hybrid brake is identified.
4. The generated torque at the disc is identified as well as the total braking torque at different velocities.
5. The overall torque hysteresis of the hybrid brake is measured and evaluated.
6. The fallback torque generation in the case of one coil failing is tested.

The respective testing procedures are documented in the following test descriptions.

6.1 Experiments to Identify the Generated Actuator Force

6.1.1 Goal

The aim of the experiment is to identify the actuator force that can be generated as a function of the air gap present, in order to examine the actuator for compliance with the requirements ($F_{\mathrm{mag}}\ (c^* = 2.5) = 8\ kN$). In addition, the electrical power loss at the required current is calculated. The experiment was part of the aforementioned student thesis[65].

6.1.2 Test Execution

The achieved magnetic force of the magnet is identified quasi-statically by means of pull-off tests, since a direct force measurement between ring and disc is not applicable without influencing the magnetic flux. For this purpose, the ring and disc are mounted on a tensile force testing machine (Figure 6-1) and quasi-statically pulled off under constant current. The required electrical voltage is also considered for power calculation. The highest tensile force measured in each case during the pull-off process is used to check whether the actuator has reached its target force. To simulate different constant air gaps, brass foils with defined thicknesses $\delta = [0; 0.1; 0.25; 0.35]$ mm are placed between the magnetic ring and the armature disc. The tolerance in thickness of the foils lies below 8 µm[66]. These have a relative magnetic

[65] Lennart Guckes: Master Thesis, Optimierung einer magnetisch aktuierten Trommelbremse (2018).

[66] Hasberg Schneider GmbH: Präzisions-Lehrenbänder und Unterlagsfolien (2022).

permeability similar to vacuum with $\mu_R \approx 1$. The used force sensor is a Zwick Roell 50 kN X-Force sensor[67].

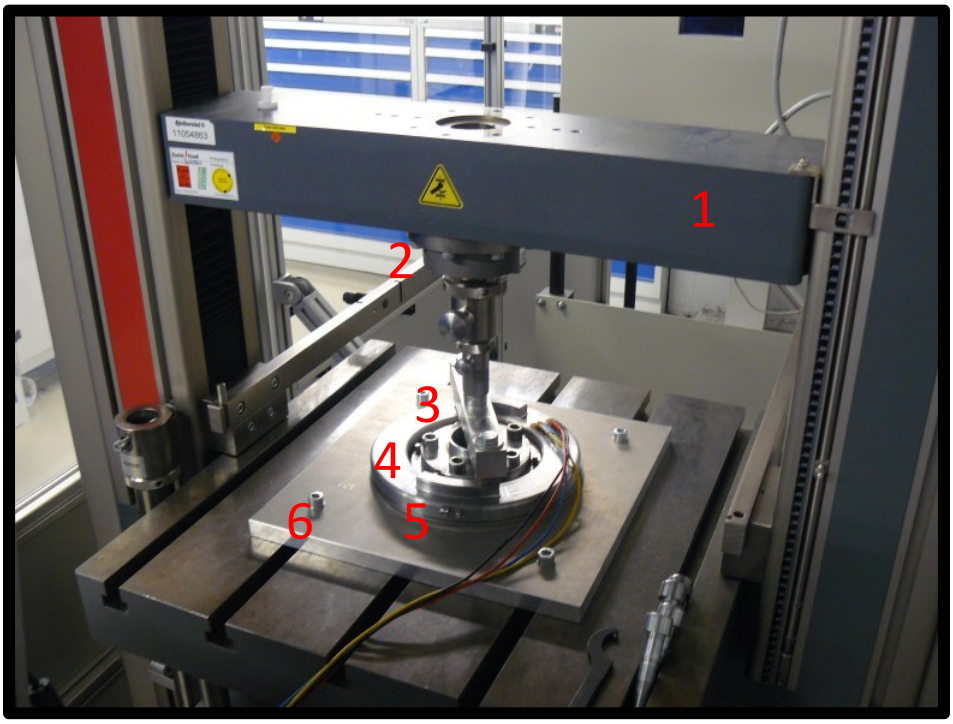

Figure 6-1: Test bench for actuation force measurements (1: portal, 2: force sensor, 3: support beam, 4: magnet actuator, 5: armature disc, 6: aluminium plate)[68]

6.1.3 Evaluation

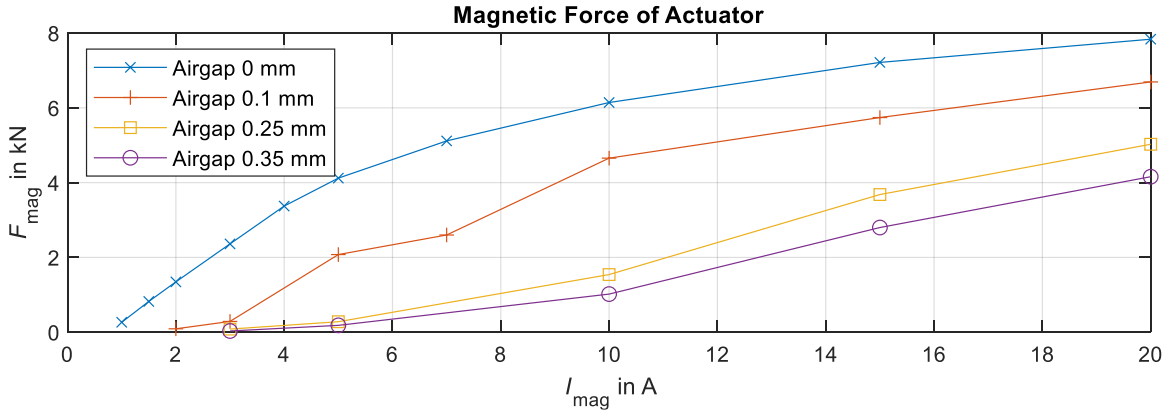

Figure 6-2: Measured holding force over current for different airgaps

The actuator achieves a maximum force of 7.8 kN with the smallest possible air gap and 20 A current and thus reaches the required actuator force with a negligible 200 N difference (Figure 6-2). The electrical resistance of the windings connected in series is $R_{\mathrm{ov}} = 0.54\ \Omega$

[67] ZwickRoell GmbH & Co. KG: Kraftaufnehmer Xforce K (2022).

[68] Lennart Guckes: Master Thesis, Optimierung einer magnetisch aktuierten Trommelbremse (2018), p. 96.

at room temperature. Thus, the electrical power at a current of 20 A results in $P_{\mathrm{el}} = R \cdot I^2 = 216\ \mathrm{W}$. The force curve at the smallest possible air gap shows the typical curve of a holding magnet operated up to saturation. For larger air gaps, the relationship between force and current resembles a linear curve more closely, which suggests that the magnet is in the lower, linear flux density range.

6.2 Tests on Current Dynamics on Application and Release

6.2.1 Goal

The goal of the experiment is to measure the dynamics of the current buildup when the disc brake is applied and released.

6.2.2 Execution

For the measurements a sample rate of 4 kHz is used to evaluate the current buildup and breakdown. The power supply consists of a 12 V battery in series with a potentiometer so that a constant voltage can be set for the magnet. A voltage of $U = 4.5\ \mathrm{V}$ is chosen for a target current of about 7 A. A relais is used to apply or release the voltage. The test is done at a velocity of $20\ \mathrm{m/s}$. The initial airgap is set to $0.5\ \mathrm{mm}$. For the current measurements a E3n series current clamp from Chauvin Arnoux[69] is used.

6.2.3 Evaluation

Figure 6-3 shows the voltage and current curves over time. It shows the typical timeline for an application of an electromagnet with the first current buildup and overshooting voltage due to induction at $t = 0\ \mathrm{s}$ and the impact of the magnet at the disc surface at about $t = 0.07\ \mathrm{s}$ after travelling through the initial airgap. The time between the voltage jump and the impact of the magnet thus amounts to $\Delta t = 70\ \mathrm{ms}$.

[69] Chauvin Arnoux: Current Clamp for AC/DC Current (2022).

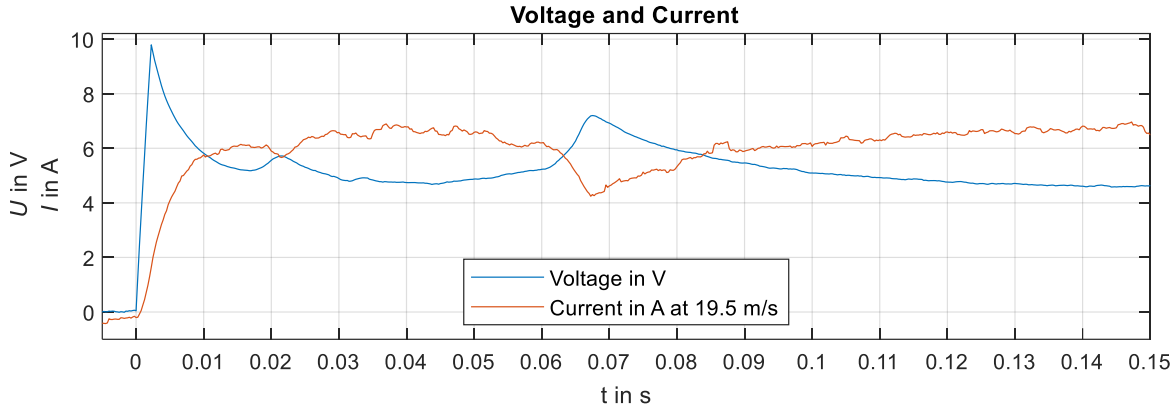

Figure 6-3: Voltage and current curve during application of the disc brake

Figure 6-4 shows the voltage and current during the release of the brake. Due to the inductance of the magnet the overall voltage drops below 0, after the switch is turned off at $t = 0$ s. The magnet detaches from the disc and the voltage drops to 0 when the magnet has moved to its initial position at $t = 0.04$ s, which results in a releasing time of the magnet of about $\Delta t = 40$ ms.

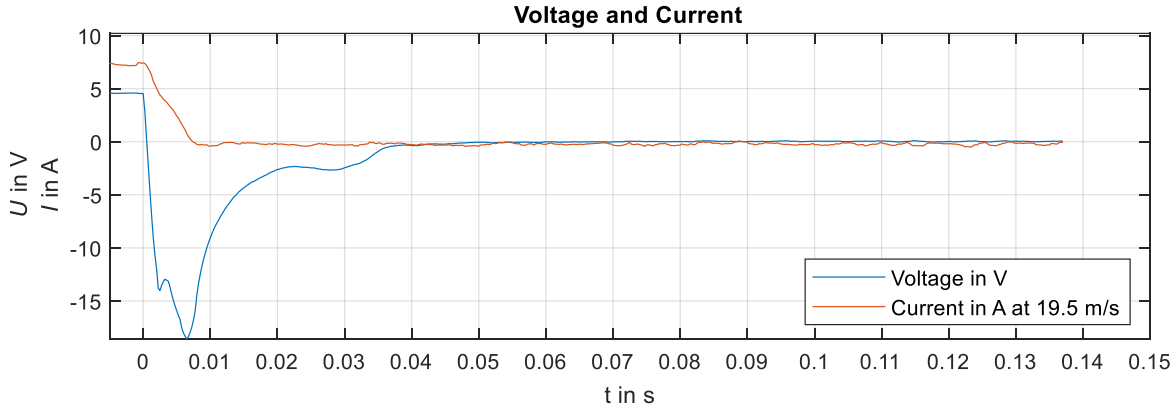

Figure 6-4: Voltage and current curve during release of the disc brake (same timescale as in application of the brake)

6.3 Test for Evaluation of System Dynamics and ABS suitability

6.3.1 Goal

The system dynamics of the hybrid brake are tested in the System Setup on a test bench to investigate the brake concept's suitability for slip control at an early prototype stage. The dependency of the torque dynamics on different wheel speeds is also evaluated.

6.3.2 Execution

The brake is controlled by means of jumps in the setpoint value. At a vehicle speed of constant $v = [9;\ 7;\ 5;\ 2]$ km/h, the magnet is exposed to voltage jumps from $0 - 12$ V and vice versa. The temperature for the ring at the start of the test is set to be below 50 °C.

To reduce the influence of random measurement deviations, the measurements are repeated three times. A measurement frequency of 10 kHz is chosen, to get a sufficient resolution on the torque response.

The slow-moving dynamometer test bench is equipped with a 25 kN force sensor U10M of HBK company[70] which is installed on a torque swivel.

6.3.3 Evaluation

The times taken to reach 90 % of the final torque are used for evaluation. For this purpose, segments of the measurements are formed, each of which consists of either a "voltage jump rising" or a "voltage jump falling". Within these segments, the duration is calculated which is required to reach 90 % of the final torque within the segment from the time of the voltage jump (Figure 6-5).

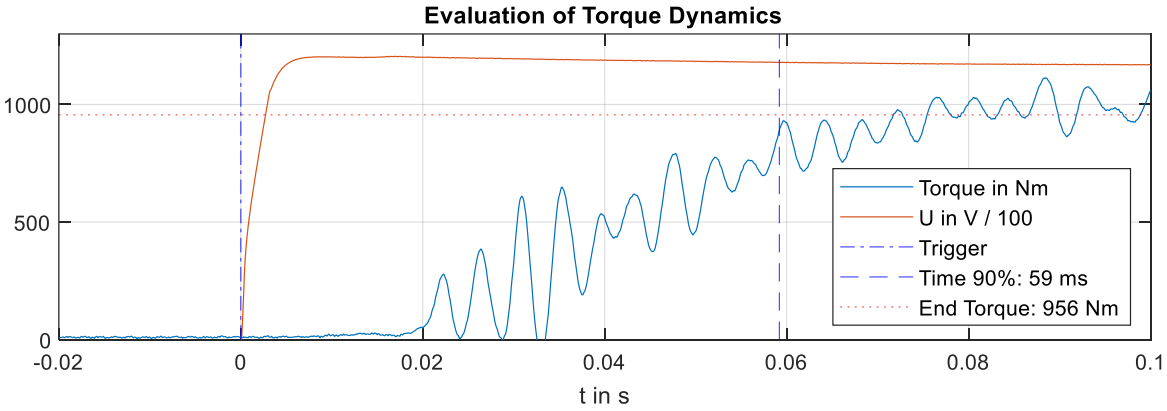

Figure 6-5: Evaluation plot for the torque dynamics for a voltage jump from 0-12 V at 9 km/h (voltage jump rising)

It can also be seen, that the torque is oscillating. The oscillation at around 230 Hz is most likely caused by a stick-slip effect, as the magnetic ring sticks and slips on the armature disk. This effect can cause NVH issues with the brake, that are not researched further in this work.

The torque dynamics achieved averaged over the three repetitions for the group "voltage jump rising" result in: $\tau_{90} = 54$ ms and for "voltage jump falling": $\tau_{90} = 57$ ms.

[70] HBK Germany: Kraftsensor U10 (2022).

For a fast change in torque, this results in a maximum possible frequency of $f = \frac{1}{\tau_{90}} \approx$ 17.6 Hz. For modern slip controllers, which control in the range up to 10 Hz in hydraulic brake systems[71], the brake can thus be considered suitable, since it can be applied at a higher frequency.

The dependency of the torque dynamics on the velocity for the rising and falling groups is shown in Figure 6-6.

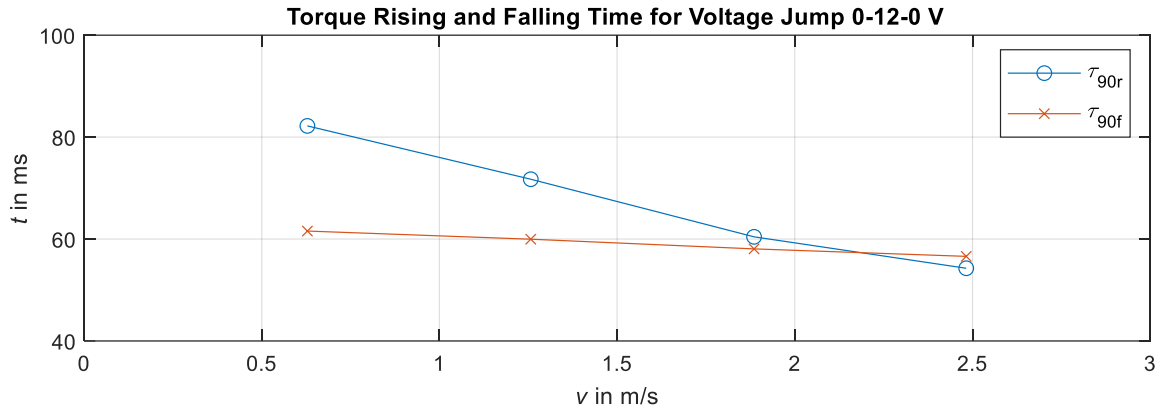

Figure 6-6: Torque dynamics depending on vehicle speed for rising and falling torque

The torque rising times are dependent on vehicle speed, which was expected. Before any torque is generated, the magnet needs to pull against the armature plate and then travel through the clearance between its teeth and the brake shoes (cp. Figure 5-1).

The maximum angular velocity that it can reach during this travel is the angular velocity of the wheel itself. The faster the wheel turns, the faster the magnet can close the clearance. For the release of the magnet the torque reacts at nearly the same time for all speeds, as the application force on the brake shoes is dropping simultaneously with the dropping axial force of the magnet, without the need of traveling through any clearance.

The trend in the diagram shows that the rising time falls below the falling time of the torque at about 2.2 m/s. If the design of the brake would require a quicker response for ABS suitability, the optimization goal should be focused on the falling time. One solution to get quicker falling times could be the installation of stronger return springs on the brake shoes.

[71] Ivanov, V. et al.: A Survey of Traction Control (2015), p. 3879.

6.4 Tests on the Torque Generation of the Overall System and the Disc Brake

For the identification of the generated torques, tests of the entire system (Hybrid Setup) as well as only of the solid disc brake (Disc Setup) are carried out.

6.4.1 Goal

The goal of the test is to identify the braking torque generated from the disc brake subsystem and in the overall disc and drum system as a function of the variables current, electrical power and velocity.

6.4.2 Execution

To identify the torque generation, a map with different velocities and current values is created and individual points of this map are tested in a stationary manner (by means of drag braking) on a brake dynamometer.

The velocities considered are $v = [2; 5; 15; 30; 55; 100; 144]\,\mathrm{km/h}$ or $v = [0.5; 1.3; 4.1; 15.3; 27.8; 40]\,\mathrm{m/s}$ with a wheel diameter of $0.3\,\mathrm{m}$ and the currents $I = 1 - 14\,\mathrm{A}$ in steps of $1\,\mathrm{A}$. To reduce the influence of random measurement deviations, the measurements are repeated three times in disc brake mode. Each test run is started after the temperature of the disc reaches a value below $40\,°\mathrm{C}$.

6.4.3 Evaluation

The evaluation of the tests is automated according to the following procedure (Figure 6-7):

1. Filtering of torque and current signal by a two-sided moving average with a span of $50\,\mathrm{ms}$ at a measurement frequency of $100\,\mathrm{Hz}$.
2. After reaching $97\,\%$ of the nominal current, the maximum torque is searched for in a time window of $150\,\mathrm{ms}$. The search period results from the time usually required to reach the maximum braking torque of $150\,\mathrm{ms}$ in a vehicle (TTL: Time to lock)[72].
3. The start time for averaging is set to when $95\,\%$ of the maximum torque found is reached.
4. The end time for averaging is set according to the duration of one complete revolution of the brake. If one revolution is not reached in the test duration (due to the low velocity), the end time is set to when the current drops below $97\,\%$ of the set current.

[72] Pinkow, S.: Cutting-edge brake technology MK C1 (2017).

By limiting the evaluation duration to one revolution, the influence of the temperature as a disturbance variable during the measurement is reduced.

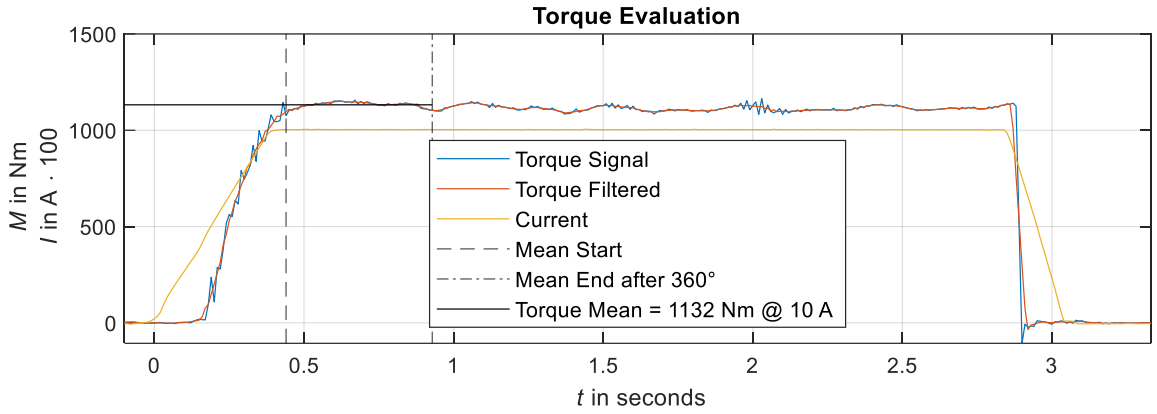

Figure 6-7: Evaluation of one drag braking test

For evaluation purposes, the achieved torques are plotted in an array of curves over current and for different velocities for both the disc brake (Figure 6-8) and the hybrid system (Figure 6-9).

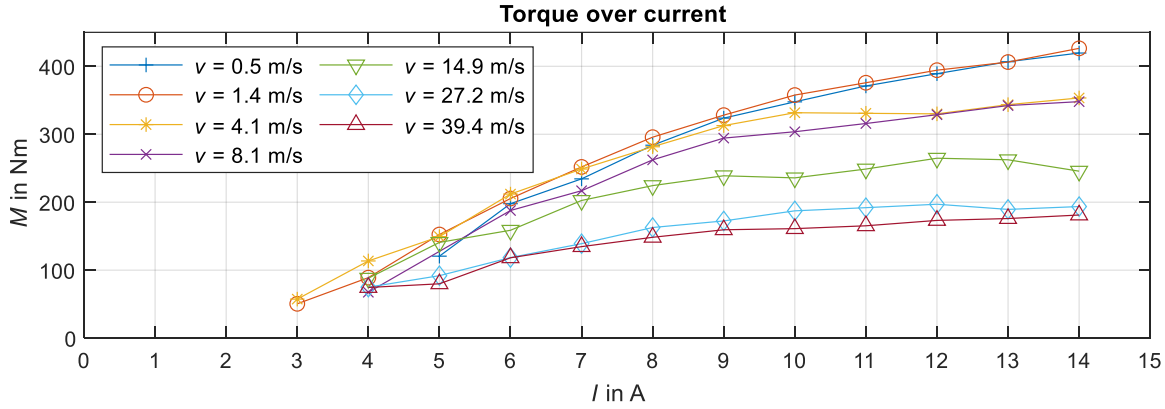

Figure 6-8: Torque over current of the disc brake

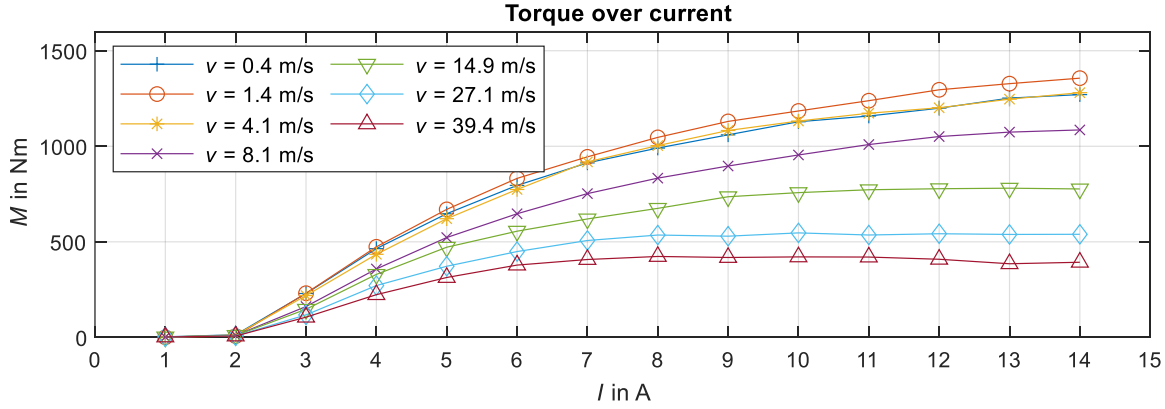

Figure 6-9: Torque over current of the hybrid brake

To evaluate the needed electric power during the braking the torque curve is plotted in Figure 6-10 over the power, which is calculated using the resistance of the coils at room temperature.

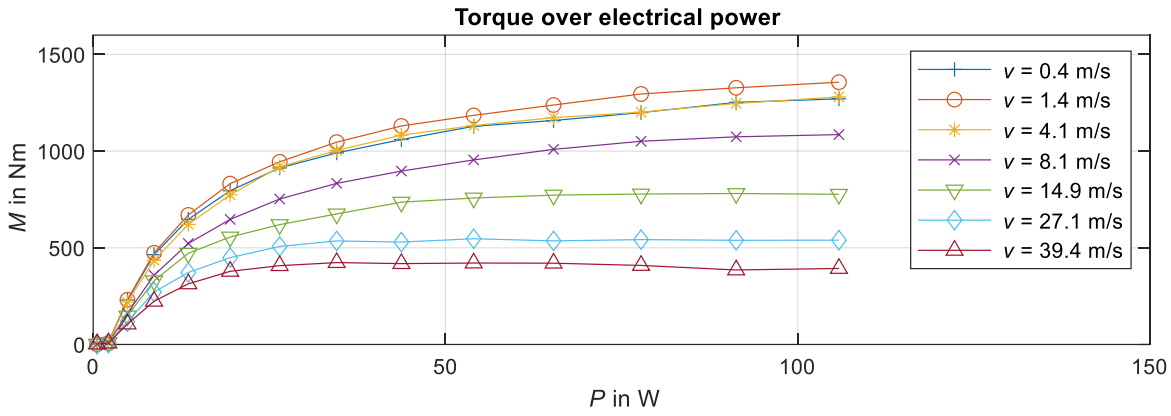

Figure 6-10: Torque of hybrid brake over electric power

For the smaller velocities up to $5\ \mathrm{m/s}$ the magnet generates a power loss of about $50\ \mathrm{W}$ during braking at the required $1100\ \mathrm{Nm}$ for the autonomous shuttle's rear axle. This value is significantly lower compared to the power ratings of the electromechanical brakes in the state of research, that use electric motors in the range of $180 - 250\ \mathrm{W}$ at the rear axle[73]. The wedge brake, however, only needs about $25\ \mathrm{W}$ during an emergency braking according to Semsch[74].

The following expected characteristics are included in the torque curves over the current:

1. As the current increases, the torque increases as a result of the higher axial force in the disc brake.
2. Due to saturation of the flux density in the flux path, the increase in torque is degressive.
3. In the range of approx. $1 - 2\ \mathrm{A}$, no torque is generated. The reason for this is the necessity to overcome the initial air gap between yoke and armature disc, which requires a minimum axial force defined by the return springs.

However, when considering the torque curve over the velocities, an unexpected behavior occurs. At all current levels, a dependence of the torque on the velocity can be observed. At the highest current level, the percentage decrease in torque in hybrid operation between slow and fast driving is 71 %. In disc mode, this decrease is 57 %. This is particularly clear from the plot of torque versus velocity (Figure 6-11 and Figure 6-12).

[73] Balz, J.: Expertengespräch zu Leistungsklassen Aktoren für Radbremsen (2022).

[74] Semsch, M. et al.: Elektromechanisch betätigte Bremse (2017), p. 497.

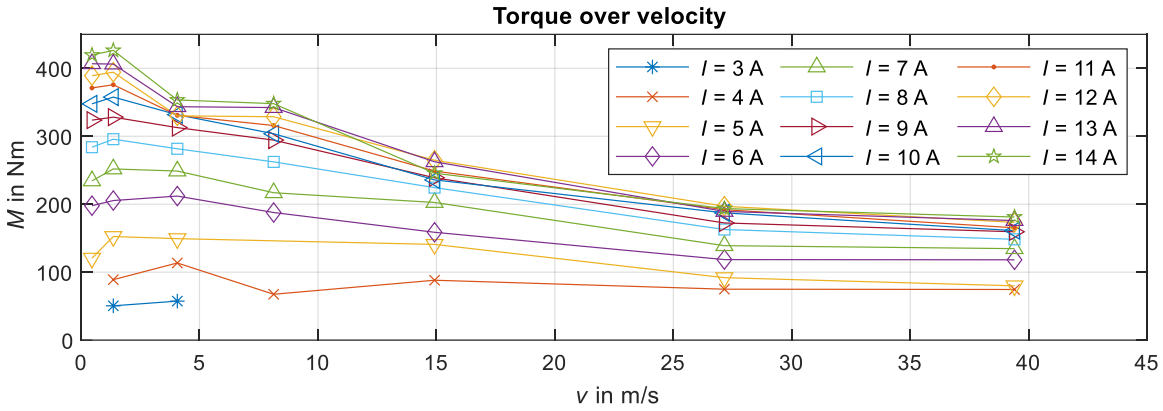

Figure 6-11: Torque generation of disc brake over velocity for different currents

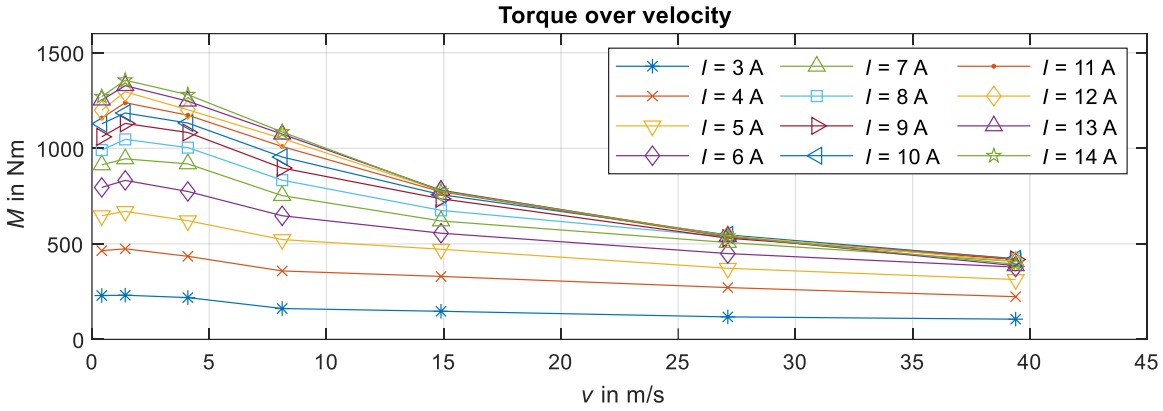

Figure 6-12: Torque generation of hybrid brake over velocity for different currents

With the two torque curves, the effective c^* can be calculated using the equation for the torque ratio:

$$c^* = \left(\frac{M_{\mathrm{Br}}}{M_{\mathrm{Di}}} - 1\right) \cdot \frac{r_{\mathrm{act}}}{r_{\mathrm{Dr}}} \tag{6-1}$$

Since the measurements are done on different days and not simultaneously, they are affected by errors and deviations that are based on the measurement setup and preparations.

The brake factor is represented via the calculated actuation force $F_{\tan} = \frac{M_{\mathrm{Di}}}{r_{\mathrm{act}}}$ and the velocity (Figure 6-13).

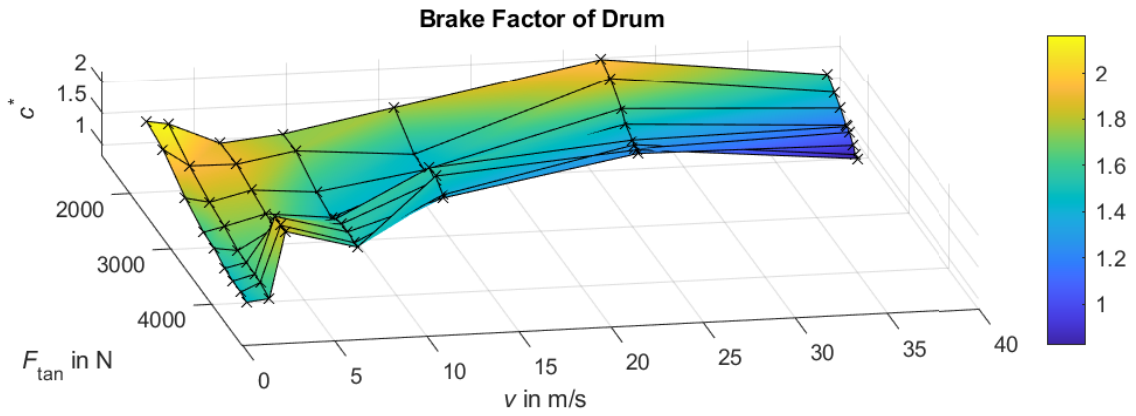

Figure 6-13: Brake factor of the drum brake

It can be seen from the diagram that the brake factor of the drum brake lies between $c^* = 0.83$ and 2.16 The value is particularly low in the range of high speeds and high actuating forces, and higher at low speeds and lower actuating forces. The calculated value based on the measured data is therefore lower than the design assumption made in Table 5-1.

With the calculated brake factor it is possible to calculate the friction coefficient between the drum and the brake shoes using the following formula for two leading brake shoes in a drum brake[75]:

$$c^* = \frac{2\mu l_3}{K_1 a_0 - r\mu} \rightarrow \mu = \frac{K_1 a_0 c^*}{2l_3 - r c^*} \tag{6-2}$$

$$K_1 = \frac{\sin(\alpha) + \alpha}{4 \cdot \sin\left(\frac{1}{2}\alpha\right)} \tag{6-3}$$

$$a_0 = \sqrt{l_1^2 + l_2^2} \tag{6-4}$$

With the following geometric values for the drum (Figure 6-14 and Table 6-1).

[75] Baumgartner, H. et al.: Nutzfahrzeugbremsen (2017), p. 254.

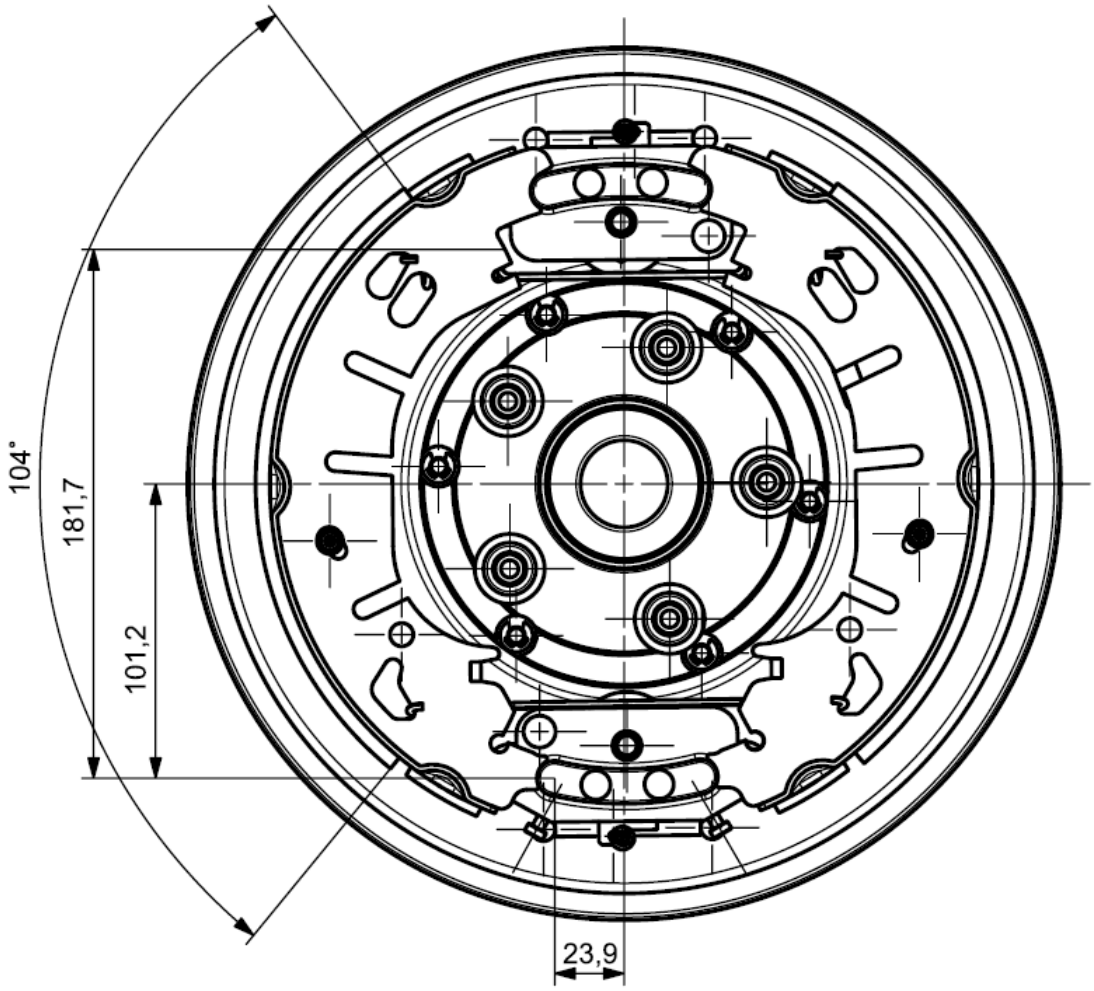

Figure 6-14: Geometric values for drum brake c* calculation

Table 6-1: Geometric values of drum brake for brake factor calculation

Geometric value	**Description**
$l_1 = 101$ mm	Vertical distance of pivot to center
$l_2 = 24$ mm	Horizontal distance of pivot to center
$l_3 = 182$ mm	Vertical distance of pivot to actuation point
$r = 127$ mm	Radius of drum
$\alpha = 104°$	Angle of coverage of brake pad on brake shoe

The results of the calculation are shown in Figure 6-15:

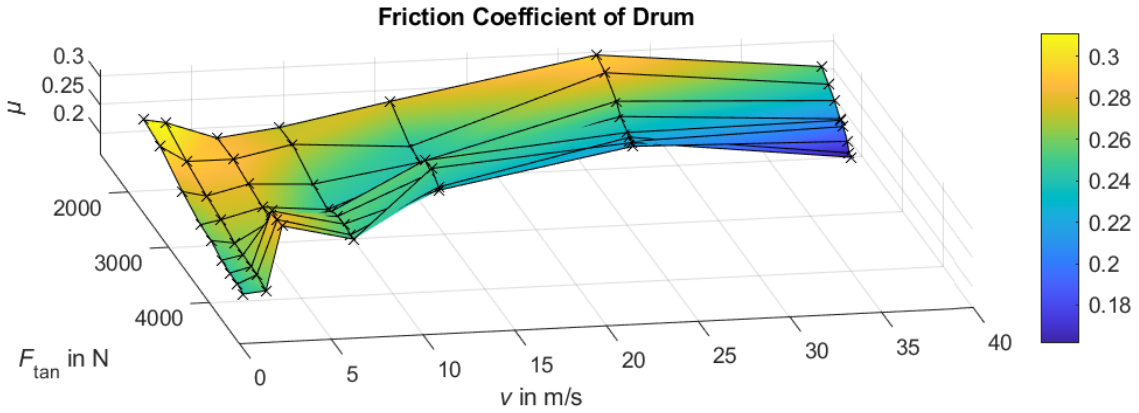

Figure 6-15: Calculated friction coefficient of the drum brake

The calculated friction coefficient of the drum brake varies between 0.31 and 0.16.

Due to the change in friction coefficient the ratio between the torques and friction powers of drum and disc brake also show a variation over current and velocity (Figure 6-16).

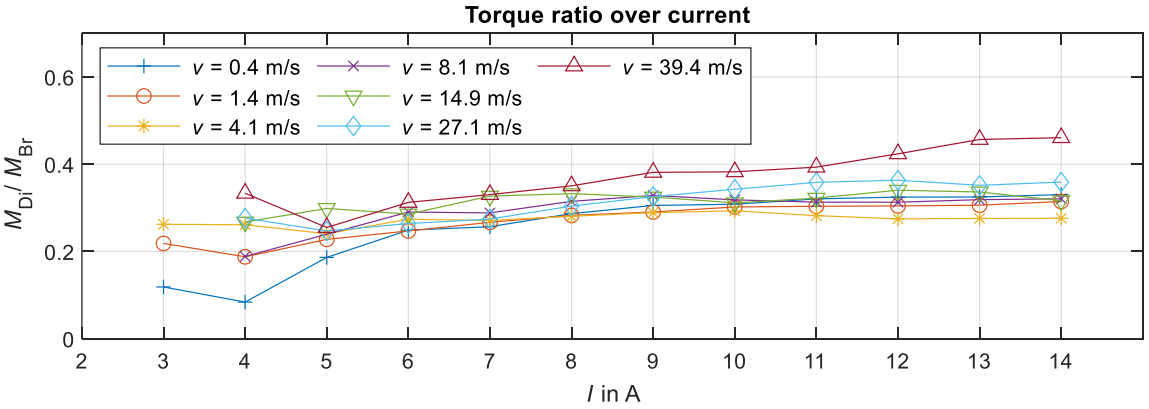

Figure 6-16: Torque ratio between disc and drum over current

The highest torque ratio of 46 % for the disc occurs at 14 A and 40 m/s. Due to the low c^* value of the drum in this area, the ratio of torque contribution is at its maximum at this point.

6.5 Test on Overall Hysteresis

6.5.1 Goal

The goal of the experiment is the evaluation of the overall hysteresis of the hybrid brake. The brake hysteresis diagram shows the torque values for an application and release of the brake over its control variable, in this case current.

6.5.2 Execution

For the test the brake is applied and released using an ascending current ramp ranging from $0 - 14$ A in 4 s followed by a descending current ramp to 0 in 4 s. The velocity of the dynamometer is set to $0.5 \frac{\mathrm{m}}{\mathrm{s}}$.

6.5.3 Evaluation

Figure 6-17 shows the measured data of current and torque on a timescale.

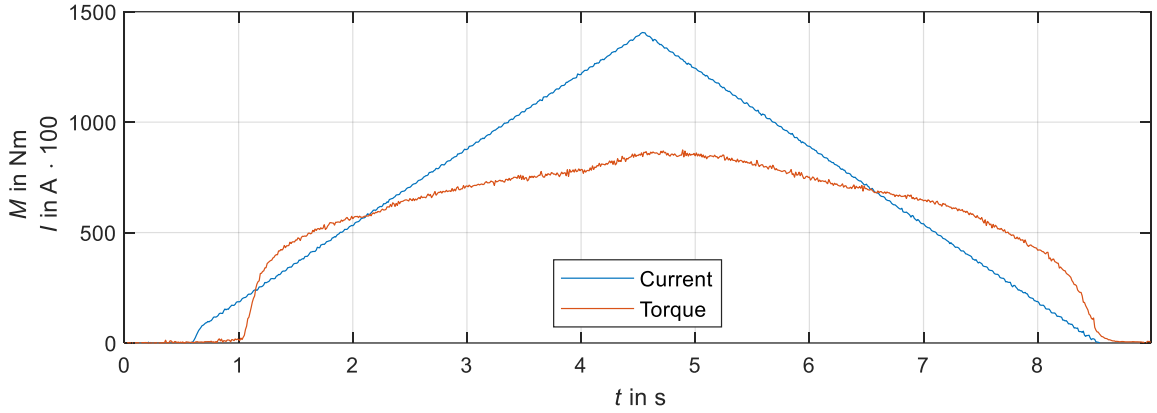

Figure 6-17: Evaluation test for overall hysteresis

To evaluate the hysteresis a diagram showing the torque over current is needed. The following steps are used to create the diagram:

1. The data is split into two parts by finding the maximum value of the current. The two parts are marked as ascending and descending corresponding to the current gradient.
2. To find the relative difference between the ascending and descending part in torque the descending data is flipped, so that the samples are in the same order as the ascending samples.
3. The difference and relative differences in torque are then calculated sample by sample.

Figure 6-18 shows the result of the evaluation.

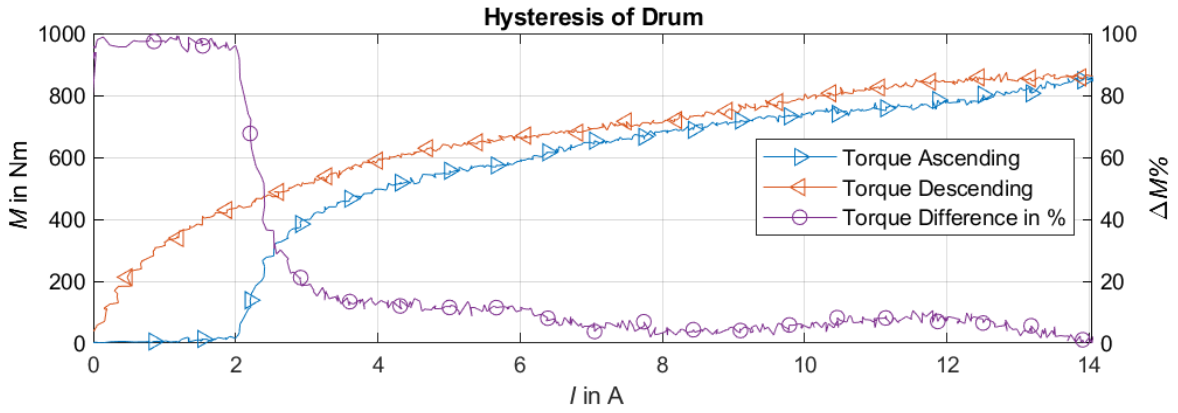

Figure 6-18: Hysteresis diagram of hybrid brake

It is important to mention, that in the case of the hybrid brake, the hysteresis diagram not only shows the influence of coulomb friction between the mechanical parts (as it does in hydraulic brakes), but also the magnetic hysteresis of the magnetized materials (see chapter 2.3.2). In short, this effect causes the magnetic field to be smaller when magnetizing the material by applying a current ramp than when releasing the current ramp. The overall hysteresis diagram in Figure 6-18 shows the combination of both effects, friction and magnetic hysteresis of the materials.

The main differences in torque are to be found in the range of small currents. The behavior of the brake in this area is due to the characteristic force curve of the magnetic actuator. Figure 6-19 shows the progression of force during the experiment.

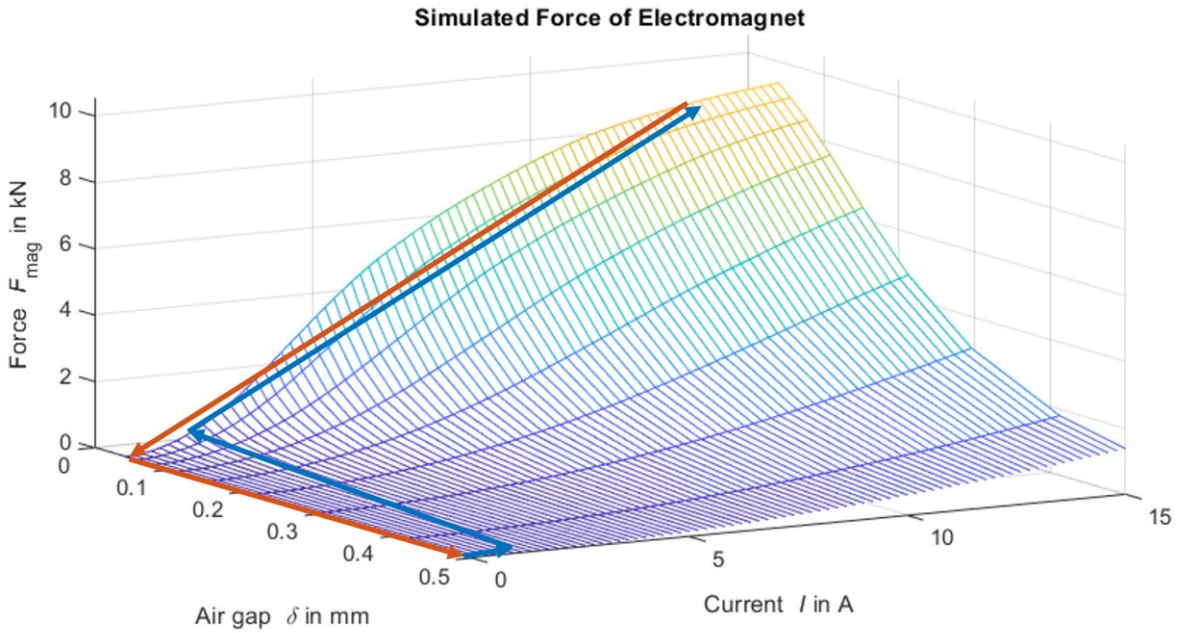

Figure 6-19: Progression of force, air gap for the hysteresis experiment in the simulated force characteristic of the actuator (blue arrows: current ascending, red arrows: current descending)

At the beginning of the braking process, the air gap between the armature disk and the magnet's yoke is at a maximum. To overcome the air gap, an initial current is required that pulls the magnet towards the armature disk against the return springs. In this case, this is about 2 A. Up to the range of 5 A, the torque increases sharply, and from this range onwards it increases linearly up to 14 A. When the brake is released, the curve closely follows the ascending curve from 14 A to approx. 4 A. The percentage deviations here are in the range of less than 10 % to about 6 A and less than 20 % to less than 3 A. Since the magnet is already in contact with the disc when the application current is lowered and therefore works at its minimum air gap, an axial force and thus a torque is generated up to almost 0 A, which is the reason for the large deviations of almost 100 % in the rising and falling torque curves in this current range.

In the range of small currents, a disadvantage of actuating a brake by means of a holding magnet becomes apparent. Due to the air gap, the generated torques in this range are dependent on the position of the magnet, which makes torque control more difficult. As soon as the magnet detaches from the armature disk, an initial current is required for the next actuation.

6.6 Tests on Torque Generation at Single Coil Failure

6.6.1 Goal

In this test the torque generation and dynamics over current shall be evaluated at a failure of one of the two coils in the magnet. An outage of one coil reduces the magnetic flux in the magnet, so that the brake only works with a degraded performance.

6.6.2 Execution

The brake is used in hybrid mode with different fallback configurations. The "Two Coil" configuration uses both coils as in the standard condition. The other two configurations are "Outer Coil", which only uses the coil with the larger diameter and the "Inner Coil" which uses the coil with the smaller diameter in the ring. The other coil is disconnected from the power supply. The test is done at constant velocities of $v = 2.5\ \mathrm{m/s}$ or $v = 9\ \mathrm{km/h}$ and constant voltages of $U = [1; 2; 3; 4; 5; 6; 7]\ \mathrm{V}$. Each test is repeated three times to reduce the influence of random measurement deviations. The temperature condition for the start of the next measurement is set to 50 °C. The tests are conducted on the slow moving dynamometer also used for the tests in chapter 6.3.

6.6.3 Evaluation

For the evaluation of the torques the torque signal and current are averaged over one rotation of the brake after its application. Figure 6-20 shows the result of the measurements for each configuration. As expected, the two coil configuration delivers the highest torques which are the baseline for the comparison for the torques reached by the fallback configurations. The outer coil reaches 708 Nm around 17 A of current, while the inner coil reaches 409 Nm. This amounts to a fallback performance of $\frac{708}{1184} = 60\ \%$ and $\frac{409}{1184} = 35\ \%$ respectively.

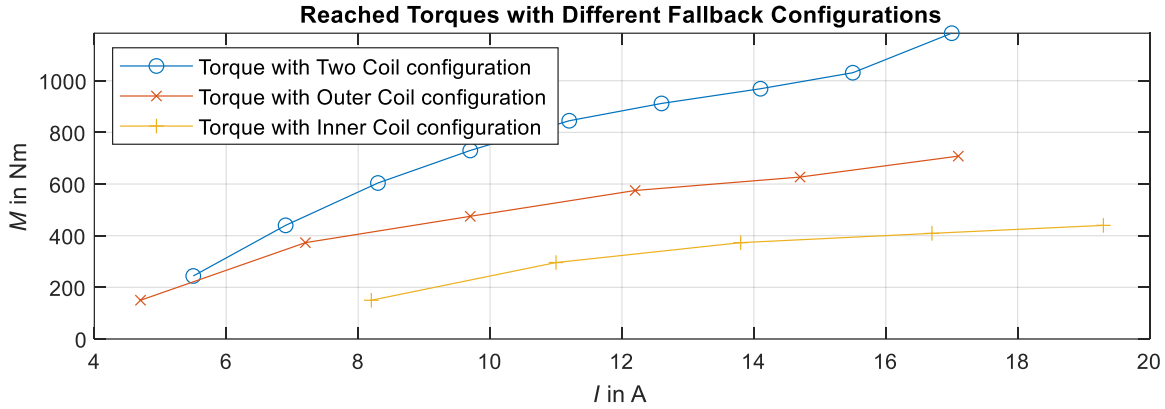

Figure 6-20: Torque over current for different fallback configurations of the magnetic hybrid brake

The dynamics of the brake application are measured and evaluated with the same method as in chapter 6.3. Figure 6-21 shows the calculated application times for 90 % of the end torque for the different configuration on a semilogarithmic scale.

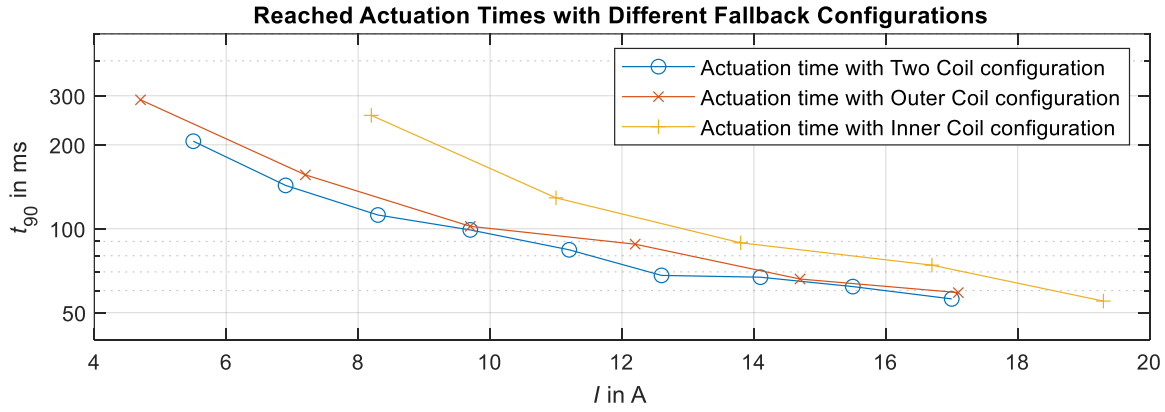

Figure 6-21: Actuation times to reach 90 % of end torque with different fallback configuration of the magnetic hybrid brake

As expected, the two coil configuration achieves the fastest dynamics as it delivers the highest magnetic forces. The outer coil achieves nearly the same dynamics, while the inner coil takes the longest to apply the brake. At around 17 A of current the two coil configuration achieves an application time of $t_{90} = 56$ ms, while the outer coil reaches 59 ms and the inner coil configuration 74 ms. All configurations achieve dynamics well below the 150 ms

mark, which is considered as a requirement for modern passenger cars for an emergency braking[76].

[76] Pinkow, S.: Cutting-edge brake technology MK C1 (2017).

6.7 Simulation of Temperatures for Developed Performance Cycles

Due to the non-achievement of braking torques at the whole velocity range, a simulation is carried out instead of a test to determine the temperature curve of the components during the developed performance tests, assuming that the brake generates the necessary torque. For this purpose, the finite volume simulation tool described in chapter 4.1.1 from Nowald et al. is used[77].

The drum geometry corresponds to the 10" drum used in chapter 4.1.1 chapter. The brake disc has the geometry shown in Figure 6-22.

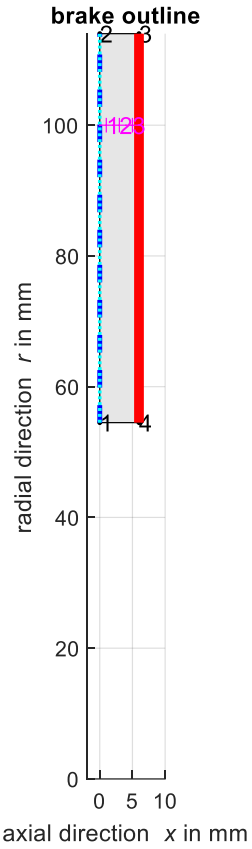

Figure 6-22: Geometric section of brake disc for thermal simulation (red: surface for heat input, magenta: points for temperature measurement, blue: surface for convection)

As the most powerful test with the highest energy input, again the STO test is used and selected as the maneuver for the simulation. To take into account the distribution of braking power between the components, 20 % of the total torque for the wheel is applied to the disc brake and the remaining 80 % to the drum brake.

[77] Nowald, G.; Siegl, B.: Thermal Simulation Tool for Early Sizing of Nonstandard Brake Concepts (2021).

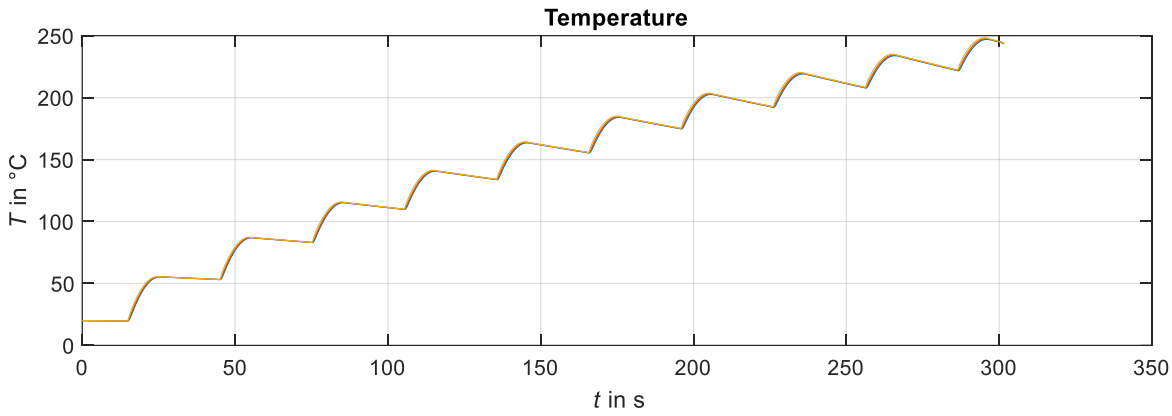

Figure 6-23: Temperature Curve for brake disc during STO Test

The temperatures at the evaluation points within the brake disc are very close to each other and differ only marginally (Figure 6-23). The maximum temperature reached is 250 °C. For the brake drum, the temperatures shown in Figure 6-24 are obtained.

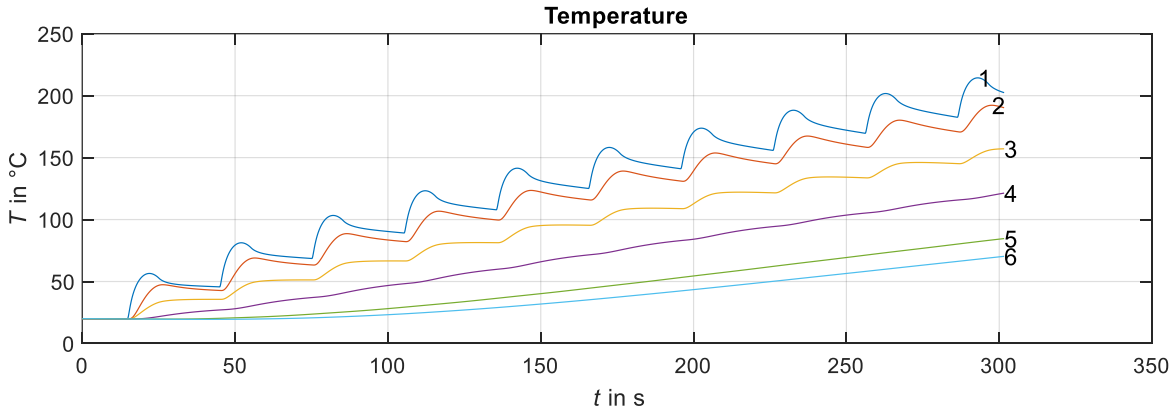

Figure 6-24: Temperature curve for brake drum during STO Test

The highest temperature reached is 215 °C at evaluation point 1. The temperature of the drum is thus far below the critical temperatures of drum brakes, which Vey places at around 400 °C[78].

With regard to the thermal design, it should be noted that the drum brake would be thermally capable of taking over a higher proportion of the braking power than the disc brake. However, this would require a shift in the torque ratio between the disc and drum brake.

[78] Vey, C.: Diss., Bremsmomentmessung für Simplex-Trommelbremsen (2021), p. 106.

6.8 Performance Identification Conclusion

The series of tests carried out to identify the concept's performance yields the following results:

- The developed actuator achieves the necessary magnetic forces which were calculated to actuate the brake.
- The dynamics of the actuator for passing through the air gap of 0.5 mm in the low current range (at 7 A) lies at approximately 70 ms, while for the release about 40 ms are needed.
- For highly dynamic actuations of the brake with high currents as in the case of an ABS control it takes 54 ms to reach 90 % of the end torque for the application and 57 ms for the release. The maximum frequency for the control thus amounts to approximately 17 Hz.
- The torque generated by the brake only meets the deceleration requirement at low velocities below 8 m/s . At high velocities, the torque drops sharply, 71 % at the maximum. The torque drop from the disc brake amounts to 57 %.
- Part of the torque loss is thus caused by the drum brake, but the majority originates from the electromagnetic disc brake. The occurring effects remain to be investigated.
- The two coil design offers an additional redundancy which enables a degraded functionality, if one of the coils fails. The fallback performance according to torque for the outer coil lies at a torque ratio of 60 % and 35 % for the inner coil. For dynamics the fallback performances lie below 75 ms for the application of the brake for high currents for emergency stops.
- The thermal simulation for the components of the hybrid brake show that for the developed brake cycles, the temperatures stay below 250 °C. The drum itself could manage a higher thermal energy intake, which would require a redesign considering the thermal heat flux ratio of the different components.

7 Effect Analysis and Discussion

To investigate the cause of the unexpected decrease in torque at higher speeds, especially in disc operation, two hypotheses are set up and falsification tests based on them are carried out. The loss in torque of the drum brake itself will not be researched further, as the disc brake component represents the center of interest for the braking concept.

1. The drop in torque is caused by a decreasing axial force over velocity due to magnetic field weakening (due to eddy currents or mechanically induced air gap fluctuations)
2. The drop in torque is caused by a velocity-dependent coefficient of friction between the magnetic ring and the armature disc

7.1 Falsification Tests for Hypothesis 1: Magnetic Field Weakening During Operation

The underlying hypothesis assumes a weakening of the magnetic force during operation as a function of the rotational speed. The magnetic force of an electromagnet largely depends on the flux density B, the flux-carrying area A and the permeability in the air gap μ_0 . Maxwell's formula of magnetic traction force[79] shows this relationship:

$$F_{\mathrm{mag}} = \frac{B^2 A}{2\mu_0} \tag{7-1}$$

The effective flux density in the prototype is influenced by the size of the air gap present, by arising eddy currents that counteract the flux density, and by saturation effects in the material through which the flux is flowing. Eddy currents occur in the electrically conducting material when there is a change in flux density. The necessary potential difference arises from the induced voltage U_{ind}, which is proportional to the change in flux density $\dot{B}$ in the material. However, if the geometry of the prototype is considered ideally and without an eccentricity, no change in the flux density can be assumed, since the flux does not change under rotation of the armature disc, i.e., when considered over the circumference (Figure 7-1).

[79] Kallenbach, E. et al.: Elektromagnete (2018), p. 77.

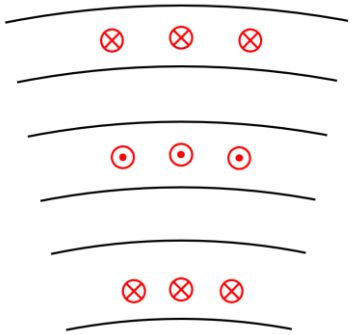

Figure 7-1: Magnetic flux through an angular cutout of the yoke ring

The same applies to the radial flux profile. In reality, however, there can be deviations in the centric arrangement between the magnetic ring and the armature disc, which can cause a radial flux density change in the disc over one rotation. The brake surface used in a Warner Brake concept however, would encounter two points of high gradients in the flux density, the first one being the entry into the magnetic field of the magnet and the second one on the exit of the same field.

A second chain of effects to weaken the flux density would be an increase of the mean air gap when the brake is applied depending on the rotational speed, which would be due to dynamic effects. If one of these phenomena were to weaken the magnetic flux density, in this case saturation would have to occur only at a higher excitation (at a higher current).

The investigation of the torque generation of the disc brake (Figure 6-8) shows a typical saturation curve of the flux density in the materials of the magnetic circuit. If there was a field weakening effect in the area of higher speeds this saturation would shift to higher excitations (meaning higher currents). Figure 7-2 shows the torque curve over currents in a normalized display, by dividing all torque values of each velocity with the torque value at 14 A. The graph shows that each curve has its point of inflection in the range of $7 - 8$ A. This observation consequently argues against the hypothesis of a field weakening effect.

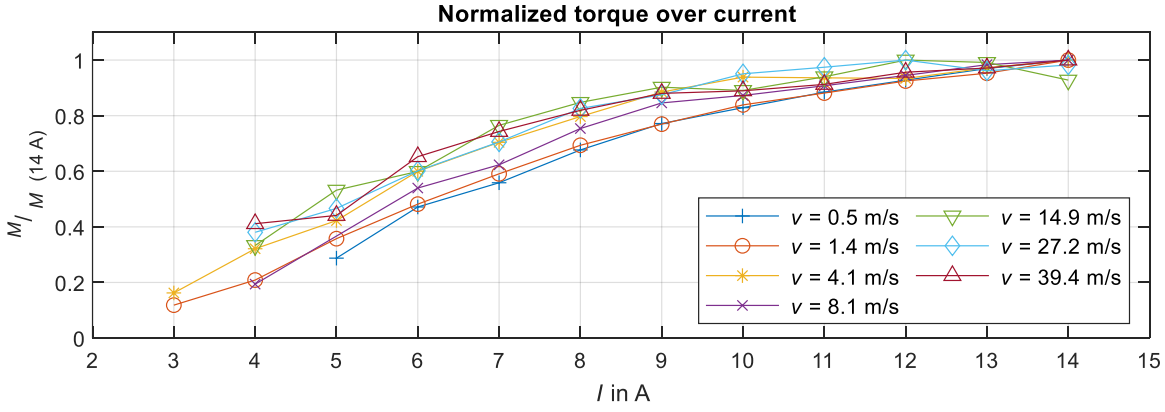

Figure 7-2: Normalized torque curve of disc brake

In order to be able to make a more substantiated statement about the effective magnetic force, the change in flux density is identified via induced voltages in a separate experiment using several measuring coils introduced into the flux path of the magnet.

7.1.1 Goal

The aim of the experiment is to identify the effective magnetic flux density at different currents and speeds and thus to estimate the axial force in the disc brake system.

7.1.2 Execution

For the experiment, fixed speeds are approached with the dyno test bench at $v = [2\ 10\ 15\ 20\ 40\ ]\ \mathrm{m/s}$ and fixed currents of $I = [8\ 12\ 16\ 20]$ A are set.

The testing method to get an estimation on the flux density was developed in a student thesis[80]. For this purpose, a new magnet design was developed, which includes six measurement coils, that are inserted into the flux path of the inner and outer leg of the magnet (Figure 7-3).

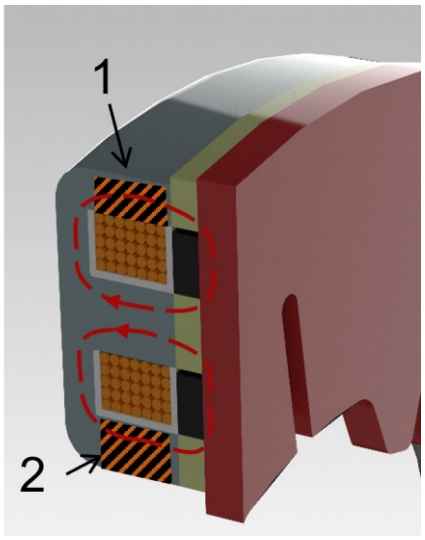

Figure 7-3: Positioning of the measurement coils in the magnetic flux path (1: outer measurement coil, 2: inner measurement coil)

To install the coils a new yoke was designed including radial slots, that enable the installation of the coils (Figure 7-4). To achieve a higher amplification, six coils were installed on the inner leg and six coils on the outer leg of the yoke ring.

[80] Schrimpf, M.: Master Thesis, Messtechnikkonzept zur Flussdichtemessung (2021).

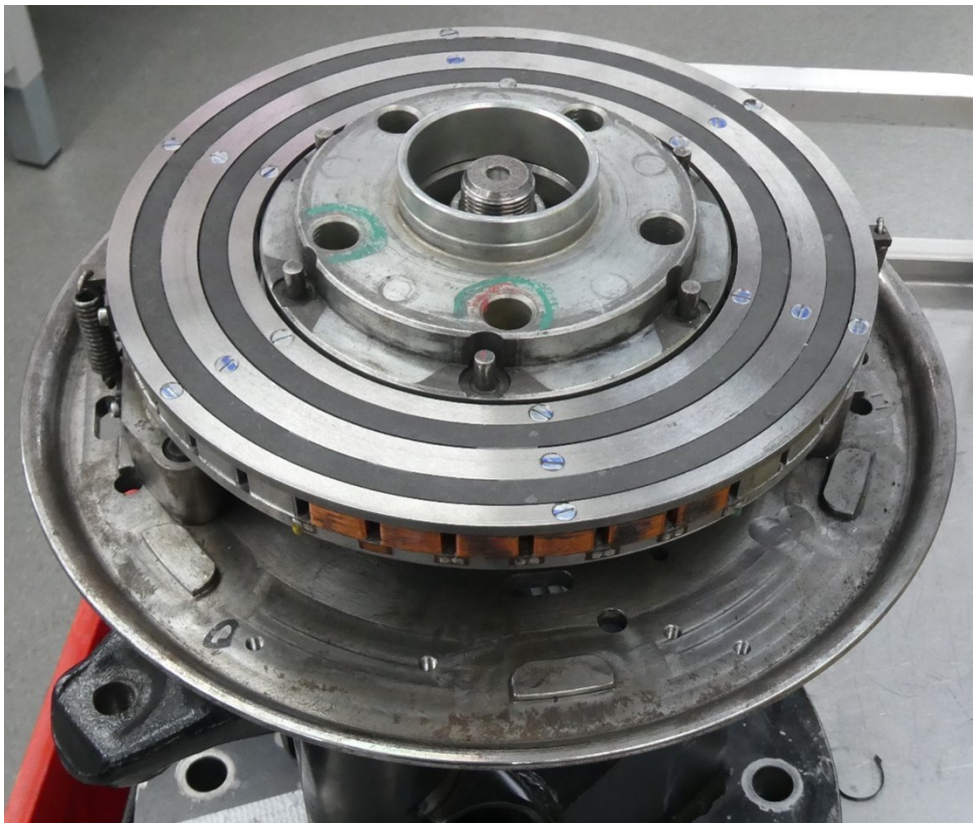

Figure 7-4: Assembled measurement yoke with six measurement coils

To measure the induced voltages of the coils a digital oscilloscope with a high measurement frequency of 30 kHz is used. The evaluation method compensates for magnetic remanence and drift of the integral due to voltage offset.

After reaching the set velocity, the induced voltages of the measuring coils are recorded during the actuation and release of the brake for a measurement period of 2 s. Figure 7-5 shows the overall setup on the full speed range dynamometer.

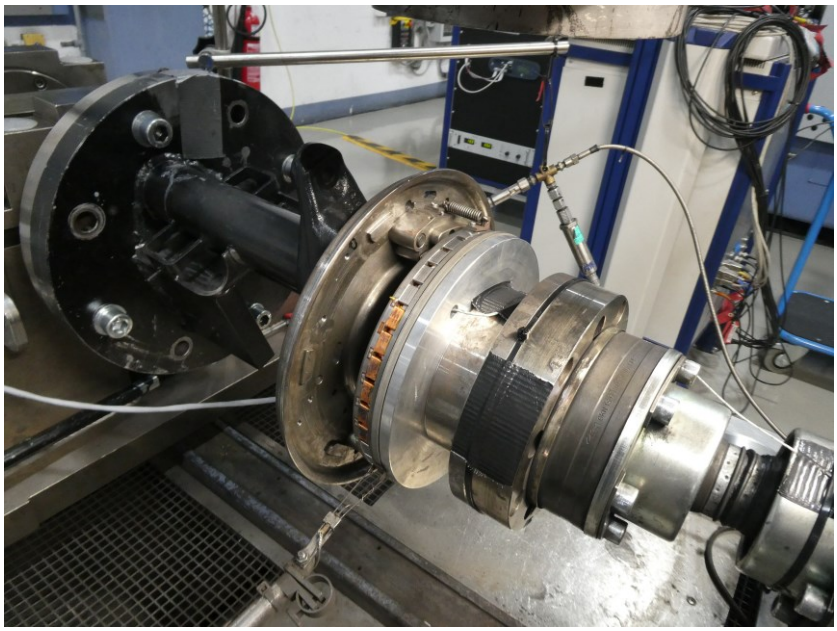

Figure 7-5: Test bench setup with measurement yoke on dynamometer in disc setup

7.1.3 Evaluation

The series of experiments yields the following flux densities versus velocity. Figure 7-6 shows the flux density over the center leg of the magnetic ring, which is calculated as the sum of the measured flux of the outer and inner leg.

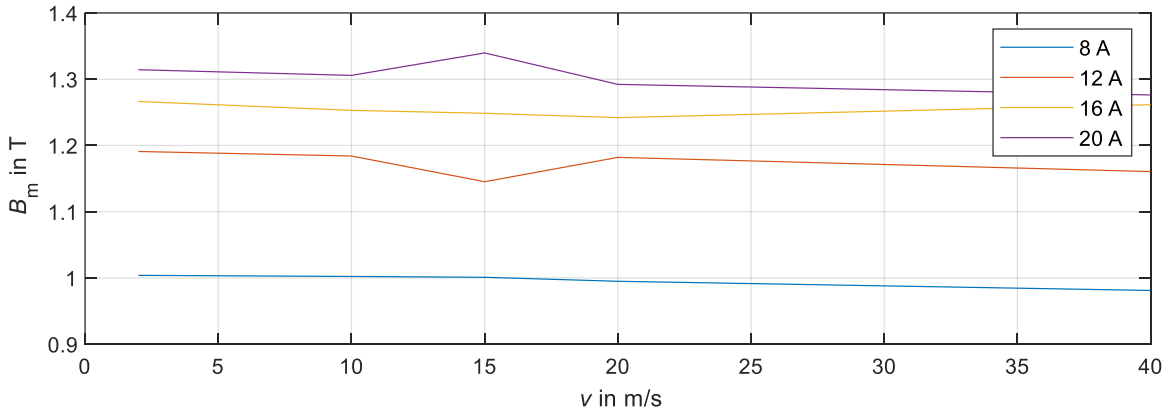

Figure 7-6: Flux density of the center leg of the yoke ring over vehicle velocity

Maxwell's formula of magnetic traction force can be used to calculate the acting axial forces considering all three legs of the yoke and to plot them against velocity (Figure 7-7).

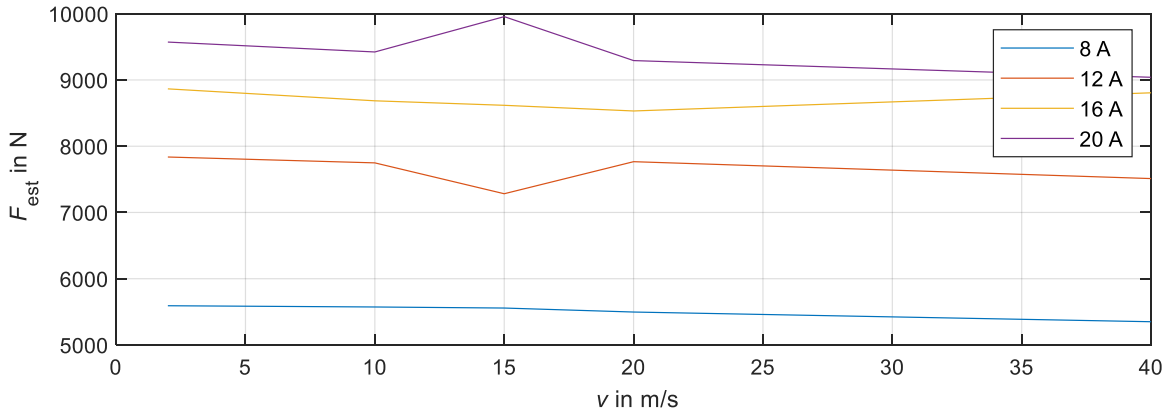

Figure 7-7: Actuator force estimation based on the calculated flux density

The estimated forces of the actuator are consistently higher than the identified pull-off forces of the actuator without measuring coils in Figure 6-2, but a direct comparison of the values is not valid due to the deviating design of the magnetic ring including the measurement coils.

The highest percentage deviation in force between slow and fast speeds can be observed at 20 A and amounts to 5.6 %, which is not sufficient to explain the 71 % drop in braking torque that was observed earlier. Consequently, the decrease of the friction torque over the velocity does not have its cause in a significant decrease of the magnetic flux density or magnetic force. The hypothesis of the drop in torque due to field weakening during operation is thus falsified.

7.2 Falsification Tests for the Hypothesis "Speed-Dependent Coefficient of Friction between Magnet and Armature Disc"

7.2.1 Goal

The aim of the experiment is to identify the coefficient of friction of the armature disc and cast friction rings as a function of speed and contact pressure. To do so, it is necessary to know the acting axial force and the resulting circumferential force.

7.2.2 Execution

For the execution of the experiments, an adaptation of the design is made. Since the magnetic force in operation can only be estimated by derivation from flux density, the full-pad disc brake is actuated by hydraulic cylinders (Figure 7-8), which provide more precise knowledge of the axial force via the hydraulic pressure. Since the axial tensile force acts only between the cast rings and the armature disc in magnetic operation, the two friction material rings are

removed for this experiment. The velocities are set to $v = [2; 10; 15; 20; 40]\,\frac{\mathrm{m}}{\mathrm{s}}$. The pressure levels are also varied with $p = [5; 10; 30; 55]$ bar, which corresponds to axial forces of $F_{\mathrm{ax}} = [1;\ 2;\ 6; 11]$ kN. To reduce the influence of random measurement deviations, the measurements are repeated three times. The test bench setup on the full speed range dynamometer can be seen in Figure 7-9. The hydraulic pressures are measured using a HBK P3 pressure sensor[81].

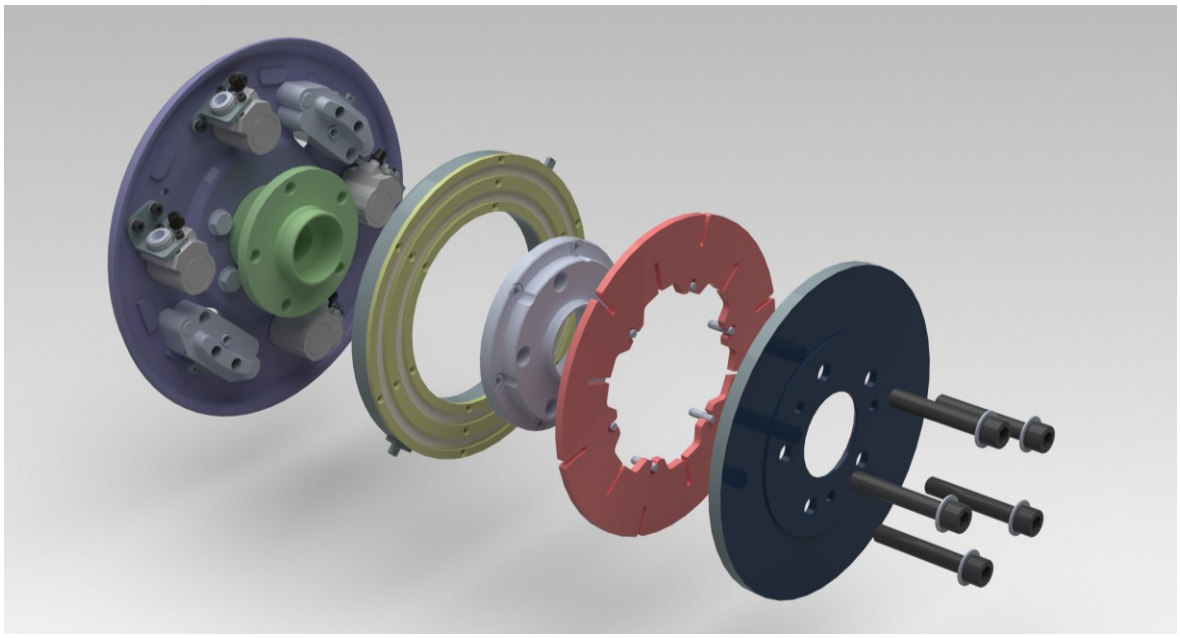

Figure 7-8: Exploded view of the assembly for hydraulic actuation of the yoke ring without friction lining rings

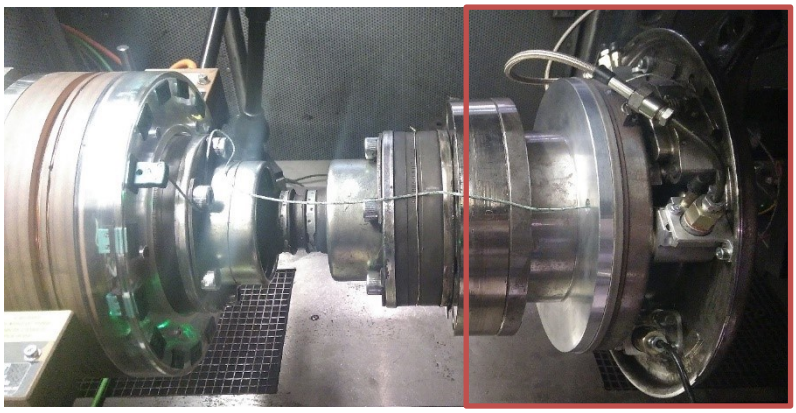

Figure 7-9: Hydraulic actuation assembly (red frame) on dynamometer test bench

[81] HBK Germany: Druckaufnehmer P3 Top Class (2022).

7.2.3 Evaluation

The evaluation shows that the coefficient of friction of the cast rings on the armature disc, which are mainly involved in the friction pairing, drops sharply over velocity (Figure 7-10). The friction values were calculated assuming a constant effective friction radius and averaged over the three repetitions in each case. The coefficient of friction also decreases with increasing contact pressure. For low speeds friction values in the range $0.37 < \mu < 0.67$, are obtained, and in the range of higher speeds only $0.11 < \mu < 0.24$, corresponding to a percentage change of 70 % and 67 %, respectively. The friction values at low speeds are much higher than the ones assumed for the initial dimensioning of the brake. Additionally, a dependency on surface pressure becomes apparent, with higher surface pressure the friction coefficient decreases.

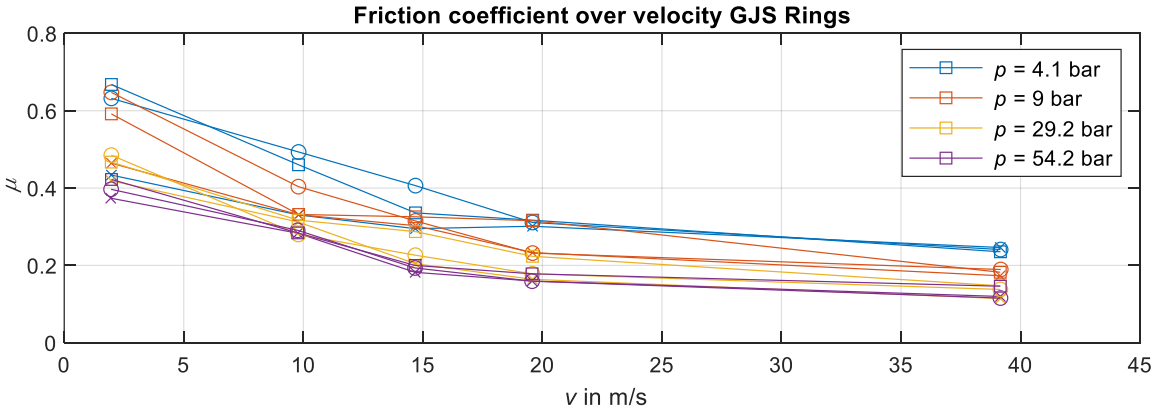

Figure 7-10: Coefficient of friction versus speed of GJS rings, including repetition of measurements marked with x and o

The result of this test shows that the hypothesis of the speed-dependent coefficient of friction cannot be falsified and therefore withstands. Looking ahead, there is the question of the involvement of the friction lining rings in friction force generation. This cannot be clarified with the hydraulic setup, since in magnetic operation the tensile forces exist only in the air-gap between the armature disc and the cast friction rings, whereas the hydraulic test setup would generate compressive forces over the entire ring's friction surface.

7.3 Tests on the Enhancement to the Lower Torque Range using Current Pre-Control

7.3.1 Goal

The goal of this test is to identify the height of a current jump that is needed, to lift the magnet from his resting position and attach it reliably to the armature disc. After the attachment a lower current can be set to reach the lower torque range of the brake, which narrows

the gap of the hysteresis curve shown in Figure 6-18. The progression through the force characteristic of the magnet using pre-control is shown in Figure 7-11.

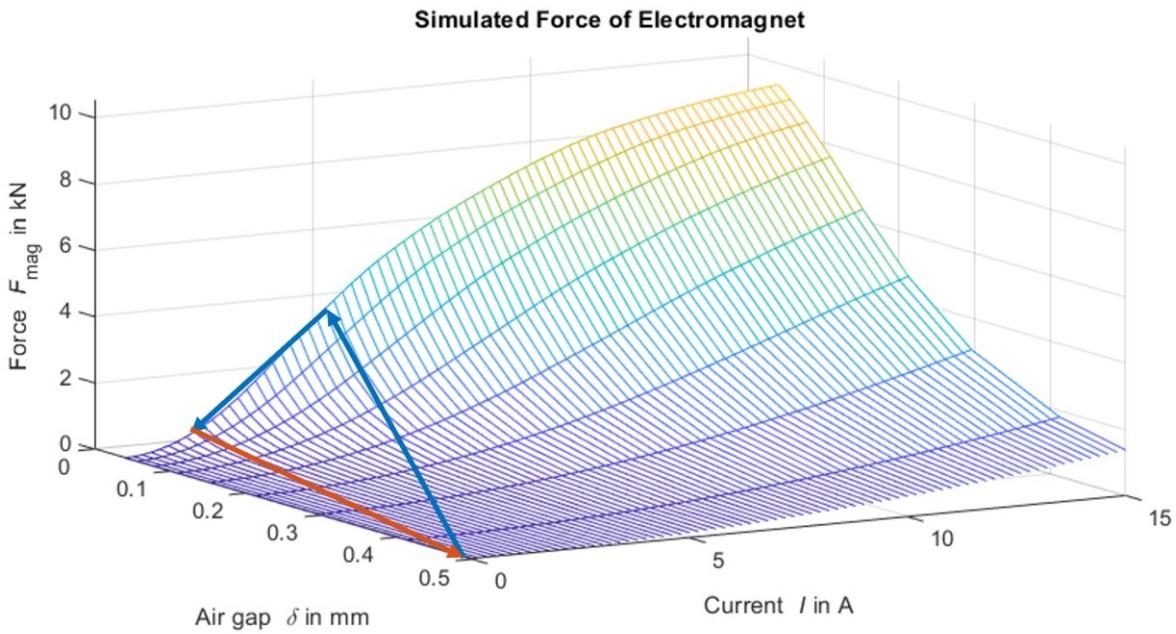

Figure 7-11: Progression through force characteristics using current pre-control to approach a set point of low torque (blue arrows: application of brake, orange arrows: release)

7.3.2 Execution

Like in all tests conducted before, an initial air gap of 0.5 mm is set using thickness gauges while assembling the prototype. To overcome the force of the return springs at the initial air gap of 0.5 mm a voltage jump of 10 V is applied. Similar to Figure 6-3, the time for the magnet to attach to the disc can be extracted from the current characteristics. This time is taken as the duration of the pre-control voltage. The voltage setpoints for the lower torque ranges are set to $U_{\mathrm{set}} = [5;\ 4;\ 3;\ 2]$ V. With those inputs a test for a voltage pre-control is performed, which adds a voltage jump before the actual smaller voltages are set to get in the lower torque ranges. To evaluate the test, the torque gradients are then compared to the maximum jerk values that are considered comfortable (Table 3-3). The tests are conducted on the slow-moving dynamometer.

7.3.3 Evaluation

Figure 7-12 shows an example run performed with the voltage pre-control method.

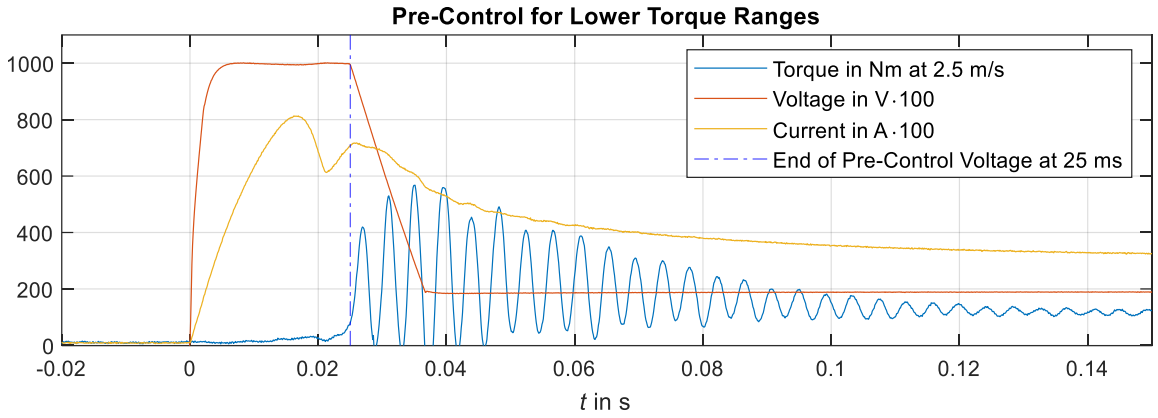

Figure 7-12: Method to advance functionality of the hybrid brake to lower torque ranges (brake in hybrid mode)

The diagram shows the pre-control phase (from $0 - 25$ ms) and the following braking phase. With a setpoint voltage of 2 V and a final current at about 3 A a torque of 115 Nm can be generated by the brake. Based on the current characteristics the magnet is fully attached to the disc at about 22 ms, the duration for the pre-control voltage was chosen as 25 ms.

The oscillations of the torque curve are probably caused by the stick-slip effect of the magnet on the armature disc. The forces acting on the magnet to cause it to slip are the forces of the brake shoes and their return springs. To decrease the torque oscillations a damping element should be installed between the magnet's teeth and the brake shoes. Unfortunately, the oscillations in torque do not allow a reasonable calculation on jerk values on the vehicle body.

For all three trials the mean torque values for one full rotation were calculated and averaged. The results are shown in Figure 7-13. At the speed of approximately 1.9 m/s the lowest reached torques at 2 V or 3.1 A are 72 Nm. At a higher speed level of 2.5 m/s the magnet tends to detach from the armature plate at a current of 3.1 A, so that the pre-control method does not generate a steady torque output at those low currents. That behaviour of the brake reveals one major challenge for the usage in low torque ranges, which is the state detection for the magnet, if it is attached to the armature disc, or not. An additional sensor would be needed to get this information, if no torque sensor is used in the brake. Another possibility is to use the pre-control voltage jumps more than once during the application of the brake, if this doesn't affect the ride comfort of the passengers due to jerk in a critical way.

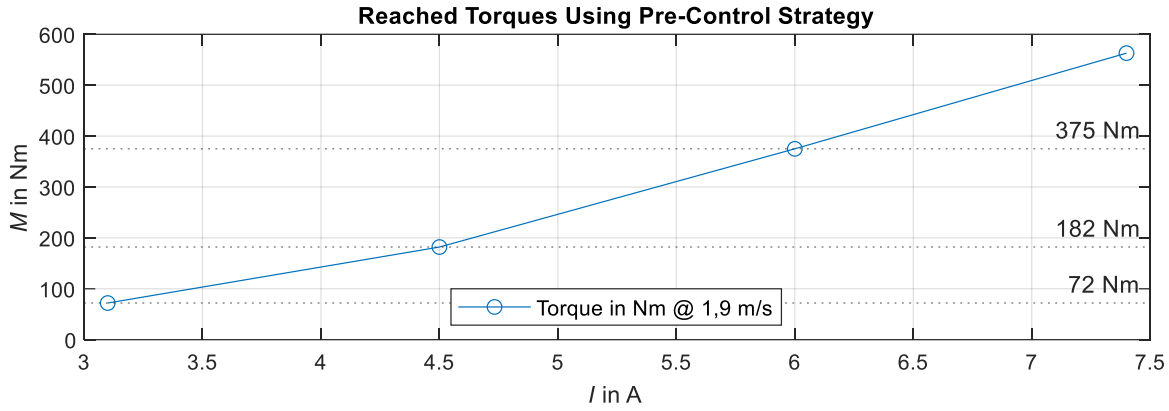

Figure 7-13: Reached torques with pre-control strategy

8 Conclusion and Outlook

The research on current development trends in the automotive industry provides the motivation to consider a group of vehicles that combines these trends and in the near future could account for a significant share of urban traffic. This group is made up of electrified, autonomous shuttles, and this thesis investigated a magnetic braking concept for the use in this group of vehicles.

8.1 Conclusion

Three research questions are addressed:

1. *What are the requirements for wheel brakes of highly automated, electrified shuttles?*
2. *Which wheel brake concepts are particularly suitable for highly automated, electrified shuttles?*
3. *Is a magnetically actuated hybrid brake able to fulfill the requirements for an autonomous shuttle and are the presumed advantages valid?*

The used method of a combined stakeholder analysis and a semantic analysis of today's passenger car requirements to answer the first research question led to the following findings:

- The major difference in requirements to today's passenger cars originates from the absence of a driver in the vehicle.
- The shuttle's ODD limits the accelerations to a comfortable level
- For collision avoidance the brake still needs to ensure the full utilization of the friction coefficient between tire and road.
- Depending on the function range of the electric drivetrain, the friction brake is mainly used for brakings in the upper deceleration ranges, e.g., for collision avoidance.
- New performance cycles had to be developed, which were based on the vehicle's ODD and driving scenarios.

Due to the change in requirements the pool of concept solutions regarding wheel brakes was examined for suitability to answer the second research question. As an alternative to electromotively actuated wheel brakes, an electromagnetical concept, the hybrid brake, was chosen for a performance identification. The actuator is designed as a holding magnet, which fits into the usual drum brake installation space completely. The concept promises significant advantages over an electromechanical drum brake, especially in terms of usage of installation space, low mechanical complexity and additional fail-safe capabilities when using both coils with separate current control circuits. To find an answer for the third research question, a prototype was set up and performance tests were conducted.

The following advantages over electromotively actuated wheel brakes were verified during the performance tests:

- In the same installation space as a hydraulic drum brake, the hybrid brake houses actuation, modulation and foundation.
- The dynamics for torque generation are sufficient for ABS braking maneuvers.

Next to the advantages one major flaw of the concept was identified:

- The torque generation is highly dependent on the angular velocity of the wheel.

The effect was analysed using hypothesis-based testing and it was found that:

- The torque loss is not based on a decrease in the effective axial force or flux density. The influence of field-weakening effects is not observable.
- The torque loss is based on the friction coefficient between the electromagnet and the disc.

The analysis of the results shows the development conflict that has arisen due to the dual function of the actuator material through which the magnetic field flows. To improve the behavior, a material is needed that has both good magnetic properties and is a good friction partner for the disc.

8.2 Outlook

With the present results and findings, further questions are raised, the investigation of which promises a gain in knowledge for the topic of electromagnetic brake actuation.

The friction instability of the cast material and the armature disc has highlighted the development conflict of the dual function of the material. An application of a sufficiently thick friction layer will cause a significant loss of force for the actuator. If a thin layer of material were to be applied to the armature, which could stabilize the friction value, it would have to remain in place over the service life of the brake and thus be extremely wear-resistant. This reveals the following research question:

Is there a material or a material pairing that sufficiently fulfils the dual function of sufficient conduction of the magnetic flux and friction coefficient stability with the armature disc?

Another solution for achieving this goal is to separate the dual function into two individual functions and assign them to individual components. However, this requires a turn from the concept of the holding magnet, which operates at a minimum air gap, since a friction material must be used to which the magnetic force must be transferred in order to achieve friction stability. In this case, the magnet itself must operate with a sufficient residual air gap so that the armature does not come to rest against the yoke itself and the magnetic force is no longer generated between the friction material and the disc like shown in Figure 8-1. Optimally, such a magnet would achieve a linear operating range by means of characteristic

optimization, so that the actuation force is independent of the magnet's air gap and wear adjustment is not required.

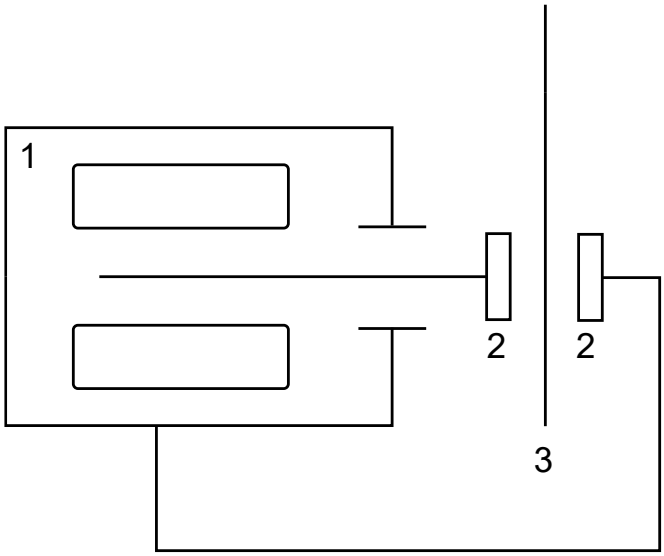

Figure 8-1: Magnetic caliper concept; 1: solenoid, with coil and armature, 2: brake pads, 3: brake disc

The associated research question is:

Is a characteristic-optimized solenoid suitable for the application of a brake?

Looking at torque control technology, the question arises as to the feasibility of a sufficient control for the hybrid brake. As only one prototype was tested in this thesis, the variation of torque between two brakes of the left and right wheels needs to be determined. If the variations are above the level of regulations, at least one torque sensor would be required for control, for example as investigated by Vey[82]. The associated, prospective research question is:

Is an additional sensor needed to consider torque variations between the left and right hybrid brake in a vehicle?

Answering the questions listed would create a deeper understanding in the pros and cons of using magnets to actuate wheel brakes.

In the area of determining requirements for wheel brakes of future mobility concepts, it must be checked whether the assumptions made prove to be valid for real traffic. At the time of the work, the vehicles mentioned in the state of the art are so far only on closed driving routes, but an extension to real traffic is being planned[83]. Such projects provide an opportunity for researchers to record data and conduct comfort evaluation studies.

[82] Vey, C.: Diss., Bremsmomentmessung für Simplex-Trommelbremsen (2021).

[83] RMV: Erste autonom fahrende On-Demand-Flotte ab 2023 (2022).

Appendix

A.1 Simulation Output of Car Maker Model

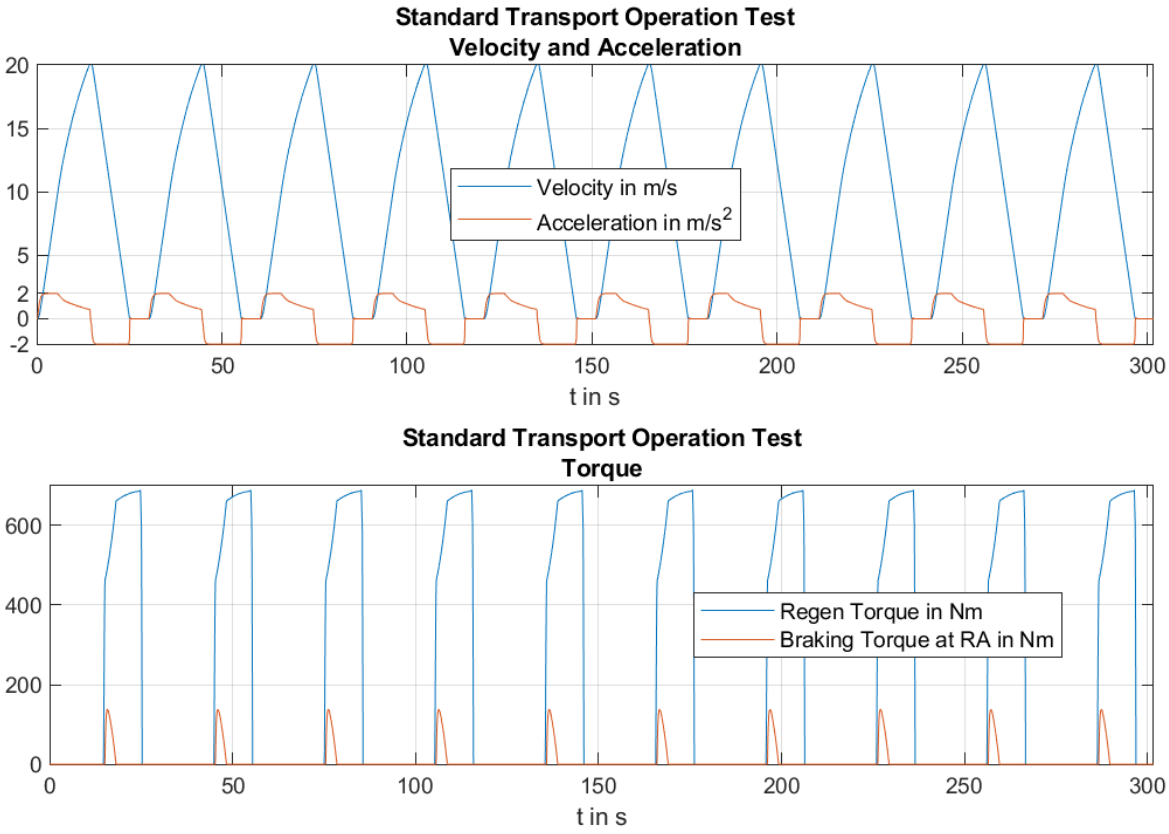

Figure 8-2: Simulation output in Standard Transport Operation Test with 50 % SoC in the beginning

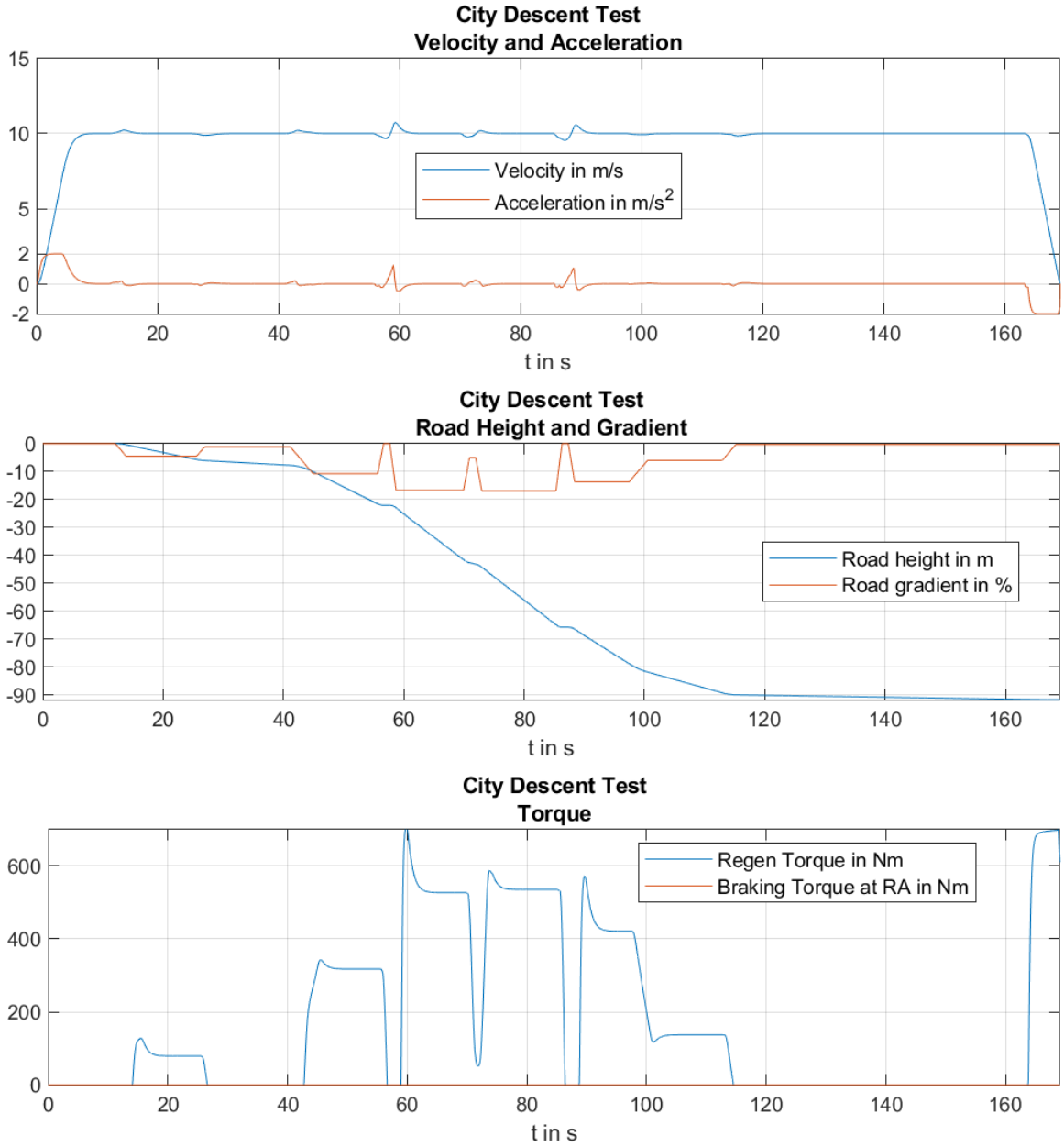

Figure 8-3: Simulation output of City Descent Test with 50 % SoC in the beginning

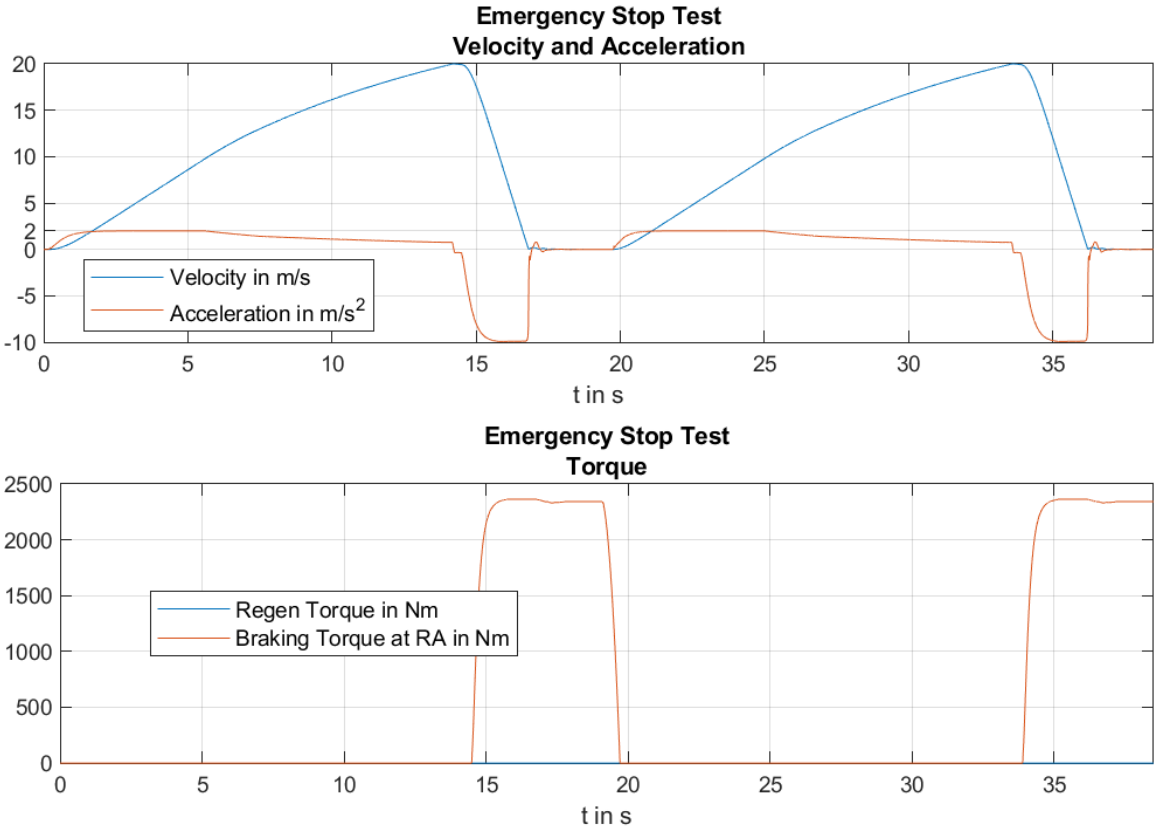

Figure 8-4: Simulation output in Emergency Stop Test without regenerative braking

Bibliography

2getthere: GRT vehicle: automated minibus (2018)
2getthere: GRT vehicle: automated minibus; https://www.2getthere.eu/grt-vehicle-automated-minibus/, 2018, Access 09.08.2019

2getthere: PRT vehicle: automated taxi (2018)
2getthere: PRT vehicle: automated taxi; https://www.2getthere.eu/prt-vehicle-automated-taxi/, 2018, Access 13.01.2020

Autoteile Ralf Schmitz Handel GmbH: Was wurde eigentlich aus der Keilbremse? (2022)
Autoteile Ralf Schmitz Handel GmbH: Was wurde eigentlich aus der Keilbremse?; https://www.at-rs.de/beitrag/items/was-wurde-eigentlich-aus-der-keilbremse.html, 2022, Access 27.07.2022

Bach, U. et al.: Trommelbremse für ein drehbares Element (2019)
Bach, Uwe; Guckes, Lennart; Gädke, Martin; Stauder, Peter; Hoffmann, Jens; Pla, Sébastien: Trommelbremse für ein drehbares Element, CONTINENTAL TEVES AG & CO OHG [DE], Patent DE102019209523 (A1), Patent application number: DE201910209523 20190628, 2019

Bae, I. et al.: Toward a Comfortable Driving Experience for a Self-Driving Shuttle Bus (2019)
Bae, Il; Moon, Jaeyoung; Seo, Jeongseok: Toward a Comfortable Driving Experience for a Self-Driving Shuttle Bus, in: Electronics (9), Issues 8, p. 943, 2019

Balz, J.: Expertengespräch zu Leistungsklassen Aktoren für Radbremsen (2022)
Balz, Jürgen: Leistungsklassen elektromechanischer Aktoren für Radbremsen, 2022

Baumgartner, H. et al.: Nutzfahrzeugbremsen (2017)
Baumgartner, Hans; Gerum, Eduard; Pahle, Wolfgang; Siebke, Alf; Pehle, Michael: Nutzfahrzeugbremsen, in: Breuer, Bert; Bill, Karlheinz H. (Eds.): Bremsenhandbuch, Springer Fachmedien Wiesbaden, Wiesbaden, 2017

Bill, K. H.: Grundlagen elektrisch betätigter Pkw-Bremssysteme (2017)
Bill, Karlheinz H.: Grundlagen elektrisch betätigter Pkw-Bremssysteme, in: Breuer, Bert; Bill, Karlheinz H. (Eds.): Bremsenhandbuch, Springer Fachmedien Wiesbaden, Wiesbaden, 2017

Breuer, B.; Bill, K. H.: Bremsenhandbuch (2017)
Breuer, Bert; Bill, Karlheinz H. (Eds.) Bremsenhandbuch, Springer Fachmedien Wiesbaden, Wiesbaden, 2017

Buffington, J.; Enns, D.: Daisy chain control allocation
Buffington, James; Enns, Dale: Daisy chain control allocation - Lyapunov stability analysis, in: Guidance, Navigation, and Control Conference

Bugatti Automobiles S.A.S.: Bugatti Veyron Technik (2022)
Bugatti Automobiles S.A.S.: Bugatti Veyron Technik; https://www.bugatti.com/de/modelle/veyron-modelle/technik/, 2022, Access 26.07.2022

Carlier, M.: Number of electric vehicles in use by type 2016-2020 (2021)
Carlier, Mathilde: Number of electric vehicles in use by type 2016-2020; https://www.statista.com/statistics/1101415/number-of-electric-vehicles-by-type/, 2021, Access 04.05.2022

Chauvin Arnoux: Current Clamp for AC/DC Current (2022)
Chauvin Arnoux: Current Clamp for AC/DC Current; https://catalog.chauvin-arnoux.com/fr_de/pince-e27.html, 2022, Access 24.11.2022

Continental AG: New Wheel Concept (2017)
Continental AG: Continental stellt erstmalig innovatives Rad- und Bremskonzept für Elektrofahrzeuge vor; https://www.continental.com/de/presse/pressemitteilungen/innovatives-radkonzept-und-bremskonzept-fuer-elektrofahrzeuge/, 2017, Access 06.06.2022

Copernicus: California Street (2020)
Copernicus: California Street, Google Earth Pro, 2020

Diehl, P.: Schraubzwinge (2015)
Diehl, Peter: Schraubzwinge, in: Auto Service Praxis (7), pp. 18–19, 2015

e.GO MOOVE GmbH: Our Concept (2020)
e.GO MOOVE GmbH: Our Concept; https://e-go-moove.com/en/our-concept/, 2020, Access 13.01.2020

FISITA: Euro Brake 2021 (2021)
FISITA (Ed.) Euro Brake 2021, 2021

Gay, S.: Diss., Contactless Magnetic Brake (2005)
Gay, Sebastien: Contactless Magnetic Brake For Automotive Applications, Dissertation Texas A&M University, 2005

Gombert, B.; Gutenberg, P.: Die elektronische Keilbremse (2006)
Gombert, Bernd; Gutenberg, Philipp: Die elektronische Keilbremse, in: ATZ - Automobiltechnische Zeitschrift (11), Issues 108, pp. 904–913, 2006

Guckes, L. et al.: Requirements and Test Cycles for Brake Systems of Autonomous Vehicle Concepts on the Example of an Autonomous Shuttle (2021)
Guckes, Lennart; Winner, Hermann; Hoffmann, Jens; Pla, Sébastien: Requirements and Test Cycles for Brake Systems of Autonomous Vehicle Concepts on the Example of an Autonomous Shuttle, in: FISITA (Ed.): Euro Brake 2021, Barcelona, 2021

Hagino, H. et al.: Laboratory testing of airborne brake wear particle emissions using a dynamometer system under urban city driving cycles (2016)
Hagino, Hiroyuki; Oyama, Motoaki; Sasaki, Sousuke: Laboratory testing of airborne brake wear particle emissions using a dynamometer system under urban city driving cycles, in: Atmospheric Environment, Issues 131, pp. 269–278, 2016

Hans Wegmüller AG: Wirbelstrombremsen (2022)
Hans Wegmüller AG: Wirbelstrombremsen; https://hwag.com/wirbelstrombremsen/, 2022, Access 26.07.2022

Harloff, T.: Warum die Trommelbremse des ID.3 sinnvoll ist (2020)
Harloff, Thomas: Warum die Trommelbremse des ID.3 sinnvoll ist; https://www.auto-motor-und-sport.de/tech-zukunft/alternative-antriebe/vw-elektroauto-warum-die-trommelbremse-des-id-3-sinnvoll-ist/, 2020, Access 06.06.2022

Hasberg Schneider GmbH: Präzisions-Lehrenbänder und Unterlagsfolien (2022)
Hasberg Schneider GmbH: Präzisions-Lehrenbänder und Unterlagsfolien; https://www.hasberg-schneider.de/leistungen/praezisions-lehrenband-sonderbreiten/, 2022, Access 22.11.2022

HBK Germany: Druckaufnehmer P3 Top Class (2022)
HBK Germany: Druckaufnehmer P3 Top Class; https://www.hbm.com/de/2480/p3-top-class-druckaufnehmer-mit-temperaturkompensation/?product_type_no=P3%20Top%20Class:%20Pr%C3%A4ziser%20Druckaufnehmer%20der%20Spitzenklasse, 2022, Access 24.11.2022

HBK Germany: Kraftsensor U10 (2022)
HBK Germany: Kraftsensor U10; https://www.hbm.com/de/2410/u10m-u10s-kraftaufnehmer-fuer-statische-und-dynamische-zug-und-druckkraefte/?product_type_no=U10, 2022, Access 24.11.2022

Hoffmann, J.; Wörsdörfer, K.-F.: End of oversizing: smart designing of brake systems for BEVs (2020)
Hoffmann, Jens; Wörsdörfer, Karl-Friedrich: End of oversizing: smart designing of brake systems for BEVs, in: Pfeffer, Peter E. (Ed.): 10th International Munich Chassis Symposium 2019, Proceedings, Springer Fachmedien Wiesbaden, Wiesbaden, 2020

Huber, A.: Continental Trommelbremse für die Vorderachse (2021)
Huber, Andreas: Continental Trommelbremse für die Vorderachse; https://www.autobild.de/artikel/continental-trommelbremse-fuer-die-vorderachse-2021-golf-gti-elektroauto-bremstechnik-20873203.html, 2021, Access 18.07.2022

Ivanov, V. et al.: A Survey of Traction Control (2015)
Ivanov, Valentin; Savitski, Dzmitry; Shyrokau, Barys: A Survey of Traction Control and Antilock Braking Systems of Full Electric Vehicles With Individually Controlled Electric Motors, in: IEEE Transactions on Vehicular Technology (9), Issues 64, pp. 3878–3896, 2015

Kallenbach, E. et al.: Elektromagnete (2018)
Kallenbach, Eberhard; Eick, Rüdiger; Ströhla, Tom; Feindt, Karsten; Kallenbach, Matthias; Radler, Oliver: Elektromagnete, 5. Edition, Vieweg, Wiesbaden, 2018

Katharina Buchholz: Cars Increasingly Ready for Autonomous Driving (2021)
Katharina Buchholz: Cars Increasingly Ready for Autonomous Driving; https://www.statista.com/chart/25754/newly-registered-cars-by-autonomous-driving-level/, 2021, Access 04.05.2022

Klumpner, A.; Klumpner, B.: Innenbackenbremse mit elektromagnetischer Betätigungseinrichtung (2011)
Klumpner, Andreas; Klumpner, Bernhard: Innenbackenbremse mit elektromagnetischer Betätigungseinrichtung, Knott GmbH, Patent DE102011100088 (A1), Patent application number: DE201110100088 20110429, 2011

Knott Group: Bremsenübersicht (2022)
Knott Group: Bremsenübersicht; https://www.knott.de/fileadmin/Knott/Resources/Public/files/KNOTT-Bremsenuebersicht-D_P07901_de_1115_web.pdf, 2022, Access 26.07.2022

Lennart Guckes: Master Thesis, Optimierung einer magnetisch aktuierten Trommelbremse (2018)
Lennart Guckes: Systematische Analyse und Optimierung einer magnetisch aktuierten Trommelbremse anhand eines Simulationsmodells, Master Thesis Technische Universität Darmstadt, Darmstadt, 2018

Local Motors: Meet Olli (2020)
Local Motors: Meet Olli; https://localmotors.com/meet-olli/, 2020, Access 13.01.2020

Marschner, H. et al.: Bremsentechnisches Versuchswesen (2017)
Marschner, Holger; Teitge, Hilmar; Semsch, Martin; Bletz, Marcus; Weiss, Dieter: Bremsentechnisches Versuchswesen, in: Breuer, Bert; Bill, Karlheinz H. (Eds.): Bremsenhandbuch, Springer Fachmedien Wiesbaden, Wiesbaden, 2017

Marschner, H. et al.: Schwingungen und Geräusche (2017)
Marschner, Holger; Pfaff, Alexander; Leibolt, Paul; Maggi-Trovato, Giuseppe: Schwingungen und Geräusche, in: Breuer, Bert; Bill, Karlheinz H. (Eds.): Bremsenhandbuch, Springer Fachmedien Wiesbaden, Wiesbaden, 2017

Miriam Baum: Entwicklungsfahrzeug CUbE
Miriam Baum: Continental treibt mit dem Entwicklungsfahrzeug CUbE Technologien für fahrerlose Fahrzeuge voran; https://www.continental-corporation.com/de/presse/pressemitteilungen/cube-technologien-74444, Access 15.02.2019

Navya: Arma Autonomous Shuttle (2020)
Navya: Arma Autonomous Shuttle; https://navya.tech/en/autonom-shuttle/, 2020, Access 13.01.2020

Nowald, G.; Siegl, B.: Thermal Simulation Tool for Early Sizing of Nonstandard Brake Concepts (2021)
Nowald, Gerrit; Siegl, Benjamin: Development of a Thermal Simulation Tool for Early Sizing of Nonstandard Brake Concepts, in: FISITA (Ed.): Euro Brake 2021, Barcelona, 2021

Oberhavel Verkehrsgesellschaft mbH: Lastenheft (2019)
Oberhavel Verkehrsgesellschaft mbH: Lastenheft; https://www.ovg-online.de/fileadmin/ovg/img/pics/Lastenheft_B_Los_3_SL.pdf, 2019, Access 11.07.2022

Pickenhahn, J.; Straub, T.: Auslegung und Simulation von Pkw-Bremsanlagen (2017)
Pickenhahn, Josef; Straub, Thomas: Auslegung und Simulation von Pkw-Bremsanlagen, in: Breuer, Bert; Bill, Karlheinz H. (Eds.): Bremsenhandbuch, Springer Fachmedien Wiesbaden, Wiesbaden, 2017

Pinkow, S.: Cutting-edge brake technology MK C1 (2017)
Pinkow, Sören: Continental's cutting-edge brake technology MK C1 enables the next step to highly automated driving; https://www.continental.com/en/press/press-releases/cutting-edge-brake-technology-mk-c1/, 2017, Access 08.06.2022

Ray: Faulty Dexter Trailer Brake (2013)
Ray: Faulty Dexter Trailer Brake; https://www.loveyourrv.com/faulty-dexter-trailer-brake/, 2013, Access 22.11.2022

Reichenbach, M.: Wir sind auf dem besten Weg zur trockenen Bremse (2022)
Reichenbach, Michael: Wir sind auf dem besten Weg zur trockenen Bremse, in: ATZ - Automobiltechnische Zeitschrift (6), Issues 124, pp. 22–25, 2022

Remfrey, J. et al.: Aufbau und Komponenten von Pkw-Bremsanlagen (2017)
Remfrey, James; Gruber, Steffen; Sendler, Jan: Aufbau und Komponenten von Pkw-Bremsanlagen, in: Breuer, Bert; Bill, Karlheinz H. (Eds.): Bremsenhandbuch, Springer Fachmedien Wiesbaden, Wiesbaden, 2017

RMV: Probefahrt in die Zukunft
Rhein-Main-Verkehrsverbund GmbH: Probefahrt in die Zukunft; https://www.probefahrt-zukunft.de/flyer%20frankfurt.pdf, Access 13.05.2022

RMV: Erste autonom fahrende On-Demand-Flotte ab 2023 (2022)
Rhein-Main-Verkehrsverbund GmbH: RMV plant erste autonom fahrende On-Demand-Flotte ab 2023; https://www.rmv.de/c/de/informationen-zum-rmv/der-rmv/rmv-aktuell/rmv-plant-erste-autonom-fahrende-on-demand-flotte-ab-2023, 2022, Access 23.07.2022

Robert Syrnik: Diss., Fahrdynamische Potenziale eines elektromotorischen Traktionsantriebs (2015)
Robert Syrnik: Untersuchung der fahrdynamischen Potenziale eines elektromotorischen Traktionsantriebs, Dissertation Technische Universität München, 2015

SAE International: Taxonomy and Definitions for Terms Related to Driving Automation Systems for On-Road Motor Vehicles (2021)
SAE International: Taxonomy and Definitions for Terms Related to Driving Automation Systems for On-Road Motor Vehicles, 2021

Schaeffler: Urbanes Fahrzeugkonzept für die Zukunft (2019)
Schaeffler: Urbanes Fahrzeugkonzept für die Zukunft; https://www.schaeffler.de/content.schaeffler.de/de/news_medien/presse/pressemitteilungen/pressemitteilungen_detail.jsp?id=82027406, 2019, Access 20.08.2019

Schrimpf, M.: Master Thesis, Messtechnikkonzept zur Flussdichtemessung (2021)
Schrimpf, Malte: Entwicklung und Inbetriebnahme eines Messtechnikkonzepts zur Flussdichtemessung in einer magnetisch aktuierten Vollbelagscheibenbremse, Master Thesis
Technische Universität Darmstadt, Darmstadt, 2021

Semsch, M.: Entwurf einer elektromechanisch betätigten Radbremse mit Selbstverstärkung (2010)
Semsch, Martin: Entwurf einer elektromechanisch betätigten Radbremse mit Selbstverstärkung, FZD Fahrzeugtechnik TU Darmstadt, Issues 721, VDI-Verl., Düsseldorf, 2010

Semsch, M. et al.: Elektromechanisch betätigte Bremse (2017)
Semsch, Martin; Feigel, Hans-Jörg; Hoffmann, Jens: Elektromechanisch betätigte Bremse, in: Breuer, Bert; Bill, Karlheinz H. (Eds.): Bremsenhandbuch, Springer Fachmedien Wiesbaden, Wiesbaden, 2017

UN: ECE R13-H (2018)
United Nations ECE R13-H; Rev. 4, 05.06.2018

UNECE: Concerning The Common Definitions of Vehicle Categories, Masses and Dimensions (2005)
United Nations Economic Commission for Europe Concerning The Common Definitions of Vehicle Categories, Masses and Dimensions, 15.09.2005

UNECE: UNECE to develop global methodology to measure particle emissions from vehicles' braking systems (2021)
United Nations Economic Commission for Europe: UNECE to develop global methodology to measure particle emissions from vehicles' braking systems; https://unece.org/environment/press/unece-develop-global-methodology-measure-particle-emissions-vehicles-braking, 2021, Access 04.05.2022

Vey, C. et al.: Design of an Electromechanical Drum Brake (2019)
Vey, Christian; Hoffmann, Jens; Semsch, Martin; Pla, Sébastien: Brakes 2025 – Design of an Electromechanical Drum Brake, Dresden, 2019

Vey, C.: Diss., Bremsmomentmessung für Simplex-Trommelbremsen (2021)
Vey, Christian: Entwicklung eines Verfahrens zur integrierten Bremsmomentmessung für Simplex-Trommelbremsen, Dissertation Dissertation, 2021

Wang, D. M. et al.: A novel high-torque magnetorheological brake with a water cooling method for heat dissipation (2013)
Wang, D. M.; Hou, Y. F.; Tian, Z. Z.: A novel high-torque magnetorheological brake with a water cooling method for heat dissipation, in: Smart Materials and Structures (2), Issues 22, p. 25019, 2013

Warner Electric: Electric Wheel Brake (2014)
Warner Electric: Electric Wheel Brake; https://www.altraliterature.com/-/media/Files/Literature/Brand/warner-electric/service-manuals/a-216-we.ashx, 2014, Access 06.06.2022

ZwickRoell GmbH & Co. KG: Kraftaufnehmer Xforce K (2022)
ZwickRoell GmbH & Co. KG: Kraftaufnehmer Xforce K; https://www.zwickroell.com/fileadmin/content/Files/SharePoint/user_upload/PI_DE/03_677_Kraftaufnehmer_Xforce_K_PI_DE.pdf, 2022, Access 24.11.2022

Own Publications

Guckes, Lennart; Winner, Hermann; Hoffmann, Jens; Pla, Sébastien:

Requirements and Test Cycles for Brake Systems of Autonomous Vehicle Concepts on the Example of an Autonomous Shuttle, in: FISITA (Hrsg.): Euro Brake 2021, Barcelona, 2021

Guckes, Lennart; Hoffmann, Jens; Schrimpf, Malte; Winner, Hermann:

Evaluation of an Electromagnetically Actuated Drum Brake Concept; https://www.researchsquare.com/article/rs-2162085/v1, Preprint, 2022, Access 17.11.2022

Supervised Student Theses

Tobias Brückner, Maschinenbau: Entwicklung und Inbetriebnahme eines Prüfaufbaus für einen magnetischen Aktor zur Bremsbetätigung. Bachelor-Thesis Nr. 1351, 2020

Malte Schrimpf, Mechatronik: Entwicklung und Inbetriebnahme eines Messtechnikkonzepts zur Flussdichtemessung in einer magnetisch aktuierten Vollbelagsscheibenbremse. Master-Thesis Nr. 805, 2021

Jiahao Wang, Maschinenbau: Simulative Bewertung von Aktuierungskonzepten magnetisch betätigter Reibbremsen. Master-Thesis Nr. 809, 2021

Jan Hölschke, Materialwissenschaften: Empirische Identifikation des Verschleißverhaltens verschiedener Reibmaterialien für eine magnetisch aktuierte Reibbremse. Bachelor-Thesis Nr. 1383, 2021

Lukas Schadt, Maschinenbau: Untersuchungen zum Einfluss tribologischer Parameter auf das Reibverhalten nasslaufender Lamellenbremsen von landwirtschaftlichen Nutzfahrzeugen. Ext. Master-Thesis Nr. 813, 2021